THE INFLUENCE OF CATAMARAN MAIN CHARACTERISTICS ON SHIP MOTIONS IN REGULAR WAVES

by

João Ricardo Centeno da Costa

Thesis submitted for the Degree of Master of Science in the

Faculty of Engineering, University of Glasgow

Department of Naval Architecture and Ocean Engineering
University of Glasgow

December, 1998

© João Ricardo Centeno da Costa 1998

ProQuest Number: 13818784

All rights reserved

INFORMATION TO ALL USERS
The quality of this reproduction is dependent upon the quality of the copy submitted.

In the unlikely event that the author did not send a complete manuscript
and there are missing pages, these will be noted. Also, if material had to be removed,
a note will indicate the deletion.

ProQuest 13818784

Published by ProQuest LLC (2018). Copyright of the Dissertation is held by the Author.

All rights reserved.
This work is protected against unauthorized copying under Title 17, United States Code
Microform Edition © ProQuest LLC.

ProQuest LLC.
789 East Eisenhower Parkway
P.O. Box 1346
Ann Arbor, MI 48106 – 1346

GLASGOW
UNIVERSITY
LIBRARY
12242-Copy 1

Declaration

Except where reference is made to the work of others, this thesis is believed to be original.

Acknowledgements

The author would like to express his gratitude to all those who have contributed to this research work.

The author gratefully acknowledges Professor C. Guedes Soares for his supervision during the research period in Lisbon at Instituto Superior Técnico - Technical University of Lisbon.

The author wishes to express sincere gratitude to Dr K. S. Varyani for his supervision, help and support throughout the research and experimental work at the University of Glasgow.

The author thanks Vosper International and FBM Marine Ltd for allowing the use of their catamarans data in this research.

The author acknowledges Mr Nuno Fonseca for the private discussions and help with the strip theory mono-hull program in which the viscous forces and twin-hull configuration were implemented.

Part of the work presented in this thesis was carried out by the author under the "Safe Passage and Navigation" (SPAN) project, which has been financed by the European Community under the BRITE/EURAM program.

The author wishes to thank also FUNDENAV for financing the tuition fees.

Finally the author wishes to express a special thanks to his parents for their great understanding and patience.

Contents

Nomenclature

$o \cdot x_0 y_0 z_0$	Space fixed coordinate system
$o \cdot x y z$	Steady translating coordinate system
$o' \cdot x' y' z'$	Ship fixed coordinate system
(x_G, y_G, z_G)	Centre of gravity
A	Wave amplitude
A_{jk}	Added mass coefficients
a_{jk}	Sectional added mass coefficients
a_l	Lift coefficient
$b(x)$	Distance between the catamaran centre line and one demi-hull centre line at section x
B	Catamaran breadth
B_{jk}	Damping coefficients
$\hat{B}_{jk}$	Viscous damping coefficients
b_{jk}	Sectional damping coefficients
B_m	Breadth of one single hull
C_D	Cross-flow drag coefficient
C_{jk}	Hydrostatic coefficients
$\hat{C}_{jk}$	Viscous restoring coefficients
C_B	Block coefficient
C_p	Prismatic coefficient
C_M	Midship section coefficient
D	Distance between hulls centre lines
$d(x)$	Hull maximum draught at section x
F_j	Exciting force and moment
F_{HS}	Hydrostatic forces
F_{HD}	Hydrodynamic forces

F_{EX}	Exciting forces
F_R	Radiation forces
F_j^I	Incident wave forces in the jth direction
F_j^D	Diffracted wave forces in the jth direction
F_j^V	Exciting viscous forces in the jth direction
F_n	Froude number
g	Gravitational constant
GM_L	Longitudinal metacentric height
GM_T	Transverse metacentric height
h	Water depth
H	Inner space between hulls
i	Imaginary unit
I_{jk}	Moments of inertia
$k_0 = \frac{\omega_0^2}{g}$	Wave number
L	Ship length at water line
LCG	Longitudinal centre of gravity
Lw	Wave length
M_{jk}	Generalised mass matrix
$\mathbf{n}$	Unit normal vector
N_j	Unit normal vector in a cross section plane
p	Pressure
r`	Position vector of a point on the body surface relative to the $o'x'y'z'$ reference system
R	Cylinder radius
S_w	Wetted body surface in unsteady flow
$\bar{S}$	Mean wetted body surface in steady flow
t	Time variable
T	Ship draught

T_e	Encounter wave period
U	Mean forward velocity of the body
$v_j(x)$	Relative velocities at section x (j=2,3)
$\mathbf{V}$	Fluid velocity vector
VCG	Vertical centre of gravity
$\mathbf{V}_s$	Body velocity vector
$V40$	Catamaran model with 40 cm between demi-hull centre lines
$V60$	Catamaran model with 60 cm between demi-hull centre lines
$V80$	Catamaran model with 80 cm between demi-hull centre lines
x_A	x coordinate of the aftermost section of the ship

Greek symbols

α	Displacement relative to the steady moving coordinate system
β	Incident wave angle with respect to the x-axis (180° is head waves)
δ_{jk}	Kronecker delta
Δ	Model displacement [Kg]
ε	Perturbation parameter Phase angle
Φ	Velocity potential
$\overline{\Phi}$	Steady velocity potential
$\widetilde{\Phi}$	Unsteady velocity potential
$\overline{\phi}$	Steady perturbation potential
ϕ_I	Incident wave potential
ϕ_D	Diffracted wave potential
ϕ_k	Radiation potential in the kth mode of motion
ϕ'_k	Two dimensional sectional potential
ξ_j	Displacements (j=1,2…6 , refer to surge, sway, heave, roll, pitch and yaw respectively)

∇	Gradient operator and Ship volume displacement
∇^2	Laplace operator
ω_0	Wave frequency
ω, ω_e	Encounter wave frequency
ω_n	Natural frequency
ω_{nh}, ω_{np}, ω_{nr}	Heave, pitch and roll natural frequencies
ω_{n3}	Symmetric resonance frequency
ω_s	Sloshing resonance frequency
ρ	Water density
ζ	Free water surface elevation
$\dot{\zeta}_v, \dot{\zeta}_h$	Vertical and horizontal velocities of the fluid induced by the incident wave

List of Figures

List of Tables

Summary

The aim of this thesis is to develop a practical approach for calculating the catamaran motions in waves and to analyse the influence of hull separation and other main characteristics on the motions. An experimental program with two different catamaran models is used to help validate the theory. The theoretical work developed in this thesis is mainly based on strip theory extended to twin-hull configurations in which viscous force components are introduced. The two-dimensional theoretical model is developed with a cross flow drag term and its predictions are compared with the ones of a three-dimensional theoretical model. Both theoretical results are compared with the experimental results.

The thesis is divided in six chapters. The first one is introductory and presents the importance of the study of the seakeeping behaviour of catamarans in waves. It also introduces the history of ship motions in waves and the latest work done concerning catamaran motions in waves.

The second chapter formulates the problem of motions of a vessel in waves. The basic fluid properties and assumptions used in the theory are explained in this chapter. Both two and three-dimensional theories used in this work are based in the potential flow theory. The coordinate systems most suited to each different kind of situation are defined and explained. The boundary conditions necessary to solve this particular problem of ship motions in waves are also defined. Since the exact boundary conditions lead to a very complex non-linear problem, the theoretical formulation is simplified through a linearisation process.

Chapter 3 develops the hydrodynamic forces associated with the catamaran motions in regular waves. All the usual forces in conventional mono-hull ships are developed as well as the viscous forces, which are particularly important in the motion responses of twin-hull ships. The viscous effects are modelled by a cross-flow drag approach developed from aerodynamic theories and are then added to the basic two-dimensional potential flow theory. The numerical implementation of the method is described.

Comparisons with published results are made for simple hull forms, like twin-cylinders and Wigley forms, as well as with a realistic catamaran model.

In chapter 4 the experimental investigation performed with two catamaran models at the Hydrodynamic Laboratory of the University of Glasgow is presented. This chapter presents the statistical data analysis performed to choose the experimented model characteristics. The instrumentation set-up used for the experiments is described. The heave and pitch experimental results are presented and compared with the two-dimensional calculations. This study shows how well both heave and pitch results are improved when the viscous forces are added to the theory. At the end of the chapter an error analysis is performed to analyse the confidence of the heave and pitch experimental results as well as to analyse the quality of the incoming wave.

In chapter 5 the catamaran hull interaction and resonance frequencies are studied and analysed in order to understand what kind of interactions occur and what is the influence of the distance between the hulls in the ship motion responses. In order to better understand the hull interactions, the resonance frequencies and the influence of the hull distance in the body responses, the twin cylinder results calculated in chapter 3 are reanalysed to explain the results near the resonance frequencies at zero and forward speeds.

The results from the experimental work are analysed and compared with two and three-dimensional theoretical calculations. The three-dimensional results do not give better results than the two-dimensional results especially near the resonance frequencies where the viscous effects are important and are not modelled by the three-dimensional theory. The experimental results from the two tested models are compared and the influence of the distance between the hulls is investigated. The experimental model results are also compared with mono-hull motion responses and the results analysed.

Two parametric studies with two different hull forms are made. One uses a hard chine hull type like the one used in the experimental work while the other uses a round displacement hull. The effect of speed, hull separation, displacement and ship main dimensions are analysed.

Finally, in the last chapter the main conclusions are drawn and some recommendations and suggestions for future work are made.

Chapter 1

Introduction

For some kinds of operations such as fast passenger transportation, special military missions or oceanographic research, the twin-hull vessel has several advantages over the mono-hull vessel. Over the last few years catamarans have been widely used as fast passenger ferries where the comfort is one of the most important issues for the final user.

The main advantages of catamarans are their large deck area, very high transverse stability, small draft, low wave resistance at high speed and in general they can maintain a higher speed in a seaway than a conventional planing craft.

It is important to study and develop appropriate tools to predict catamaran behaviour at sea, because of increasing use of catamarans all over the world. Since catamarans have been used mainly for passenger transportation, from the passenger's point of view, the most important characteristics in the vessel are good seaworthiness and voyage time, which is related to the ship speed. From the naval architect's point of view there are two important points to be considered, the seakeeping behaviour of the ship and the global structural loading. The seakeeping behaviour is related to operational limits and economic viability, especially for passenger transportation operations. While in the past, most existing catamarans were small ships where the global hydrodynamic forces were not structurally important, nowadays with the advancement of new hull forms with higher speeds and larger dimensions the global hydrodynamic forces play a crucial role in the catamaran structural design.

The study of the seakeeping behaviour of mono hull vessels started in the 1950s by St.Denis and Pierson (1953) and Korvin-Kroukovsky and Jacobs (1955,1957). The first theory suitable for numerical computations based on a two-dimensional approach, was presented by Korvin-Kroukovsky and Jacobs, and is commonly referred to as the strip-theory. Since then much work has been developed and improved by many other authors, such as Gerritsma and Beukelman (1967), Salvesen et al. (1970). The first mathematical justification of strip theory was presented by Ogilvie and Tuck (1969). Later Newman (1978) presented a complete formulation of

the theory of ship motions. These theories are based on the assumption of potential flow, slender ships and small amplitude motions. Conventional strip theories do not consider forward speed effects on the free surface and the speed effects on the hull boundary condition are approximated in a simplistic way. The main problem of strip theory is in fact the treatment of forward speed effects.

The application of strip theory to multi-hulls started in the 1970s with the work of Ohkusu and Takaki (1971), Lee, Jones and Bedel (1971) and Lee et al. (1973).

Three-dimensional theoretical models were developed, first to predict the response of large offshore structures and then these models were extended to ships and multi-hulls with forward speed (Inglis and Price (1982a,b), Chan (1993), Hudson et al (1995)). These three-dimensional models are theoretically more correct but they are difficult to implement and the calculations are very complicated and time consuming.

Ohkusu (1970) proposed an approximate method to calculate hydrodynamic forces and moments on multiple cylinders with arbitrary cross section and with forced heave, sway and roll motion. Ohkusu and Takaki (1971) calculated the seakeeping qualities using the strip theory method and using the hydrodynamic forces previously developed by Ohkusu (1970). The theoretical results were compared with experimental results and were found to be satisfactory.

Lee, Jones and Bedel (1971) presented a theoretical method to calculate the two dimensional hydrodynamic coefficients associated with the motion of catamarans. This method was applied to twin cylinders. The mathematical tool adopted to solve the problem is the method of source distribution on the cross sectional contour of both cylinders. This is the same method adopted by Frank (1967) to one cylinder. Some experimental work was done with different shapes of twin cylinders and where the results from the theory and experiment were compared they showed good agreement.

Later, Lee, Jones and Curphey (1973) also used the strip theory method and the two dimensional hydrodynamic coefficients to calculate motions and hydrodynamic loads on catamarans. The theoretical results were also compared with experimental work and they were found to be satisfactory, except for some discrepancies resulting from inadequate account for viscous effects and three dimensional effects. The discrepancies on the theoretical results can be seen, specially near the resonant encounter frequencies, where the motion amplitudes are overestimated and increase

with the forward speed. For SWATH vessels the discrepancies are particularly more pronounced.

Following the same line of development, Lee (1976) presented a theoretical method to predict SWATH motions in waves, considering the viscous effects through an adequate representation of the viscous damping in the hydrodynamic forces. With this work he concluded that the effects of viscous damping on SWATH motions can be predicted by combining the cross flow approach with strip theory. Even if theoretically it cannot be fully justified, for practical purposes this approach is acceptable.

Ohkusu and Faltinsen (1990) presented a practical approach to predict three dimensional hydrodynamic interaction between two hulls of a catamaran oscillating and with forward speed. Chapman's (1976) approach is used with a full linear free surface condition including the forward speed effects. The predicted hydrodynamic forces agree generally well at high speed with the model test results and they concluded that hydrodynamic interaction between hulls is weak at high speeds.

Faltinsen and Zhao (1991a, 1991b) presented a generalisation of Chapman's method based on strip theory and a full linearised free surface boundary condition with the forward speed effect term, to calculate ship motion at high forward speed. Faltinsen et al. (1992) extended the above theory further to calculate motions and loads of catamarans in waves. At high speeds if the hulls are not too close to each other and the waves generated on one hull do not influence the pressure distribution on the other, it can be assumed that the hulls are hydrodynamically independent of each other.

Van't Veer and Siregar (1995) also studied the interaction effects on a catamaran travelling with forward speed in waves. They used a strip theory but they considered three different kind of interference between hulls, depending on the ship speed. For very small speeds the hull interaction can be considered two-dimensional and can be well predicted with strip-theory. At very high speed the authors say that there is no wave interaction between the hulls and it is only at medium speed that there is a longitudinal wave interaction. At high speed the waves generated by one hull do not reach the other hull and as a result there is no interaction between the hulls. A correction scheme was included in order to take into consideration the 3D effects in

the medium speed range. The results obtained by this method are an improved version of previously developed conventional strip theory results.

Chan (1993) proposed a three dimensional linearised potential theory associated with a cross flow approach for taking viscous effects into account for the prediction of motions and loads of twin-hull ships. The cross-flow approach is similar to the approach made by Lee (1976). The theoretical and experimental results show good agreement for a catamaran and a SWATH ship, except for some discrepancies that are believed to be caused by neglecting forward speed effects on the free surface boundary condition.

Hudson, Price and Temarel (1995) compared experimental model tests with catamarans at different speeds with a two dimensional and a three dimensional theoretical model. They concluded that both 2D and 3D theoretical models are suitable for catamarans with small hull separation and low speed. But as speed increases the results are not so good as they over predict the experimental results.

Fang, Chan and Incecik (1996) presented a two dimensional method based on the strip theory with a cross flow approach for taking viscous effects into account to study the motion response of catamaran in waves. Some experimental work was done and compared with numerical results. They concluded that the two dimensional method correlates well with the measurements of small amplitude motions except near the resonance frequencies. However it is shown that the theoretical results can be improved if the effects of viscous damping are added to the theory.

The objective of this work is to develop a practical approach to predict catamaran motions in regular waves and to study the influence of the distance between the two hulls in the catamaran motions.

Some theoretical calculations are based on a strip-theory model. The strip-theory is a very fast prediction tool, is widely used and is suitable to predict catamaran motions in regular waves, but some results show discrepancies near the resonant frequencies. To correct these discrepancies, the viscous flow effects modelled with a cross flow approach will be incorporated into the basic strip-theory formulation.

The resonance frequencies are analysed both theoretically and experimentally. Besides the response peak, of the first natural frequency, there is also in the theoretical results

a second peak that has to be properly studied because it is not evident in the experimental results.

To validate the theoretical method some experimental work on a Vosper International catamaran was carried out at the Hydrodynamic Laboratory of the University of Glasgow. The experimental work was carried out for two different hull separations, at four different forward speeds, head waves, one wave height and for several wave frequencies. The strip-theory results are compared with experimental results and Chan's (1990) three-dimensional theory.

At high speed the interaction effects between the hulls are weak. For a certain hull separation and after a certain speed, the waves generated by one hull do not have sufficient time to reach the other hull. The main objective of the experimental test program was to validate the theoretical results and to observe the relation between forward speed and hull separation distance.

Chapter 2

Formulation of the problem

2.1 *Introduction*

To calculate ship motions in regular waves it is necessary to determine the fluid motion around the travelling ship. The ship is considered as an unrestrained rigid body with six degrees of freedom. The interaction between the moving body and the fluid flow is very complex but can be considered as a system that involves only a limited number of hydrodynamic forces.

One of the most common mathematical formulations used to solve this problem is based on potential flow theory. As shown in chapter 1, two and three-dimensional solutions have already been developed based on this theory. The potential flow theory is based on the assumption of the ideal fluid. This allows several simplifications and makes the solution of the problem more feasible. Nevertheless other simplifications will have to be made. The problem has to be formulated setting some appropriate boundary conditions. The full development of the boundary conditions under this potential flow theory will lead to non-linear terms, which are once again very difficult to solve. In order to simplify the solution, the formulation will go through a linearisation process by using the perturbation expansion technique.

In this chapter all these aspects are developed and the formulation that is used to calculate the hydrodynamic forces and the solution of the motion problem is described later in chapter 3.

The formulation and assumptions made in this chapter are similar to the theories presented by Newman (1978) and Chan (1990).

2.2 *Fluid Properties*

The motion of a fluid is governed by the well known Navier-Stokes equations but in the formulation of this problem some simplifications have to be made in order to

make the solution feasible. The fluid is considered incompressible and homogenous. For the main problem of ship motions in waves the first simplification is that the viscous stress tensor, in the full Navier-Stokes equation, is not considered and so the fluid can be analysed as an inviscid, incompressible and homogeneous fluid. Under these assumptions and assuming an irrotational flow, the problem will be formulated using a potential flow analysis as described below.

The fundamental equations in this problem formulation are the continuity equation and Euler's equations. Consider the fluid velocity vector $\mathbf{V}(x_0, y_0, z_0, t) = (u, v, w)$ in a Cartesian coordinate system (x_0, y_0, z_0). The velocity vector must satisfy the continuity equation for an incompressible fluid:

$$\nabla \cdot \mathbf{V} = 0 \quad \text{or} \quad \left(\frac{\partial}{\partial x_0}, \frac{\partial}{\partial y_0}, \frac{\partial}{\partial z_0} \right) \cdot \mathbf{V} = 0 \tag{2.1}$$

and the Euler equations for an ideal fluid:

$$\frac{\partial \mathbf{V}}{\partial t} + (\mathbf{V} \cdot \nabla)\mathbf{V} = -\frac{1}{\rho} \nabla p + \frac{1}{\rho} \mathbf{F} \tag{2.2}$$

where p is the pressure and $\mathbf{F}$ is the vector of body forces. In this case the only body force is the gravitational force which acts vertically downward. On the coordinate system the vertical axis is the z_0-axis which is positive upward and $z_0 = 0$ is set as the mean free-surface level. So the vertical gravitational force is $\mathbf{F} = (0, 0, -\rho g)$.

It can be shown (Newman 1977) that, if the fluid is inviscid and incompressible the fluid motion may be considered irrotational or:

$$rot\, \mathbf{V} = \nabla \times \mathbf{V} = 0 \tag{2.3}$$

If the velocity vector $\mathbf{V}$ is irrotational then it can be represented simply as the gradient of a scalar function $\Phi(x_0, y_0, z_0, t)$:

$$\mathbf{V} = \nabla \Phi \quad \text{or} \quad \mathbf{V} = (u, v, w) = \left(\frac{\partial \Phi}{\partial x_0}, \frac{\partial \Phi}{\partial y_0}, \frac{\partial \Phi}{\partial z_0} \right) \tag{2.4}$$

The scalar function $\Phi(x_0, y_0, z_0, t)$ is the velocity potential.

If the velocity **V**, or the gradient of the velocity potential $\nabla\Phi$, is substituted into the continuity equation, then the Laplace equation is obtained:

$$\nabla^2\Phi = 0 \quad \text{or} \qquad \frac{\partial^2\Phi}{\partial x_0^2} + \frac{\partial^2\Phi}{\partial y_0^2} + \frac{\partial^2\Phi}{\partial z_0^2} = 0 \tag{2.5}$$

So if the fluid is inviscid, incompressible and irrotational, and satisfies the continuity equation, then it also satisfies the Laplace equation.

The fluid motion irrotational property can be confirmed by recalling from vector analysis that the curl of a gradient is zero.

Through Euler's equations a relation can be seen between the fluid velocity, the pressure and body forces. By integrating the Euler's equations, an explicit equation for the pressure can be obtained, which is the well known Bernoulli equation. The Euler's equation takes the form:

$$\frac{\partial \mathbf{V}}{\partial t} + (\mathbf{V}\cdot\nabla)\mathbf{V} = -\frac{1}{\rho}\nabla\left(p + \rho g z_0\right) \tag{2.6}$$

Using the vectorial identity

$$(\mathbf{V}\cdot\nabla)\mathbf{V} \equiv \nabla\left(\frac{1}{2}\mathbf{V}^2\right) - \mathbf{V}\times(\nabla\times\mathbf{V}) \tag{2.7}$$

and substituting in Euler's equation

$$\frac{\partial \mathbf{V}}{\partial t} + \nabla\left(\frac{1}{2}\mathbf{V}^2\right) - \mathbf{V}\times(\nabla\times\mathbf{V}) = -\frac{1}{\rho}\nabla\left(\rho g z_0 + p\right) \tag{2.8}$$

using the velocity potential $\mathbf{V} = \nabla\Phi$ the previous equation becomes,

$$\frac{\partial}{\partial t}\nabla\Phi + \nabla\left(\frac{1}{2}\mathbf{V}^2\right) - \mathbf{V}\times(\nabla\times\mathbf{V}) = -\frac{1}{\rho}\nabla\left(\rho g z_0 + p\right) \tag{2.9}$$

Because of the irrotational fluid property, $rot\,\mathbf{V} = \nabla\times\mathbf{V} = 0$, so equation (2.9) can be written in the form:

$$\nabla\left(\frac{\partial\Phi}{\partial t} + \frac{1}{2}\mathbf{V}^2 + \frac{p}{\rho} + g z_0\right) = 0 \tag{2.10}$$

Integrating with respect to the space variables, results in the explicit equation of the pressure:

$$p = -\rho\left(\frac{\partial\Phi}{\partial t} + \frac{1}{2}|\nabla\Phi|^2 + gz_0\right) + C(t) \tag{2.11}$$

The "constant" $C(t)$ is independent of the space variables and can be set equal to zero or it can be set equal to some other desired value such as the atmospheric pressure. $C(t)$ can be absorbed into the velocity potential by defining a function *f(t)* such that,

$$C(t) = \frac{\partial f(t)}{\partial t} \tag{2.12}$$

and then a new potential: $\Phi(x,y,z,t) = \Phi(x,y,z,t) + f(t)$

The value of $C(t)$ is related to the velocity potential but has no effect on the velocity vector, since the gradient is not time dependent.

2.3 Coordinate Systems

To describe the fluid motion and the ship motion, three Cartesian coordinate systems will be adopted, one fixed and two moving ones. Define $o - x_0y_0z_0$ as fixed in space, $o'-x'y'z'$ fixed with respect to the ship, and $o - xyz$ moving in steady translation with the mean forward speed of the ship.

The space fixed system $o - x_0y_0z_0$ is the simplest one to express the free-surface boundary condition. The ship fixed system $o'-x'y'z'$ is the best one to derive the boundary condition on the ship's wetted surface. The steady-translating system $o - xyz$ is an inertial reference frame with the x-axis translating on the undisturbed free-surface with the same mean forward velocity as the ship.

In the space fixed system, the plane $o - x_0y_0$ coincides with the undisturbed free surface, hence $z_0 = 0$ is the plane of the undisturbed free surface. The z_0-axis is positive upward. The x_0-axis is positive in the direction of the ship's forward velocity. The y_0-axis is positive in the port direction. The steady-translating coordinate system $o - xyz$ is related to the space-fixed system $o - x_0y_0z_0$ by the linear transformation

$$\mathbf{x} = (x,y,z) = (x_0 - Ut, y_0, z_0) \tag{2.13}$$

with U as the mean forward velocity of the ship. From the previous relation it can be seen that the steady-translating system coincides with the fixed coordinate system when the forward velocity of the ship is zero.

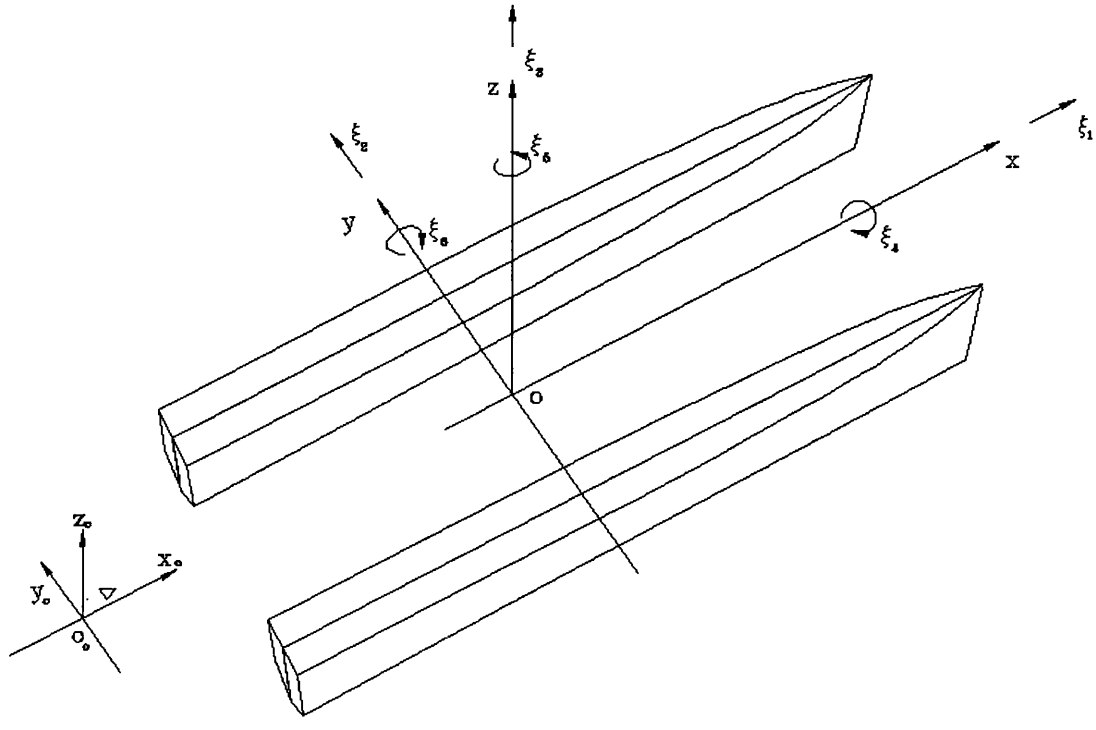

Figure 2.1 - Coordinate Systems

The steady-translating system $o-xyz$ is used to describe the body motion in six degrees of freedom. The origin is at the intersection of the undisturbed free-surface and the vertical plane which contains the centre of gravity. The translational displacements in the *x, y,* and *z* directions with respect to the origin are ξ_1, ξ_2 and ξ_3, respectively. The angular displacement of the rotational motion about the *x, y,* and *z* axis are ξ_4, ξ_5 and ξ_6, respectively. Here $\xi_1, \xi_2, \xi_3, \xi_4, \xi_5, \xi_6$ refer to surge, sway, heave, roll, pitch and yaw motions respectively and as shown in figure 2.1.

The $o'-x'y'z'$ reference system is the oscillatory translating system, fixed with the ship. The difference α between the coordinates of a point in the steady translating reference system $o-xyz$ and the ship fixed system $o'-x'y'z'$ gives the local oscillatory displacement (these two reference systems are equal in a steady state equilibrium).

$$\alpha = \mathbf{x} - \mathbf{x}' \tag{2.14}$$

or

$$\alpha = (\xi_1, \xi_2, \xi_3) + (\xi_4, \xi_5, \xi_6) \times \mathbf{r}' \tag{2.15}$$

$$\alpha = \xi + \Omega \times \mathbf{r}'$$

where $\mathbf{r}'$ is the position vector of a point on the body surface, relative to the $o'-x'y'z'$ reference system.

2.4 Boundary Conditions

For the analysis of fluid motions of any physical systems it is necessary to impose appropriate physical conditions on the boundaries of the system domain. In fact, it is precisely these boundary conditions that distinguish different flow problems.

Based on the fluid assumptions made on section 2.2, the velocity potential of the flow must satisfy the Laplace equation:

$$\nabla^2 \Phi = 0 \tag{2.16}$$

and the boundary conditions that will allow the exact solution of the problem to be found. Under the assumptions of this problem, there are two types of boundary conditions: a kinematic and a dynamic condition. The kinematic condition is related to the velocity of the fluid on the boundary while the dynamic condition is related to the forces on the boundary.

The boundary conditions for the problem of the motion of surface ships in regular waves are the body boundary condition, the free surface boundary conditions, the bottom or sea bed boundary condition and a wave radiation condition.

2.4.1 Body Boundary Condition

The body boundary condition is a kinematic condition imposed on the wetted ship surface. This condition expresses impermeability, i.e. that no fluid enters or leaves the

body surface. The normal component $\mathbf{V} \cdot \mathbf{n}$ of the fluid velocity must be equal to the normal velocity $\mathbf{V}_s \cdot \mathbf{n}$ of the boundary body surface.

$$\mathbf{V} \cdot \mathbf{n} = \mathbf{V}_s \cdot \mathbf{n} \qquad \text{on the wetted body surface } S_w . \tag{2.17}$$

where $\mathbf{n}$ is the unit normal vector to the body surface. The vector $\mathbf{n}$ is defined to point out of the fluid domain. The body velocity $\mathbf{V}_s$ is the local velocity of the wetted body surface S_w relative to the body-fixed reference system $o'-x'y'z'$.

$$\mathbf{V}_S = \alpha_t \qquad \text{on } S_w \tag{2.18}$$

where the subscript t, means differentiation in respect to time.

2.4.2 Free Surface Boundary Condition

On the surface boundary two conditions will be imposed: the kinematic and the dynamic boundary conditions.

Kinematic boundary condition.

The free water surface is defined by its elevation $\zeta(x_0, y_0, t)$. Define a function $F(x_0, y_0, z_0, t)$, such that

$$F(x_0, y_0, z_0, t) = z_0 - \zeta(x_0, y_0, t) = 0 \quad \text{on the free surface}$$

Assuming that a fluid particle on the free surface stays on the free surface, this means that it satisfies the previous equation and the substantial derivative is zero, i.e. $\frac{DF}{Dt} = 0$. This substantial derivative expresses the rate of change with time of the function F if one follows a fluid particle in space. Mathematically it is expressed as

$$\frac{DF}{Dt} = \frac{\partial F}{\partial t} + \mathbf{V} \cdot \nabla F \tag{2.19}$$

Applying that expression to the function F:

$$\frac{D}{Dt}\left(z_0 - \zeta(x_0, y_0, t)\right) = 0 \qquad \text{on } z_0 = \zeta$$

and remembering that $\mathbf{V} = \nabla\Phi$, the free surface kinematic condition is obtained

$$\frac{\partial}{\partial t}\left[z_0 - \zeta(x_0, y_0, t)\right] + \nabla\Phi \cdot \nabla\left[z_0 - \zeta(x_0, y_0, t)\right] = 0 \quad \text{on } z_0 = \zeta \qquad (2.20)$$

Dynamic boundary condition.

The dynamic free surface condition requires that the pressure on the free surface is equal to the constant atmospheric pressure p_a. If the term *C(t)* in the Bernoulli equation (2.11) is set equal to the atmospheric pressure then the Bernoulli equation becomes

$$\frac{\partial\Phi}{\partial t} + \frac{1}{2}|\nabla\Phi|^2 + gz_0 = 0 \qquad \text{on } z_0 = \zeta$$

The free surface conditions (kinematic and dynamic) are non linear. The position of the free surface is not known before the problem is solved. However, by linearizing the free surface conditions it is possible to simplify the problem and still get useful information for many practical cases. The linearization will be done in the following section 2.5. This boundary condition can be used to determine the free surface elevation from the implicit equation

$$\zeta = -\frac{1}{g}\left(\frac{\partial\Phi}{\partial t} + \frac{1}{2}|\nabla\Phi|^2\right)_{z_0=\zeta} \qquad (2.21)$$

Substituting equation (2.21) into (2.20) leads to

$$\frac{\partial}{\partial t}\left[gz_0 + \left(\frac{\partial\Phi}{\partial t} + \frac{1}{2}|\nabla\Phi|^2\right)\right] + \nabla\Phi \cdot \nabla\left[gz_0 + \left(\frac{\partial\Phi}{\partial t} + \frac{1}{2}|\nabla\Phi|^2\right)\right] = 0$$

then

$$\Phi_{tt} + 2\nabla\Phi \cdot \nabla\Phi_t + \frac{1}{2}\nabla\Phi\nabla(\nabla\Phi \cdot \nabla\Phi) + g\Phi_{z_0} = 0 \quad \text{on } z_0 = \zeta \qquad (2.22)$$

where the subscript t and z mean differentiation in respect to time and to the z coordinate respectively.

2.4.3 Bottom Boundary Condition

The bottom or the sea bed boundary condition implies that there cannot be flow through the bottom boundary. It is a kinematic boundary condition where the boundary is stationary, so the fluid particle on the bottom has zero velocity normal to the boundary. It is assumed that the sea bed is flat and the normal is in the vertical direction.

$$\frac{\partial \Phi}{\partial z} = 0 \qquad \text{on } z = -h$$

where h is the water depth. Since a deep water condition, with infinite depth, is assumed, the bottom boundary condition is:

$$\frac{\partial \Phi}{\partial z} = 0 \qquad \text{as } z \rightarrow -\infty$$

2.4.4 Far Field Radiation Condition

The three previous boundary conditions, i.e., body surface, free surface and bottom boundary conditions, are not enough to guarantee a unique solution to the motion problem. Physically, the radiation condition is necessary to ensure that the waves generated by the body propagate away from the body and decay to the infinite.

2.5 The Linearised Problem

As mentioned in previous sections, the determination of the velocity potential gives the velocity of a fluid particle in the problem domain. The velocity potential must satisfy the Laplace equation and the boundary conditions. In the previous sections, the exact boundary conditions used in this problem were formulated. The exact body boundary condition on the unsteady body surface S_w and the exact free surface condition are non-linear formulations. The solution of the problem using the exact non-linear boundary conditions is mathematically complicated. This is a difficult problem because the non-linearities associated with the free-surface and the unsteady body surface interact. In order to simplify the solution, the problem has to be

linearised. The linearisation method, is one in which all the second-order terms are neglected because they are considered sufficiently small.

The velocity potential Φ is assumed to be represented by a convergent power series

$$\Phi(\mathbf{x}_0, t; \varepsilon) = \Phi^{(0)} + \varepsilon\Phi^{(1)} + \varepsilon^2\,\Phi^{(2)} + \ldots$$

as well as the free surface elevation ζ

$$\zeta(x_0, y_0, t; \varepsilon) = \zeta^{(0)} + \varepsilon\zeta^{(1)} + \varepsilon^2\,\zeta^{(2)} + \ldots$$

The power series in the perturbation expansion are convergent if and only if the perturbation parameter ε exists and is less than unity.

The velocity potential will be defined first and then the boundary conditions will be linearised. The flow field consists of a steady flow due to the presence of the ship advancing with forward motion through the calm water surface and an unsteady flow due to the incident wave and due to the diffraction and radiation wave caused by the presence and motion of the body.

According to the following transformation $x_0 = x + Ut$, the velocity potential $\Phi(\mathbf{x}_0, t)$ can be represented in the steady moving reference frame by $\phi(x, y, z, t)$

$$\Phi(\mathbf{x}_0, t) = \Phi(x + Ut, y, z, t) \equiv \phi(x, y, z, t)$$

thus the time differentiation (Newman 1978) is given by

$$\Phi_t = \frac{\partial}{\partial t}\phi(x_0 - Ut, y_0, z_0, t) = \left(\frac{\partial}{\partial t} - U\frac{\partial}{\partial x}\right)\phi(x, y, z, t)$$

2.5.1 Linearised Free Surface Condition

The perturbation expansion is used to linearise the free surface condition to the first order, and a Taylor series expansion is used to transform the exact free surface ζ to some known surface such as the undisturbed free surface.

The total velocity potential in the steady moving reference is separated into steady and unsteady potentials

$$\phi(x,y,z,t) = \overline{\Phi}(\mathbf{x}) + \widetilde{\Phi}(\mathbf{x},t) \tag{2.23}$$

where $\overline{\Phi}$ is the steady and $\widetilde{\Phi}$ is the unsteady contributions to the velocity potential.

Steady flow problem

For a steady flow problem, the velocity potential $\overline{\Phi}$ due to the steady forward motion of the body (Chan 1990) is given by

$$\overline{\Phi}(\mathbf{x}) = -Ux + \overline{\phi}(\mathbf{x}) \tag{2.24}$$

where the first term is due to the mean forward speed of the body and $\overline{\phi}(\mathbf{x})$ is the steady perturbation potential. The velocity field of the steady flow relative to the steady translating coordinate system $o-xyz$ is

$$\mathbf{W}(\mathbf{x}) = \nabla\overline{\Phi}(\mathbf{x}) = \nabla\left(-Ux + \overline{\phi}(\mathbf{x})\right)$$

Using the dynamic free surface condition on the steady free surface elevation $\overline{\zeta}$ and the steady potential,

$$\left(\frac{\partial}{\partial t} - U\frac{\partial}{\partial x}\right)\overline{\phi} + \frac{1}{2}\left(\nabla\overline{\phi}\right)^2 + gz = 0 \tag{2.25}$$

since $\overline{\phi}_t = 0$ and $\overline{\phi} = \overline{\Phi} + Ux$

$$-U\frac{\partial}{\partial x}\left(\overline{\Phi} + Ux\right) + \frac{1}{2}\left(\nabla\left(\overline{\Phi} + Ux\right)\right)^2 + gz = 0 \qquad \text{on } z = \overline{\zeta}$$

$$-U\left(\frac{\partial\overline{\Phi}}{\partial x} + U\right) + \frac{1}{2}\left(\nabla\overline{\Phi}^2 + 2U\overline{\Phi}_x + U^2\right) + gz = 0$$

then the steady free surface elevation is given by

$$\overline{\zeta} = -\frac{1}{2g}\left(\left|\nabla\overline{\Phi}\right|^2 - U^2\right) \qquad \text{on } z = \overline{\zeta} \tag{2.26}$$

The non linear free surface condition for the steady flow problem is

$$\frac{1}{2}\nabla\overline{\Phi}\cdot\nabla\left(\nabla\overline{\Phi}\cdot\nabla\overline{\Phi}\right) + g\,\overline{\Phi}_z = 0 \qquad \text{on } z = \overline{\zeta} \tag{2.27}$$

which is similar to the total non-linear free surface condition (2.22) without the time dependent terms.

Substituting the steady potential $\overline{\Phi}(\mathbf{x}) = -Ux + \overline{\phi}(\mathbf{x})$ into (2.27) and retaining the first order terms

$$\frac{1}{2}\nabla\left(-Ux+\overline{\phi}\right)\cdot\nabla\left(\nabla\left(-Ux+\overline{\phi}\right)\nabla\left(-Ux+\overline{\phi}\right)\right)+g\frac{\partial}{\partial z}\left(-Ux+\overline{\phi}\right)=0$$

and developing the expression,

$$U^2\overline{\phi}_{xx} - U\nabla\overline{\phi}\overline{\phi}_{xx} + \nabla\overline{\phi}\nabla\left(\nabla\overline{\phi}\right)^2 - \frac{1}{2}(U,0,0)\nabla\left(\nabla\overline{\phi}\right)^2 + g\overline{\phi}_z = 0$$

and retaining the first order terms, the linear free surface condition for the steady flow problem is

$$U^2\overline{\phi}_{xx} + g\overline{\phi}_z = 0 \qquad \text{on } z = 0$$

Unsteady flow problem

For the unsteady flow problem the free surface condition is derived by introducing the velocity potential (2.23) in

$$\left(\frac{\partial}{\partial t} + \mathbf{V}\cdot\nabla\right)\left(\Phi_t + \frac{1}{2}(\nabla\Phi)^2 + gz_0\right) = 0 \qquad \text{on } z = \zeta$$

which comes from the combination of the non linear kinematic and dynamic free surface boundary conditions, then

$$\left(\frac{\partial}{\partial t} + \left(\nabla\overline{\Phi} + \nabla\widetilde{\Phi}\right)\cdot\nabla\right)\left(\widetilde{\Phi}_t + \frac{1}{2}\left(\nabla\overline{\Phi} + \nabla\widetilde{\Phi}\right)\left(\nabla\overline{\Phi} + \nabla\widetilde{\Phi}\right) + gz\right) = 0 \qquad \text{on } z = \zeta$$

After some manipulation and neglecting the quadratic terms of $\widetilde{\Phi}$, i.e. coefficients of $O(\varepsilon^2)$ in $\widetilde{\Phi}$, the free surface of the unsteady flow is obtained.

$$\begin{aligned}&\widetilde{\Phi}_{tt} + 2\nabla\overline{\Phi}\nabla\widetilde{\Phi}_t + \frac{1}{2}\nabla\overline{\Phi}\nabla\left(\nabla\overline{\Phi}\nabla\overline{\Phi}\right) + \nabla\overline{\Phi}\nabla\left(\nabla\overline{\Phi}\nabla\widetilde{\Phi}\right) + g\overline{\Phi}_z + \\ &\frac{1}{2}\nabla\widetilde{\Phi}\nabla\left(\nabla\overline{\Phi}\nabla\overline{\Phi}\right) + g\widetilde{\Phi}_z = 0 \qquad \text{on } z = \zeta\end{aligned} \tag{2.28}$$

The free surface elevation of the unsteady flow is obtained by superposing $\tilde{\Phi}$ over $\bar{\phi}$ in equation (2.25) as follows

$$\left(\frac{\partial}{\partial t}-U\frac{\partial}{\partial x}\right)\left(\bar{\phi}+\tilde{\Phi}\right)+\frac{1}{2}\left(\nabla\bar{\phi}+\nabla\tilde{\Phi}\right)\left(\nabla\bar{\phi}+\nabla\tilde{\Phi}\right)+gz=0 \qquad \text{on } z=\zeta \quad (2.29)$$

Substituting $\bar{\phi}=\bar{\Phi}+Ux$ into (2.29) and neglecting the quadratic terms of $\tilde{\Phi}$ in ε, leads to,

$$\zeta=-\frac{1}{g}\left(\tilde{\Phi}_t+\frac{1}{2}\left(\left|\nabla\bar{\Phi}\right|^2-U^2\right)+\nabla\bar{\Phi}\nabla\tilde{\Phi}\right) \qquad \text{on } z=\zeta$$

To transform the free surface ζ to $\bar{\zeta}$, a Taylor series expansion is used for the previous equation. The two first terms of the expansion are

$$\zeta=-\frac{1}{g}\left(\tilde{\Phi}_t+\frac{1}{2}\left(\left|\nabla\bar{\Phi}\right|^2-U^2\right)+\nabla\bar{\Phi}\nabla\tilde{\Phi}\right)_{z=\bar{\zeta}}$$
$$-\left(\zeta-\bar{\zeta}\right)\frac{1}{g}\frac{\partial}{\partial z}\left(\tilde{\Phi}_t+\frac{1}{2}\left(\left|\nabla\bar{\Phi}\right|^2-U^2\right)+\nabla\bar{\Phi}\nabla\tilde{\Phi}\right)_{z=\bar{\zeta}}+\ldots$$

as seen before $\bar{\zeta}=-\frac{1}{2g}\left(\left|\nabla\bar{\Phi}\right|^2-U^2\right) \qquad \text{on } z=\bar{\zeta}$

and $\frac{\partial}{\partial z}U^2=0$ and $\frac{1}{2}\frac{\partial}{\partial z}\left|\nabla\bar{\Phi}\right|^2=\nabla\bar{\Phi}\nabla\bar{\Phi}_z$

Substituting ζ, $\bar{\zeta}$ and $\bar{\Phi}$ in the perturbation series expansion and neglecting the terms $O(\varepsilon^2)$ then

$$\zeta=\bar{\zeta}-\frac{1}{g}\left(\tilde{\Phi}_t+\nabla\bar{\Phi}\nabla\tilde{\Phi}\right)_{z=\bar{\zeta}}-\left(\zeta-\bar{\zeta}\right)\frac{1}{g}\left(\nabla\bar{\Phi}\nabla\tilde{\Phi}\right)_{z=\bar{\zeta}}$$

$$g\left(\zeta-\bar{\zeta}\right)+\left(\zeta-\bar{\zeta}\right)\left(\nabla\bar{\Phi}\nabla\tilde{\Phi}\right)_{z=\bar{\zeta}}=-\left(\tilde{\Phi}_t+\nabla\bar{\Phi}\nabla\tilde{\Phi}\right)_{z=\bar{\zeta}}$$

and

$$\left(\zeta-\bar{\zeta}\right)=-\frac{\left(\tilde{\Phi}_t+\nabla\bar{\Phi}\nabla\tilde{\Phi}\right)}{\left(g+\nabla\bar{\Phi}\nabla\tilde{\Phi}\right)} \qquad \text{on } z=\bar{\zeta}$$

A similar expansion using Taylor series and perturbation series expansion of ζ, $\bar{\zeta}$ and $\tilde{\Phi}$ is used to develop the free surface condition of the unsteady flow (2.28) from the unsteady position ζ to the steady position $\bar{\zeta}$.

$$\tilde{\Phi}_{tt} + 2\nabla\bar{\Phi}\nabla\tilde{\Phi}_t + \nabla\bar{\Phi}\nabla\left(\nabla\bar{\Phi}\nabla\tilde{\Phi}\right) + \frac{1}{2}\nabla\tilde{\Phi}\nabla\left(\nabla\bar{\Phi}\nabla\bar{\Phi}\right) + g\tilde{\Phi}_z$$
$$-\left(\tilde{\Phi}_t + \nabla\bar{\Phi}\nabla\tilde{\Phi}_t\right)\left[\frac{1}{2}\frac{\partial}{\partial z}\left(\nabla\bar{\Phi}\cdot\nabla\left|\nabla\bar{\Phi}\right|^2\right) + g\bar{\Phi}_{zz}\right] \Big/ \left(g + \nabla\bar{\Phi}\nabla\bar{\Phi}_z\right) = 0$$

$$\text{on } z = \bar{\zeta} \qquad (2.30)$$

The general solution of this equation is at the present time difficult. One simplification is to reduce the effects of steady flow by the assumption of small steady perturbation flow due to forward motion (Chan 1990). All terms associated with the perturbation steady potential are neglected in the first order free surface condition for the unsteady flow. Hence

$$\mathbf{W} = \nabla\bar{\Phi} = \left(-U,0,0\right)$$

is assumed and the first order free surface condition (2.30) takes the form

$$\tilde{\Phi}_{tt} - 2U\tilde{\Phi}_{xt} + U^2\tilde{\Phi}_{xx} + g\tilde{\Phi}_z = 0 \qquad \text{on } z = 0$$

or

$$\left(\frac{\partial}{\partial t} - U\frac{\partial}{\partial x}\right)^2 \tilde{\Phi} + g\tilde{\Phi}_z = 0 \qquad \text{on } z = 0 \qquad (2.31)$$

2.5.2 Linearised Body Boundary Condition

The body boundary condition (2.17) is defined on the wetted body surface S_w relative to the body fixed reference system $o'-x'y'z'$. The linearised body boundary condition is defined on the mean wetted body surface $\bar{S}$. The boundary on its steady state position takes the form

$$\mathbf{W}\cdot\mathbf{n} = 0 \qquad \text{on } \bar{S} \qquad (2.32)$$

where

$$\mathbf{W}(\mathbf{x}) = \nabla\overline{\Phi}(\mathbf{x}) = \nabla\left(-Ux + \overline{\phi}(\mathbf{x})\right) \tag{2.33}$$

From equation (2.17) and (2.18) we get

$$\mathbf{V}\cdot\mathbf{n} = \alpha_t \cdot \mathbf{n} \tag{2.34}$$

The velocity **V** is the gradient of the velocity potential, hence equations (2.23) and (2.24) lead to

$$\mathbf{V} = \nabla\Phi = \nabla\left(-Ux + \overline{\phi}(\mathbf{x}) + \widetilde{\Phi}(\mathbf{x},t)\right) \tag{2.35}$$

and with equations (2.34) and (2.35)

$$\left(\nabla\left(-Ux + \overline{\phi}\right) + \nabla\widetilde{\Phi}\right)\cdot\mathbf{n} = \alpha_t \cdot \mathbf{n}$$

and using (2.33)

$$\widetilde{\Phi}_n = \alpha_t \cdot \mathbf{n} - \mathbf{W}\cdot\mathbf{n} \qquad \text{on } S_w \tag{2.36}$$

The normal vector **n** is expanded through perturbation series as

$$\mathbf{n} = \mathbf{n}^{(0)} + \varepsilon\mathbf{n}^{(1)} + O\left(\varepsilon^2\right)$$

where

$$\mathbf{n}^{(0)} = \mathbf{n}$$
$$\mathbf{n}^{(1)} = \Omega \times \mathbf{n} = \left(\xi_4, \xi_5, \xi_6\right) \times \mathbf{n}$$

Similarly **W** can be expanded in a similar way

$$\mathbf{W} = \mathbf{W}^{(0)} + \varepsilon\mathbf{W}^{(1)} + O\left(\varepsilon^2\right)$$

where

$$\mathbf{W}^{(0)} = \mathbf{W} = (u, v, w)$$
$$\mathbf{W}^{(1)} = \xi\mathbf{W} = (\alpha_t \cdot \nabla)\mathbf{W}$$

The dot product of **W** and **n** using the previous expansions and remembering that $\mathbf{W}\times\Omega = -\Omega\times\mathbf{W}$ is

$$(\mathbf{W}\cdot\mathbf{n})_S = \left(\left[\mathbf{W} - \Omega\times\mathbf{W} + (\alpha\cdot\nabla)\mathbf{W}\right]\right)_S \qquad \text{on } S_w,\ \overline{S} \tag{2.37}$$

Substituting equation (2.37) into equation (2.36) and using the condition $\mathbf{W}\cdot\mathbf{n} = 0$ on S_w.

$$\tilde{\Phi}_n = \left(\alpha_t + \Omega \times \mathbf{W} - (\alpha \cdot \nabla)\mathbf{W}\right) \cdot \mathbf{n} \qquad \text{on } S_w,\ \bar{S} \tag{2.38}$$

The last equation is presented in a different way using $\alpha = \xi + \Omega \times \mathbf{r}'$ and the following vector identity

$$(\mathbf{W} \cdot \nabla)\alpha = (\mathbf{W} \cdot \nabla)\xi + [(\mathbf{W} \cdot \nabla)\Omega] \times \mathbf{r}' + \Omega \times [(\mathbf{W} \cdot \nabla)\mathbf{r}'] \tag{2.39}$$

The vectors ξ and Ω have zero divergence because they are independent of the spatial coordinate, so the first two terms on the right hand side of the equation (2.39) are zero and the equation reduces to

$$(\mathbf{W} \cdot \nabla)\alpha = \Omega \times \mathbf{W}$$

Substituting into equation (2.38)

$$\tilde{\Phi}_n = \left(\alpha_t + (\mathbf{W} \cdot \nabla)\alpha - (\alpha \cdot \nabla)\mathbf{W}\right) \cdot \mathbf{n} \qquad \text{on } S_w,\ \bar{S} \tag{2.40}$$

The first two terms in brackets give the rate of change of α in a frame of reference moving with the stationary flow.

$$\tilde{\Phi}_n = \left(\left(\frac{\partial}{\partial t} + \mathbf{W} \cdot \nabla\right)\alpha - (\alpha \cdot \nabla)\mathbf{W}\right) \cdot \mathbf{n} \qquad \text{on } S_w,\ \bar{S} \tag{2.41}$$

Using the following vector identity

$$\nabla \times (\alpha \times \mathbf{W}) = (\mathbf{W} \cdot \nabla)\alpha - (\alpha \cdot \nabla)\mathbf{W} + \alpha(\nabla \cdot \mathbf{W}) - \mathbf{W}(\nabla \cdot \alpha)$$

Since α and $\mathbf{W}$ have zero divergence, the last two terms on the right hand side of the foregoing equation are zero, hence equation (2.38) becomes

$$\tilde{\Phi}_n = (\alpha_t + \nabla \times (\alpha \times \mathbf{W})) \cdot \mathbf{n} \qquad \text{on } S_w,\ \bar{S}$$

If the perturbation of the steady flow field due to the ship is neglected, then $\mathbf{W} = \nabla\bar{\Phi} = (-U,0,0)$ is assumed and equation (2.41) becomes

$$\begin{aligned}\tilde{\Phi}_n &= \left(\left(\frac{\partial}{\partial t} + \mathbf{W} \cdot \nabla\right)\alpha\right) \cdot \mathbf{n} = \left[\alpha_t + \Omega \times (-U,0,0)\right] \cdot \mathbf{n} \qquad \text{on } S_w,\ \bar{S} \\ &= \left[\alpha_t - U(\Omega \times \mathbf{i})\right] \cdot \mathbf{n}\end{aligned}$$

The term proportional to U can be interpreted as the product of the ship's forward speed and the angle of attack due to pitch and yaw.

2.6 Linear Decomposition of the Unsteady Potential

In the linearisation process, the velocity potential Φ is separated into steady and unsteady potential (2.23). Assuming the wave amplitude and the unsteady motions are small, the unsteady velocity potential $\tilde{\Phi}$ is decomposed linearly into separate components due to the incident waves, diffraction waves and radiation waves. The decomposition of the potential into separate components allows the solution of the several hydrodynamic problems separately. The incident waves have small amplitude and are sinusoidal and harmonic in time. Hence the unsteady motions, the diffraction and radiated waves are also sinusoidal and harmonic with the frequency of encounter ω. Under these assumptions, the translational and rotational displacements of the rigid body are denoted:

$$\xi = (\xi_1, \xi_2, \xi_3)e^{-i\omega t}$$

$$\Omega = (\xi_4, \xi_5, \xi_6)e^{-i\omega t}$$

with this notation, the unsteady component of the velocity potential is expressed as:

$$\tilde{\Phi}(\mathbf{x},t) = \left[A(\phi_I + \phi_D) + \sum_{j=1}^{6} \xi_j \phi_j \right] e^{-i\omega t}$$

where ϕ_I is the incident wave potential of unit amplitude, ϕ_D is the diffraction wave potential, ϕ_j is the radiation wave potential in the jth mode of motion, A is the wave amplitude and ω is the encounter frequency.

The diffraction wave problem considers the waves produced by the diffraction of the incident waves when the body is restrained from oscillating. The radiation wave problem considers the waves generated by the oscillating body motion in calm water.

The encounter frequency is

$$\omega = \omega_0 - Uk_0 \cos\beta$$

where U is the mean body forward speed, ω_0 is the incident wave frequency, β is the angle of incidence of the wave with the x-axis (180° is head sea) and k_0 is the wave number.

The wave number for finite water depth h, is given by the dispersion relation

$$\frac{\omega_0^2}{g} = k_0 \tanh(k_0 h)$$

and for infinite water depth, the wave number is

$$\frac{\omega_0^2}{g} = k_0$$

where g is the gravitational acceleration.

The incident wave potential of unit amplitude given by linear wave theory is

$$\phi_I = -i\frac{g}{\omega_0} e^{k_0 z} e^{ik_0(x\cos\beta - y\sin\beta)}$$

which satisfies the Laplace equation (2.16) and the linearised free surface boundary condition (2.31).

The unknown wave potentials must satisfy the Laplace equation, the free surface boundary condition and the body boundary condition.

In the diffraction problem, the body is assumed to be restrained from oscillating with respect to the body fixed reference system $o'-x'y'z'$ so that $\alpha = 0$ and the linearised body boundary condition (2.41) becomes

$$\frac{\partial}{\partial n}(\phi_I + \phi_D) = 0 \qquad \text{on } \bar{S} \qquad (2.42)$$

or

$$\frac{\partial \phi_I}{\partial n} = -\frac{\partial \phi_D}{\partial n} \qquad \text{on } \bar{S}$$

The linearised free surface condition for the diffraction problem is

$$\left(i\omega + U\frac{\partial}{\partial x}\right)^2 \phi_D + g\frac{\partial \phi_D}{\partial z} = 0 \qquad \text{on } z = 0$$

and for the radiation problem it is:

$$\left(i\omega + U\frac{\partial}{\partial x}\right)^2 \phi_j + g\frac{\partial \phi_j}{\partial z} = 0 \quad ,j = 1,2...6 \qquad \text{on } z = 0$$

In the radiation problem the radiated waves are generated as if the body is forced to oscillate with the wave excitation frequency in any rigid body motion mode. In the radiation problem, there are no incident waves. Under these assumptions the linearised body boundary condition (2.40) for the radiation potential takes the form

$$\sum_{j=1}^{6} \xi_j \frac{\partial \phi_j}{\partial n} = (\alpha_t + (\mathbf{W}\cdot\nabla)\alpha - (\alpha\cdot\nabla)\mathbf{W})\cdot\mathbf{n} \qquad \text{on } S_w,\ \bar{S}$$

From the foregoing equation and the vector displacement $\alpha = \xi + \Omega \times \mathbf{r}'$ and following Ogilvie and Tuck (1969), the body boundary condition becomes

$$\frac{\partial \phi_j}{\partial n} = -i\omega n_j + U m_j \qquad j=1,2,..6 \qquad \text{on } S_w,\ \bar{S}$$

where

$$(n_1, n_2, n_3) = \mathbf{n}$$

$$(n_4, n_5, n_6) = \mathbf{r} \times \mathbf{n}$$

and the forward speed coefficients m_j are

$$(m_1, m_2, m_3) = \mathbf{m} = -(\mathbf{n}\cdot\nabla)\mathbf{W}$$

$$(m_4, m_5, m_6) = -(\mathbf{n}\cdot\nabla)(\mathbf{r}\times\mathbf{W})$$

If the ship hull geometry is thin, slender or the mean forward speed is low, $\bar{\phi}$ is small enough to be negligible in the unsteady flow and keeping the assumption $\mathbf{W} = (-U, 0, 0)$, then

$$m_j = 0 \qquad j=1,2,3,4$$

$$m_5 = n_3$$

$$m_6 = -n_2$$

Under these assumptions, the body boundary condition becomes

$$\frac{\partial \phi_j}{\partial n} = -i\omega n_j \qquad j=1,2,3,4$$

$$\frac{\partial \phi_5}{\partial n} = -i\omega n_5 + U n_3$$

$$\frac{\partial \phi_6}{\partial n} = -i\omega n_6 + U n_2$$

2.7 Concluding Remarks

The formulation of the problem based on potential flow theory is described. The basic fluid properties and assumptions are presented. The coordinate systems used to solve the problem in the more suitable way are set and the initial boundary conditions that define the ship motion problem are presented. Since at the moment the non-linear solution of this problem is not feasible a linearisation process is presented.

Chapter 3

Hydrodynamic Forces and Motions in Regular Waves

3.1 Introduction

A ship advancing at a steady forward speed with arbitrary heading in regular waves moves in six degrees of freedom. The ship motion is decomposed into three translation components, surge, sway and heave and three rotation components, roll, pitch and yaw. In order to solve the six degrees of freedom problem, linear ship motion theories are used successfully with reasonable accurate results over a wide range of parameters (Guedes Soares et al., 1997). The most used linear theory based on a two-dimensional approach and commonly referred to as the strip-theory is the basis of the following theoretical development. The theory is based on the assumption of potential flow, slender ships and small amplitude motions.

The strip theory was first developed to predict mono-hull seakeeping characteristics, but it has also been used for twin-hull ships by Ohkusu and Takaki (1971), by Lee, Jones and Bedel (1971), by Lee et al. (1973) and several other authors since then.

Strip theory applied to twin-hull ships gives results that are in good agreement with experimental results except for some discrepancies near the resonance frequencies, where the theoretical amplitudes are overestimated and increase with the forward speed. These overestimated results are a consequence of an inadequate account for viscous effects in the strip theory model. While in a mono-hull the wave making damping plays a dominant role, in the twin-hull configuration this role is no longer so important, because of the relatively smaller water plane area, and the viscous damping starts to become important, (Lee 1976, Rathje and Schellin 1997).

To consider this viscous damping component, a method is proposed and numerically implemented in this thesis. The viscous effects are introduced in a strip theory mathematical model through a method based on a cross flow approach developed from aerodynamics theory, (Thwaites 1960).

In this chapter a general description of the strip theory program used in this work will be made and a more detailed description of the new implementation of the viscous forces is presented. A flowchart with the changes and the new routines added to the code of the original strip theory program is presented.

Calculations are made for a twin-cylinder and two catamarans with different hull forms and the results from these calculations are compared with other authors results (Ohkusu and Takaki 1971 and van't Veer 1995).

3.2 Hydrodynamic and Hydrostatic Forces

Three force components (F_1, F_2, F_3) and three moments (F_4, F_5, F_6) are obtained by integrating the fluid pressure distribution over the mean wetted hull surface.

$$F_{Hj} = \iint_{\bar{S}} p \cdot n_j \, dS \qquad j=1,2,\ldots 6 \tag{3.1}$$

where $\bar{S}$ is the mean wetted hull surface, p is the fluid pressure and n_j is the generalised unit normal vector to the hull surface as defined in section 2.6. The normal vector **n** is defined to point out of the fluid domain. Since the whole theory is based on potential flow the fluid pressure is given by Bernoulli's equation in terms of total velocity potential. The fluid pressure is separated into hydrostatic and hydrodynamic components and the forces are also separated as follows

$$F_{Hj} = F_{HSj} + F_{HDj} \qquad j=1,2,\ldots 6$$

To calculate the hydrodynamic forces the flow potential is decomposed linearly into separate components due to incident waves, diffraction waves and radiation waves as shown in chapter 2. The hydrodynamic forces are separated into two distinct sets of forces, as follows

$$F_{HDj} = F_{EXj} + F_{Rj} \qquad j=1,2,\ldots 6$$

where F_{EXj} are the exciting forces in the jth direction and are equal to the exciting force component due to incident waves (usually called the Froude-Krylov force) and the exciting force component due to diffracted waves, and is expressed as

$$F_{EXj} = \{F_j^I + F_j^D\} e^{-i\omega t} \qquad j=1,2,\ldots 6$$

F_{Rj} is the radiation forces in the jth direction due to forced oscillatory motion in the kth direction.

The pressure equation is used to calculate the forces after expanding in a Taylor series and then linearizing up to the first order terms.

3.2.1 Hydrostatic Forces

In linear theory the hydrostatic integral need only to be carried out on the body wetted surface up to the calm water level. Taking the hydrostatic term $-\rho gz$ of the pressure equation (2.11) and integrating in the mean wetted surface $\bar{S}$, one obtains the hydrostatic force F_{HSj},

$$F_{HSj} = -\rho g \iint_{\bar{S}} z \cdot n_j dS \qquad j=1,2,\ldots 6$$

Developing the integral according to the hydrostatic theory (Newman 1977) leads to

$$F_{HSj} = -\sum_{k=1}^{6} C_{jk} \xi_k \, e^{-i\omega t} \qquad j=1,2,\ldots 6$$

where C_{jk} are the hydrostatic restoring coefficients and ξ_k is the body displacement. The hydrostatic restoring coefficients give the force acting on the body in the jth direction due to unit displacement in the kth mode of motion.

C_{jk} are given by the following expressions where the integrals are taken over the length of the ship.

$$\begin{aligned} C_{33} &= 2\rho g \int B_m(x) dx = \rho g A_w \\ C_{35} &= C_{53} = -2\rho g \int x B_m(x) dx = -\rho g A_y \\ C_{55} &= \rho g GM_L \\ C_{44} &= \rho g \nabla GM_T \end{aligned} \tag{3.2}$$

All other terms are equal to zero, $C_{jk} = 0$

$B_m(x)$ is the demi-hull breadth at section x ; GM_T is the transverse metacentric height ; GM_L is the longitudinal metacentric height, A_w is the waterplane area at $z=0$; A_y is the

first moment of the waterplane area at $z=0$ and ∇ is the displaced volume of the catamaran.

3.2.2 Exciting Forces

The exciting forces are the ones that excite the motions of the body. As mentioned in previous sections, exciting forces are separated into two components, the incident and the diffraction component.

$$F_{EXj} = \{F_j^I + F_j^D\}e^{-i\omega t} \qquad j=1,2,\ldots 6$$

The exciting force F_j^I due to incident waves is calculated by integration over the mean wetted body surface of the pressure, which would exist in the wave system if the body was not present. Assuming that the motion of the body is small and the pressure at a point on the hull is expanded in a Taylor series and the high order terms on the Bernoulli equation are dropped, the unsteady pressure equation becomes.

$$p = -\rho\left(\tilde{\Phi}_t - U\frac{\partial\tilde{\Phi}}{\partial x}\right)$$

The exciting force due to incident waves is easily calculated because the incident wave potential ϕ_I and its associated pressure are known and it only needs to be integrated over the mean wetted body surface in order to obtain the force.

$$F_j^I = \rho\iint_{\bar{S}} n_j\left(i\omega + U\frac{\partial}{\partial x}\right)\phi_I dS \qquad j=1,2,\ldots 6 \qquad (3.3)$$

The incident exciting force accuracy increases as the wavelength of the incident waves increases relative to the body dimensions, (Lewis 1989). For short wave lengths the diffraction potential cannot be neglected and in the limit of very short waves the total exciting force is approximately doubled over the incident wave force. The diffraction force becomes important when the dimension of the body increases relative to the waves.

The diffraction wave force F_j^D is caused by the diffraction of the incident waves due to the presence of the hull and is associated with the diffracted potential ϕ_D and is given by

$$F_j^D = \rho \iint_{\bar{S}} n_j \left(i\omega + U \frac{\partial}{\partial x} \right) \phi_D dS \qquad j=1,2,\ldots 6 \qquad (3.4)$$

3.2.3 Radiation forces

The radiation forces result from the radiation of waves from a hull forced to oscillate in calm water. The radiation forces in the *j*th direction resulting from the motion in the *k*th direction are given by

$$\begin{aligned} F_{Rj} &= \rho \iint_{\bar{S}} n_j \left(i\omega + U \frac{\partial}{\partial x} \right) \left(\sum_{k=1}^{6} \xi_k \phi_k e^{-i\omega t} \right) dS \\ &= \sum_{k=1}^{6} \left[\rho \iint_{\bar{S}} n_j \left(i\omega + U \frac{\partial}{\partial x} \right) \phi_k dS \right] \xi_k e^{-i\omega t} \end{aligned} \qquad j=1,2,\ldots 6 \qquad (3.5)$$

For convenience the above quantity in brackets can be designated T_{jk}, so that

$$T_{jk} = \rho \iint_{\bar{S}} n_j \left(i\omega + U \frac{\partial}{\partial x} \right) \phi_k dS \qquad j=1,2,\ldots 6$$

and

$$F_{Rj} = \sum_{k=1}^{6} T_{jk} \xi_k e^{-i\omega t} \qquad j=1,2,\ldots 6$$

T_{jk} is effectively a transfer function from the unit motion in the *k*th mode to hydrodynamic force in the *j*th mode.

The hydrodynamic radiation forces are expressed in phase with the body acceleration and in phase with the velocity and takes the form

$$T_{jk} = \omega^2 A_{jk} + i\omega B_{jk}$$

$$F_{Rj} = \sum_{k=1}^{6} \left(\omega^2 A_{jk} + i\omega B_{jk} \right) \xi_k e^{-i\omega t}$$

where A_{jk} are the added mass coefficients and B_{jk} are the damping coefficients. The term added mass comes from the apparent increase in inertia of the body which moves in a fluid and spends some kinetic energy to accelerate the surrounding fluid. The term damping coefficient is related to the velocity of the motion and represents a measure of energy dissipation through the radiated waves in the potential flow theory. The added mass and damping coefficients are given by

$$A_{jk} = -\frac{\rho}{\omega^2}\mathrm{Re}\left[\iint_{\bar{S}} n_j\left(i\omega + U\frac{\partial}{\partial x}\right)\phi_k\right]dS$$

$$B_{jk} = -\frac{\rho}{\omega}\mathrm{Im}\left[\iint_{\bar{S}} n_j\left(i\omega + U\frac{\partial}{\partial x}\right)\phi_k\right]dS \tag{3.6}$$

3.3 Viscous Forces

While in a mono-hull the wave making damping plays a dominant role in the overall damping, in the twin-hull configuration, this role is no longer so important and the viscous damping starts having a larger relative value because of the smaller water plane area of this type of hull. To consider this important damping component, the viscous effects are added to the mathematical model through a cross flow approach, developed from simplified aerodynamics theory, (Thwaites 1960). The application of this cross flow approach to twin-hull ships was made before by several authors, Lee (1976), Chan (1993) and Schellin and Rathje (1995).

The force acting on an incremental length of a body with projected area dA_p include two components: the lift force L and the drag force D resolved normal to and along the relative fluid velocity as shown in Figure 3.1.

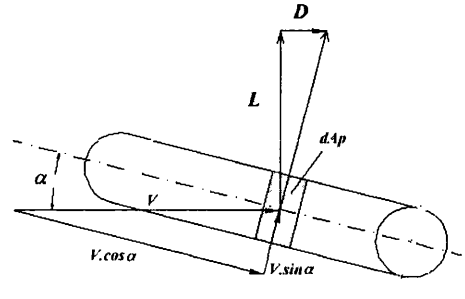

Figure 3.1 – Viscous forces on incremental length of hull

The total force due to viscous lift and cross flow drag on an incremental body length dAp is expressed as

$$F = \frac{1}{2}\rho V dA_p \sin\alpha\left(a_l |V\cos\alpha| + C_D |V\sin\alpha|\right) \tag{3.7}$$

where α is the angle of attack, V is the relative fluid velocity, A_p is the projected area, a_l and C_D are the lift and drag coefficients respectively.

The first term of equation (3.7) represents the hydrodynamic lift force and is due to vortex shedding around a slender body in steady-state translation. The second term is the drag force term and it arises from the boundary layer growth and flow separation. Viscous drag and lift coefficients depend on body geometry, mode of motion and frequency of oscillation but for simplicity these coefficients are assumed constant in all conditions. Commonly, these coefficients have to be obtained experimentally.

The viscous forces given by the general equation (3.7) is developed and separated into viscous damping forces, viscous restoring forces and viscous excitation forces in the form

$$\hat{F}_j = \sum_{k=1}^{6}\left(\hat{B}_{jk}\dot{\xi}_k + \hat{C}_{jk}\xi_k\right) - F_j^V \qquad ,j=1,2,..6 \tag{3.8}$$

where F_j^V is the exciting viscous force and $\hat{B}_{jk}$ and $\hat{C}_{jk}$ are the viscous damping and restoring coefficients respectively.

For a harmonically oscillating hull with constant forward speed and small motion amplitudes, the viscous force equation takes the following form:

$$\hat{F}_j = \frac{1}{2}\rho A_j\left(U^2 a_l \alpha_j + C_D v_j |v_j|\right) \qquad ,j=1,2,3 \tag{3.9}$$

where α_j is the angle of attack of the flow, U is the ship forward speed, v_j is the relative fluid velocity with respect to the body in the jth mode of motion, A_j is the projected area of the body in the jth direction, a_l and C_D are the lift and drag coefficients respectively.

A pseudo steady-state condition is assumed and the particle velocities are calculated from the potential of the incident wave ϕ_I. The relative velocities are determined from

the fluid velocity and the ship velocity components at the centre of action of the incremental hull length. The vertical ξ_v and horizontal ξ_h displacements at any point *(x,y,z)* in the hull are given by

$$\xi_v = \xi_3 - x\xi_5 + y\xi_4$$

$$\xi_h = \xi_2 + x\xi_6 + z\xi_4$$

The vertical relative velocity of the fluid at a section *x*, with respect to the port and starboard hull, is given by

$$\begin{aligned} v_{3P}(x) &= \dot{\xi}_3 - x\dot{\xi}_5 + b(x)\dot{\xi}_4 - \dot{\zeta}_v(x,+b(x),-d_3(x)) = U\left(\alpha_{3P}(x) - \xi_5\right) \\ v_{3S}(x) &= \dot{\xi}_3 - x\dot{\xi}_5 - b(x)\dot{\xi}_4 - \dot{\zeta}_v(x,-b(x),-d_3(x)) = U\left(\alpha_{3S}(x) - \xi_5\right) \end{aligned} \tag{3.10}$$

and the horizontal relative velocity is

$$\begin{aligned} v_{2P}(x) &= \dot{\xi}_2 + x\dot{\xi}_6 + d_2(x)\dot{\xi}_4 - \dot{\zeta}_h(x,+b(x),-d_2(x)) = U(\alpha_{2P}(x) + \xi_6) \\ v_{2S}(x) &= \dot{\xi}_2 + x\dot{\xi}_6 + d_2(x)\dot{\xi}_4 - \dot{\zeta}_h(x,-b(x),-d_2(x)) = U(\alpha_{2S}(x) + \xi_6) \end{aligned} \tag{3.11}$$

$\dot{\zeta}_v$ and $\dot{\zeta}_h$ are respectively the vertical and horizontal velocity of the fluid induced by the incident wave. The ship velocity in the *k*th mode of motion is $\dot{\xi}_k$. The distance d_2 and d_3 specify respectively the local vertical distance of the lateral and plane centres of action of the hull section, measured from the still water line. *b(x)* is the distance between the catamaran centre line and one demi-hull centre line.

From the foregoing equations, the angle of attack at a section of the body in the two modes of motion can be written as

$$\alpha_{3i}(x) = \frac{v_{3i}(x)}{U} + \xi_5 \qquad , i=S,P$$

$$\alpha_{2i}(x) = \frac{v_{2i}(x)}{U} - \xi_6 \qquad , i=S,P$$

In the vertical relative velocity, the term $b(x)\dot{\xi}_4$ will not contribute to the vertical force $\hat{F}_3$ because of the symmetry of the catamaran geometry with respect to the centre line.

Using the strip concept, together with the assumption of small angles of attack and no viscous interaction between the hulls, the viscous force in all incremental hull sections can be integrated over the two demi-hulls and the vertical force becomes

$$\hat{F}_3(x) = \frac{1}{2}\rho \sum_{i=S,P} \int_L B_m(x)\left(U^2 a_l \alpha_{3i}(x) + C_D v_{3i}(x)\left|v_{3i}(x)\right|\right)dx$$

and developing leads to

$$\hat{F}_3(x) = \frac{1}{2}\rho \int_L B_m(x)\left(2U^2 a_l \xi_5 + U a_l\left(v_{3S}(x) + v_{3P}(x)\right) + \right.$$
$$\left. C_D\left(v_{3S}(x)\left|v_{3S}(x)\right| + v_{3P}(x)\left|v_{3P}(x)\right|\right)\right)dx$$

where $B_m(x)$ is the maximum demi-hull breadth at section x.

Doing the same kind of development for the horizontal force

$$\hat{F}_2(x) = \frac{1}{2}\rho \int_L d(x)\left(-2U^2 a_l \xi_6 + U a_l\left(v_{2S}(x) + v_{2P}(x)\right) + \right.$$
$$\left. C_D\left(v_{2S}(x)\left|v_{2S}(x)\right| + v_{2P}(x)\left|v_{2P}(x)\right|\right)\right)dx$$

where $d(x)$ is the hull maximum draught at section x.

The viscous moments are obtained by multiplying the previous vertical and horizontal viscous forces by their respective moment arms. The expressions obtained for the viscous moments are given by the following expressions.

After some simplifications because of the catamaran symmetry, the roll moment becomes

$$\hat{F}_4(x) = \frac{1}{2}\rho \int_L d_2(x)d(x)\left(-2U^2 a_l \xi_6 + U a_l\left(v_{2S}(x) + v_{2P}(x)\right) + \right.$$
$$\left. C_D\left(v_{2S}(x)\left|v_{2S}(x)\right| + v_{2P}(x)\left|v_{2P}(x)\right|\right)\right)dx$$
$$+\frac{1}{2}\rho \int_L B_m(x)b(x)\left(U a_l\left(v_{3P}(x) - v_{3S}(x)\right) + \right.$$
$$\left. C_D\left(v_{3P}(x)\left|v_{3P}(x)\right| - v_{3S}(x)\left|v_{3S}(x)\right|\right)\right)dx$$

The pitch moment

$$\hat{F}_5(x) = -\frac{1}{2}\rho \int_L x B_m(x)\left(2U^2 a_l \xi_5 + U a_l\left(v_{3S}(x) + v_{3P}(x)\right) + \right.$$
$$\left. C_D\left(v_{3S}(x)\left|v_{3S}(x)\right| + v_{3P}(x)\left|v_{3P}(x)\right|\right)\right)dx$$

The yaw moment

$$\hat{F}_6(x) = \frac{1}{2}\rho \int_L x\, d(x)\Big(-2U^2 a_l \xi_6 + U a_l \big(v_{2S}(x) + v_{2P}(x)\big) + C_D\big(v_{2S}(x)|v_{2S}(x)| + v_{2P}(x)|v_{2P}(x)|\big)\Big)dx$$

The vertical and horizontal fluid velocities are obtained respectively from the vertical and horizontal differentiation of the incident potential velocity ϕ_I.

$$\dot{\zeta}_v(x,y,z) = \frac{\partial \phi_I}{\partial z}$$

$$\dot{\zeta}_h(x,y,z) = \frac{\partial \phi_I}{\partial y}$$

The cross flow drag terms in the viscous force equations are non-linear, hence they cannot be directly introduced into the linear equations of motions. To linearise the problem Lee (1976) applied the Fourier series to the even function as shown below

$$\cos\theta|\cos\theta| = A_0 + A_1\cos\theta + A_2\cos 2\theta + A_3\cos 3\theta + \ldots$$

where the Fourier coefficients are defined as

$$A_0 = 0$$

$$A_n = 0 \qquad \text{for } n \text{ even}$$

$$A_n = (-1)^{\frac{n+1}{2}} \frac{8}{n(n^2-4)\pi} \qquad \text{for } n \text{ odd}$$

so

$$A_1 = 8/3\pi$$

$$A_3 = 8/15\pi$$

If the body harmonic motion is given by $x = x_0 \cos\omega t$, then an approximation of $\dot{x}|\dot{x}|$ is

$$\dot{x}|\dot{x}| \cong \frac{8}{3\pi}\omega x_0 \dot{x} \tag{3.12}$$

This approximation is often called the equilinearization method, Lee (1976), and it is used frequently for dynamic systems with weakly non-linear behaviour.

This equilinearization method requires the previous knowledge of the motion amplitude x_0 as in the case shown in equation (3.12). The motion solution is an iterative process that uses the previous calculated motion amplitude until a reasonable convergence of the solution is found.

As said before, the equations of the viscous forces and moments (3.8) are separated into viscous damping, restoring and excitation.

$$\hat{F}_j = \sum_{k=1}^{6}\left(\hat{B}_{jk}\dot{\xi}_k + \hat{C}_{jk}\xi_k\right) - F_j^V \qquad ,j=1,2,..6$$

These viscous forces are then added to the equations of motion, as shown in the next section. The full developed viscous coefficients and viscous forces are given in Appendix I.

3.4 Equations of Motion

The solution of the equations of motion gives the response of the oscillating rigid body in regular waves. Newton's second law provides the equations, which relates the external forces and the inertial forces.

$$\sum_{k=1}^{6} M_{jk}\ddot{\xi}_k = F_j \quad ,j=1,2,..6 \tag{3.13}$$

where F_j are the external forces and $\ddot{\xi}_k$ are the six degree of freedom body acceleration, M_{jk} are the components of the generalized mass matrix for the jth force induced by the kth mode of motion:

$$M_{jk} = \begin{bmatrix} M & 0 & 0 & 0 & Mz_G & -My_G \\ 0 & M & 0 & -Mz_G & 0 & Mx_G \\ 0 & 0 & M & 0 & -Mx_G & 0 \\ 0 & -Mz_G & 0 & I_{44} & I_{45} & -I_{46} \\ Mz_G & 0 & -Mx_G & I_{54} & I_{55} & I_{56} \\ -My_G & Mx_G & 0 & -I_{64} & I_{65} & I_{66} \end{bmatrix} \tag{3.14}$$

where M is the body mass, the coordinates of the centre of gravity are given by (x_G, y_G, z_G) and I_{jk} are the moments of the inertia of the body,

$$I_{jk} = \iiint_V \rho\left[r_j^2 \delta_{jk} - (1-\delta_{jk}) x_{j-3} \cdot x_{k-3}\right] dV, \quad j,k = 4,5,6$$

where $\delta_{jk} = \begin{cases} 0 & , \quad k = j \\ 1 & , \quad k \neq j \end{cases}$, is the Kronecker delta function, r_j is the distance of the mass element to the corresponding axis of rotation about the origin, and (x_1, x_2, x_3) are the coordinates (x, y, z) in the body reference system.

It can be demonstrated (Abkowitz 1969) that for a body with a longitudinal plane of symmetry and with the origin of the coordinate system in the longitudinal and transversal centre of gravity, $x_G=0$, $y_G=0$ then $I_{45}=I_{54}=I_{56}=I_{65}=0$ and the M_{jk} matrix can be simplified and written as

$$M_{jk} = \begin{bmatrix} M & 0 & 0 & 0 & Mz_G & 0 \\ 0 & M & 0 & -Mz_G & 0 & 0 \\ 0 & 0 & M & 0 & 0 & 0 \\ 0 & -Mz_G & 0 & I_{44} & 0 & -I_{46} \\ Mz_G & 0 & 0 & 0 & I_{55} & 0 \\ 0 & 0 & 0 & -I_{46} & 0 & I_{66} \end{bmatrix}$$

The full equations of the six rigid body motion are obtained substituting in Newton's equation all the hydrodynamics forces developed in the previous sections.

$$\sum_{k=1}^{6} \left\{ (M_{jk} + A_{jk})\ddot{\xi}_k + (B_{jk} + \hat{B}_{jk})\dot{\xi}_k + (C_{jk} + \hat{C}_{jk})\xi_k \right\} = \\ = \left\{ F_j^I + F_j^D + F_j^V \right\} e^{-i\omega t} \qquad ,j=1,2,\ldots 6 \qquad (3.15)$$

For a regular harmonic wave excitation of frequency ω, the equation of motion is written as

$$\sum_{k=1}^{6} \left\{ -\omega^2 (M_{jk} + A_{jk}) - i\omega (B_{jk} + \hat{B}_{jk}) + (C_{jk} + \hat{C}_{jk}) \right\} \xi_k = F_j^I + F_j^D + F_j^V \quad ,j=1,2,\ldots 6$$

where A_{jk} are the components of the added mass coefficients, B_{jk} are the damping coefficients, C_{jk} are the restoring coefficients and ξ is the body displacement. F_j^V is the exciting viscous force and $\hat{B}_{jk}$ and $\hat{C}_{jk}$ are the viscous damping and restoring

coefficients respectively. The indexes j and k indicate the fluid force direction and the mode of motion respectively.

The longitudinal symmetry of the hull leads to decoupling the vertical modes of motion from the horizontal plane modes. The six equations of motion are reduced to two sets of equations, one of three coupled equations for surge, heave and pitch, and the other for sway, roll and yaw. If one assumes that the ship has a long slender hull form in addition to lateral symmetry, then it can be shown (Salvesen et al. 1970) that the hydrodynamic forces associated with the surge motion are much smaller than the forces associated with the other modes of motion. Hence the three surge-heave-pitch equations reduce to two coupled equations heave-pitch.

3.5 Numerical Implementation

The numerical implementation of the present method used as starting point the strip theory code that was the building block of the non-linear theory of Fonseca (1994) and Fonseca and Guedes Soares (1994). This code is based on the theory of Salvesen et al. (1970) and calculates the hydrodynamic coefficients using the Frank close-fit method (Frank 1967).

To evaluate numerically the hydrodynamic forces from the potential flow theory some simplifications are assumed. It is necessary to remove the main three dimensional characteristics of the fluid flow in such a way that the general three dimensional boundary value problem presented in chapter 2 is reduced to a set of two dimensional boundary value problems.

The ship is represented by a finite number of cylinders with the shape of the cross sections along the body length (21 sections are used in this work). Each section is represented by a finite number of straigth line segments (14 segments are used, see appendix II). The hydrodynamic forces for each cylinder are calculated independently and integrated along the ship length to obtain the forces acting on the ship. If the ship is slender (beam and draught much smaller than the length), the forward speed relatively small, and the frequency of the oscillation relatively high, then it is assumed that the flow at any ship cross section does not affect the flow at the adjacent sections, thus the flow is considered two-dimensional. For low frequency oscillations (long waves) the flow tend to be three-dimensional due to convective effects associated to

the ship forward speed. The hypothesis of high frequency of the oscillation is necessary to reduce the tree-dimensional free surface boundary condition to a two-dimensional one. However, practice has proven that strip theory works fine also at the low frequency range, and the reason is that in this case the hydrostatic forces become predominant, thus a poor prediction of the radiation and diffraction forces will not affect significantly the final result (Salvesen et al. 1970).

Using the former assumptions, the expressions derived for the hydrodynamic forces are simplified to a form suitable to numerical calculations as shown in Appendix II.

The original code was applicable to mono-hulls and did not account for viscous effects. The contribution of this thesis is to adopt the above approach to catamarans and to take into account the viscous effects. The viscous effects were introduced through a cross flow approach, as explained in section 3.3.

The DATAD subroutine was changed in order to receive the information for a full demi-hull section away from the ship centre line. The flowchart of the initial program and the added routines are shown below. The new routines added to the existing program are shown in the flow chart as shadow boxes while the original routines are in normal boxes.

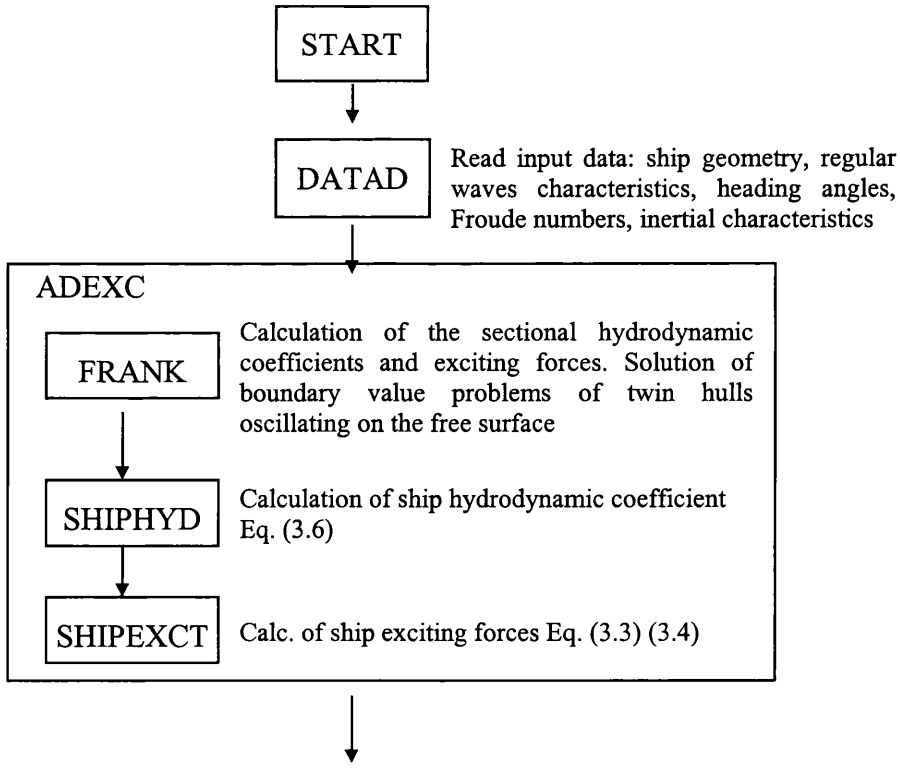

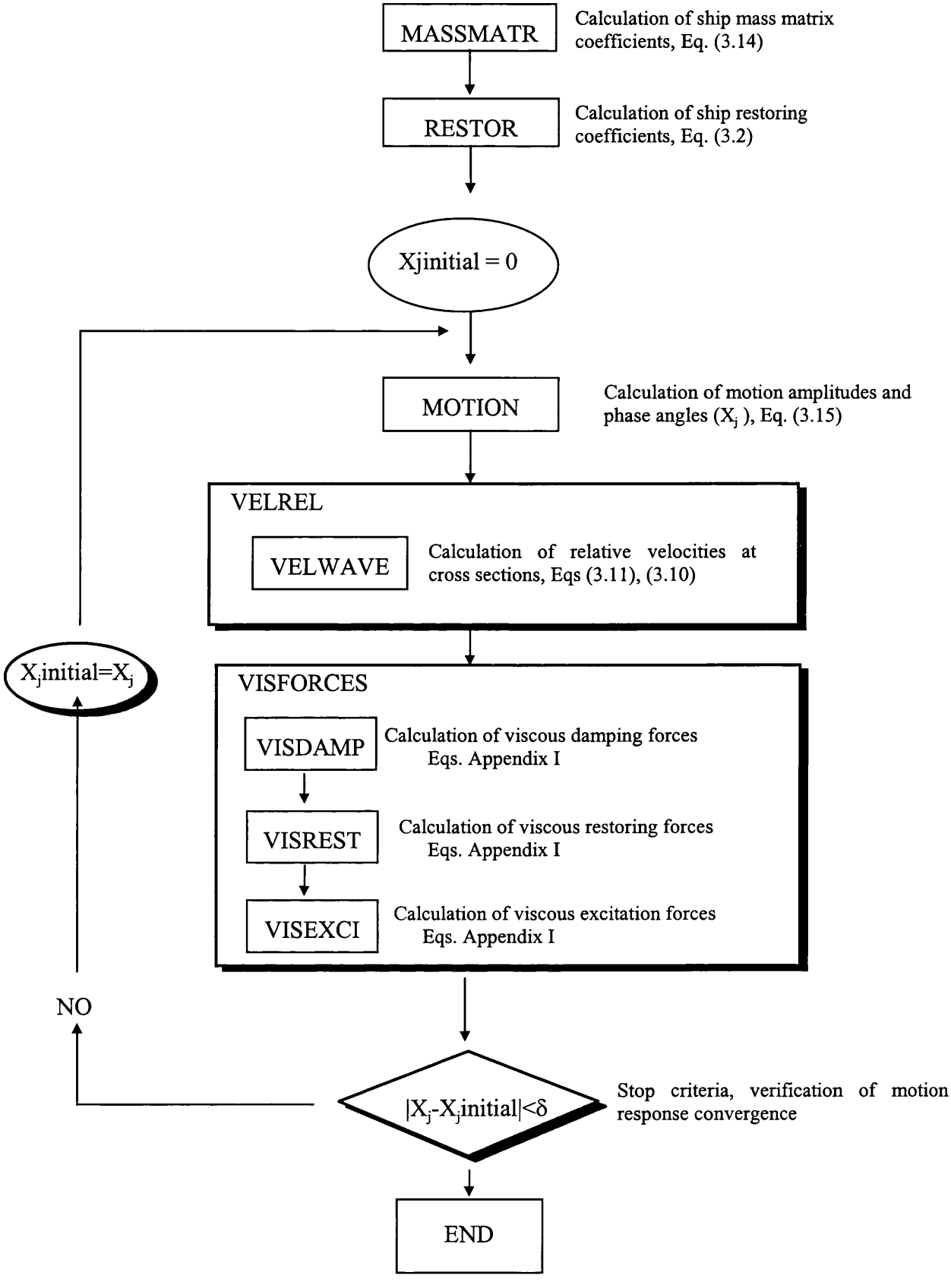

Figure 3.2 – Program flowchart

3.6 *Comparisons with Existing Results*

The results from the implemented strip theory are compared with other strip theories and with some published experimental results in order to validate the numerical implementation. Calculations were performed with twin-cylinders and also with two catamarans already analysed and published by other authors (Ohkusu 1971 and van't Veer 1995).

3.6.1 Twin Cylinders Added Mass and Damping Coefficients

Twin-cylinders are an easy and good way to validate theoretical results because they have been widely studied by many authors (Frank 1967, Wang and Wahab 1971, Ohkusu 1970, Varyani 1988).

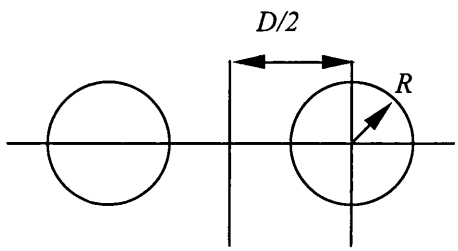

Figure 3.3 – Twin-cylinder configuration

Number of panels = 98

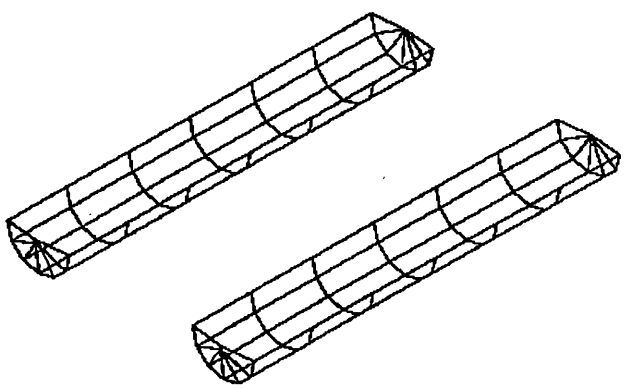

Figure 3.4 – Three-dimensional discretization.

The twin-cylinder configuration is shown in Figure 3.3, where D is the distance between the two cylinders and R is the cylinder radius. In Figure 3.4 the model with 98 panels used in the three-dimensional calculations is presented. In this three-dimensional theory the velocity potential is obtained by means of a three-dimensional distribution of unknown strength sources in each panel.

The heave added mass is calculated for two different twin-cylinder configurations where the D/R ratio takes the following values: $D/2=1.5\ R$ and $D/2=3\ R$.

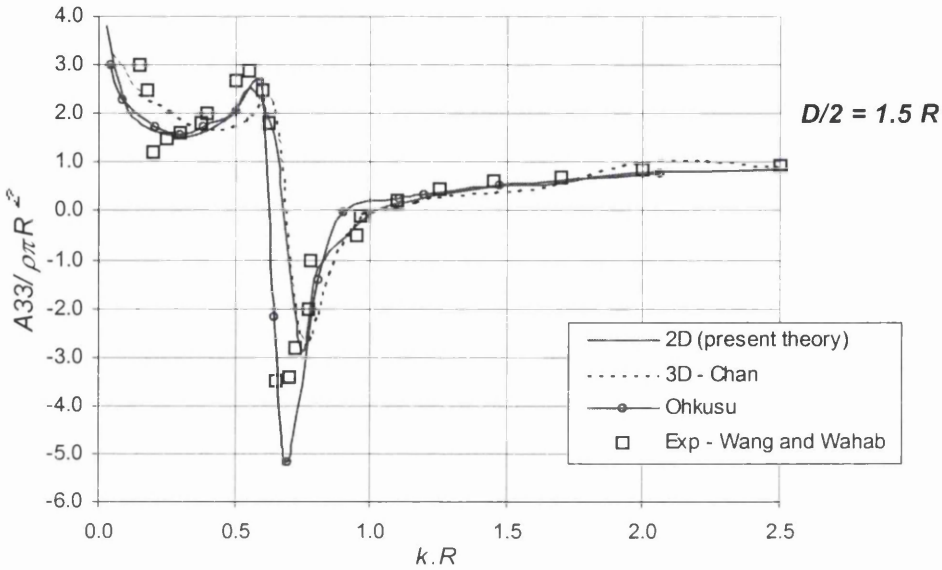

Figure 3.5 – Twin-cylinder heave added mass, $D/2=1.5\ R$ at $Fn=0.0$

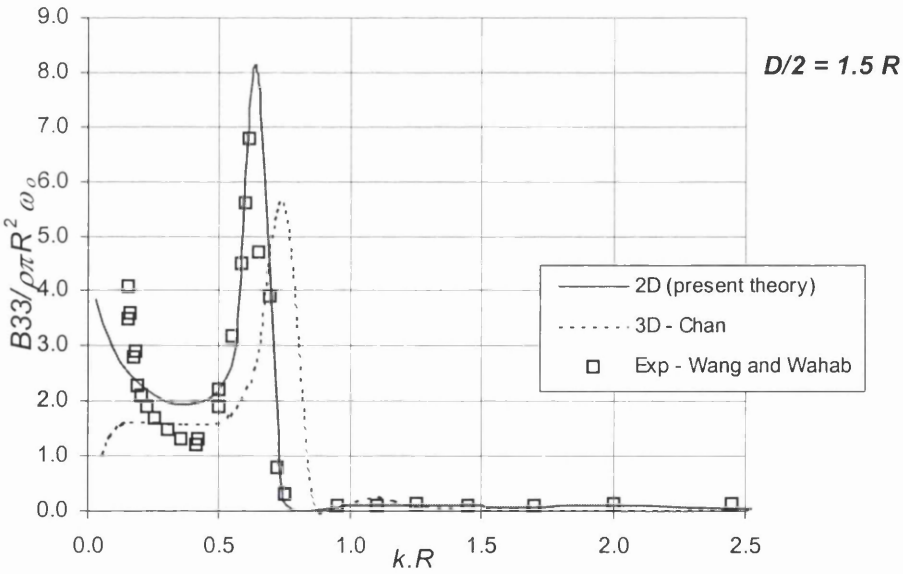

Figure 3.6 – Twin-cylinder damping coefficient, $D/2=1.5\ R$ at $Fn=0.0$

The added mass and damping coefficient for the configuration $D/2 = 1.5\,R$ are presented in Figure 3.5 and Figure 3.6 respectively. In Figure 3.5 and Figure 3.6 the experimental results presented by Wang and Wahab (1971) are compared with theoretical results calculated by the present strip theory method, by the three-dimensional method (Chan 1990) and by the theoretical work performed by Ohkusu (1970).

The theoretical and experimental results shown in Figure 3.5 agree very well. The two-dimensional damping coefficients also agree well with the Wang experimental results but it looks like the three-dimensional results have a small shift to the right when compared with the experimental results.

The same calculations are performed for a wider twin-cylinder configuration where $D/2 = 3R$ and the results are presented in Figure 3.7 and Figure 3.8. In this case the three-dimensional results do not agree at low frequencies, but on the other hand the three-dimensional results agree better than the two-dimensional and Ohkusu results at high frequencies near the second trough in the added mass figure.

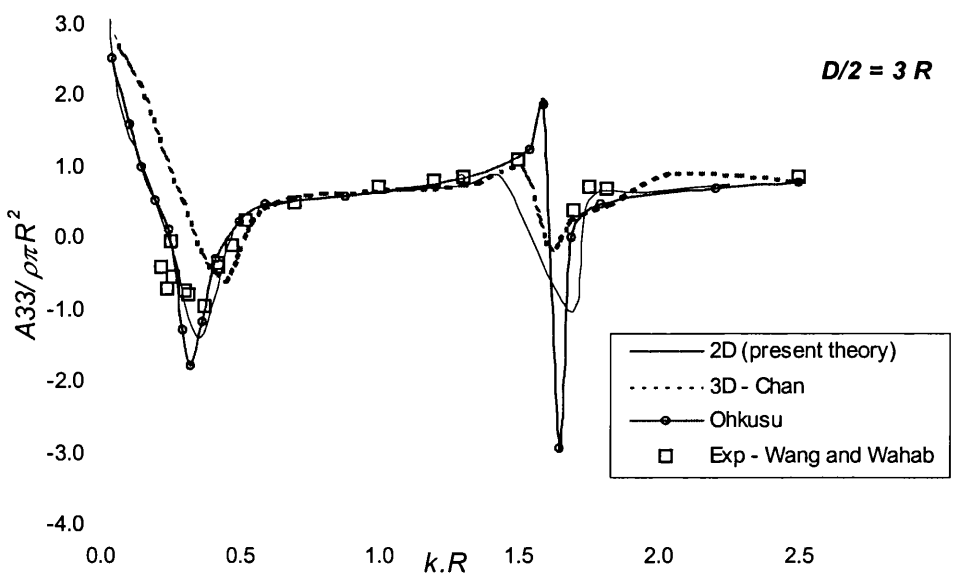

Figure 3.7– Twin-cylinder heave added mass, $D/2 = 3\,R$ at $Fn=0.0$

The second trough in the added mass curve (Figure 3.7) only occurs in the wider configuration because it is due to the standing wave generated between the two cylinders. This wave is a function of the distance between the cylinders and the wider the distance the smaller the frequency at which this phenomenon occurs. This wave

frequency is called symmetric resonance frequency and it will be analysed in more detail in section 5.2.2.

In Figure 3.8 the two-dimensional results give again better predictionns than the three-dimensional results. At very low frequencies the 2D and 3D theoretical methods exhibit distinct behaviours, i.e., while 2D results are increasing the 3D results are decreasing. Also in Figure 3.8 at that symmetric resonance frequency (near $K.R \approx 1.6$) the damping coefficient shows a small hump. This hump increases in relative magnitude with the increase of the distance between the cylinders as in Wang and Wahab (1971).

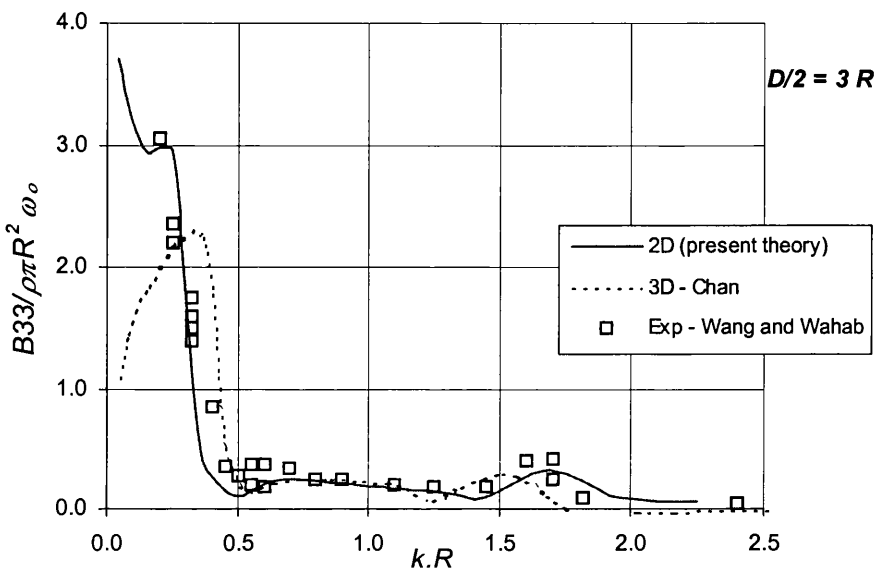

Figure 3.8 – Twin-cylinder damping coefficient, $D/2 = 3\ R$ at $Fn=0.0$

3.6.2 Wigley Results

Figure 3.10 and Figure 3.11 compare the theoretical results obtained with a Wigley catamaran with the results obtained by van't Veer (1995). The Wigley hull is a mathematical hull that is described by the following formula:

$$y = \left(1-\zeta^2\right)\left(1-\xi^2\right)\left(1+\frac{1}{5}\xi^2\right)+\zeta^2\left(1-\zeta^8\right)\left(1-\xi^2\right)^4$$

where ξ represents the x-coordinate with $\xi \in [-1,1]$ and where ζ represents the z-coordinate with $\zeta \in [-1,0]$.

The main characteristics of this Wigley catamaran are given in Table 3.1, where in this particularly case B is the demi-hull breadth, T is the draught and H is the inner space between the hulls. The body plan of the Wigley catamaran is given in Figure 3.9.

Main Characteristics	*Wigley Cat*
Length	2.5 m
Breadth *B*	1.1 m
Draught *T*	0.139 m
Displacement	0.138 m^3
H/B	2.1

Table 3.1 - Wigley Model

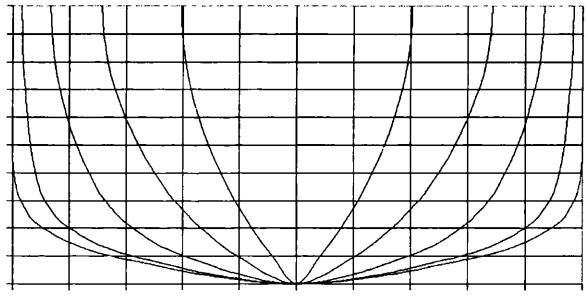

Figure 3.9 - Wigley body plan

In Figure 3.10 and Figure 3.11 two different results calculated with the present theory are shown: for with and without viscous effects. As is seen from the figures there is a considerable decrease in the amplitude response at the resonance peak when the viscous effects are included. As should be expected, van't Veer results, which do not include any of the viscous effects, are similar to the results obtained by the present theory without the viscous effects. The lift and the cross flow drag coefficients used in the present calculations are a_l =0.07 and C_D = 0.01 respectively. These values were obtained from literature as mention in section 4.5.1.

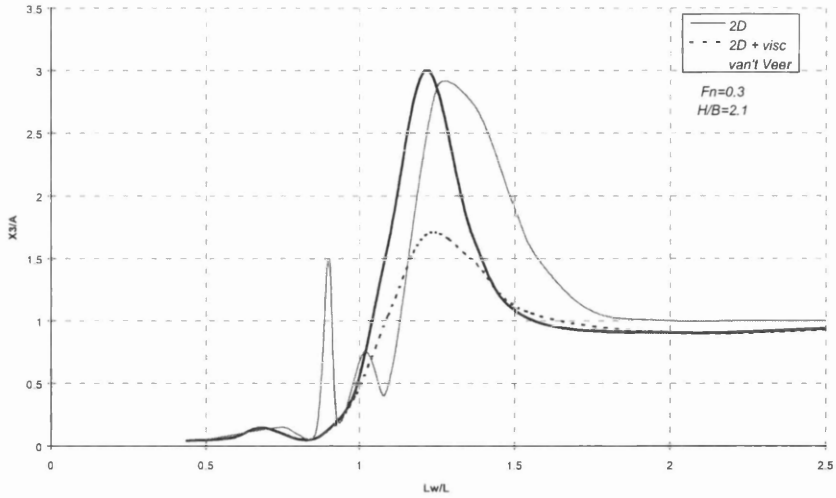

Figure 3.10 – Heave motion at *Fn=0.3* and head waves, *Wigley* model.

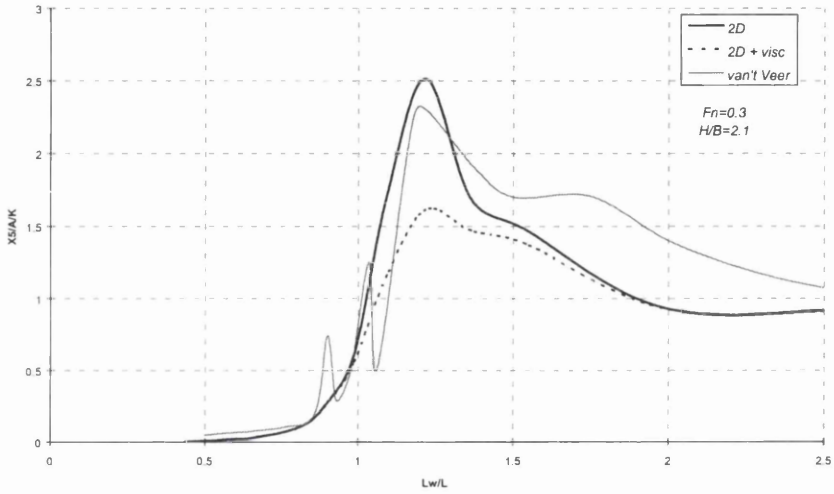

Figure 3.11 – Pitch motion at *Fn=0.3* and head waves, *Wigley* model.

3.6.3 Ohkusu Results

Figure 3.13 to Figure 3.16 show theoretical and experimental results of the *TW1* and *TW2* catamaran models studied by Ohkusu (1971). The *TW1* model is characterised by *2P/T=3* where *2P* is the distance between the centre lines of the two hulls and *T* is the draught. The *TW2* model is characterised by *2P/T=5*. The main characteristics of these two models and the hull form are given in Table 3.2 and Figure 3.12 respectively.

Main Characteristics	*TW1*	*TW2*
Length between perpendiculars	4.0 m	4.0 m
Breadth *B*	0.9 m	1.26 m
Draught *T*	0.18 m	0.18 m
Displacement	.414 m^3	.414 m^3
2*P/T*	3.0	5.0

Table 3.2 - Ohkusu Models

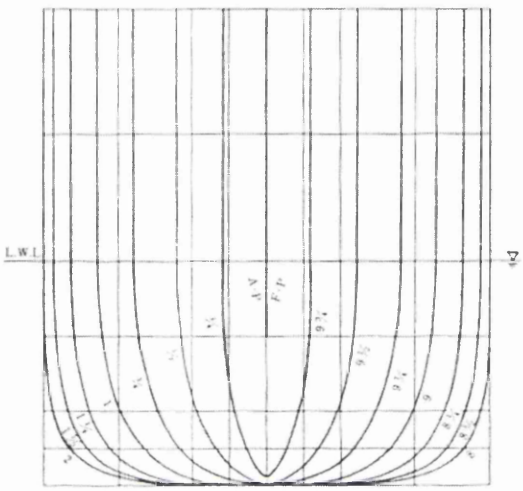

Figure 3.12 – Ohkusu's model body plan

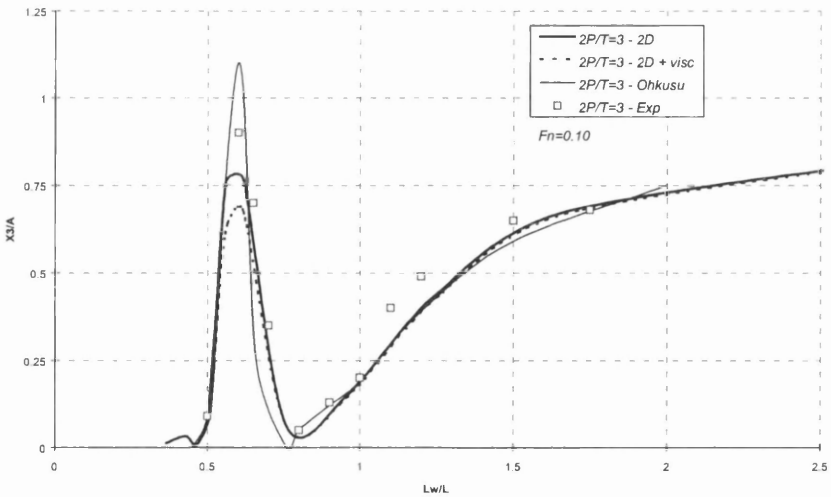

Figure 3.13 – Heave motion at *Fn=0.1* and head waves, *TW1* Ohkusu model.

As in the Wigley results, there is a decrease in the amplitude of the motion response when the present theory includes the viscous forces. In this case, since the forward speed is not as high as in the Wigley case, the viscous effects are smaller, and this is reflected in the amplitude at the peak frequency.

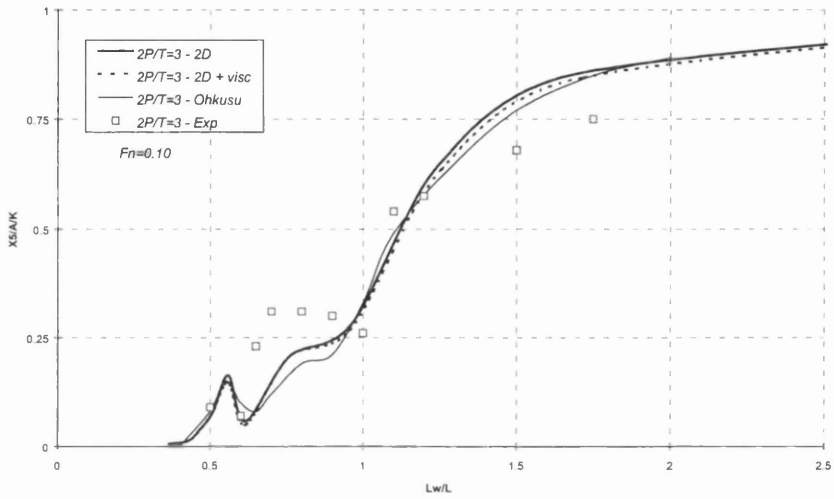

Figure 3.14 – Pitch motion at *Fn=0.1* and head waves, *TW1* Ohkusu model.

As regards the pitch response (Figure 3.14) both theoretical results agree very well. Both heave theoretical results presented in Figure 3.13 agree well except at the high frequency peak where the theoretical amplitude responses are slightly different. Nevertheless, at that high frequency peak the amplitude of the experimental results obtained by Ohkusu is almost in the middle of the two theoretical peaks.

Analysing the results of the *TW2* catamaran, which is wider than *TW1*, it can be seen that both heave and pitch results (Figure 3.15 and Figure 3.16) also agree well. In this case, as in the *TW1* case some differences are also observed in the heave amplitude response between theoretical and experimental results at the resonance peak frequency.

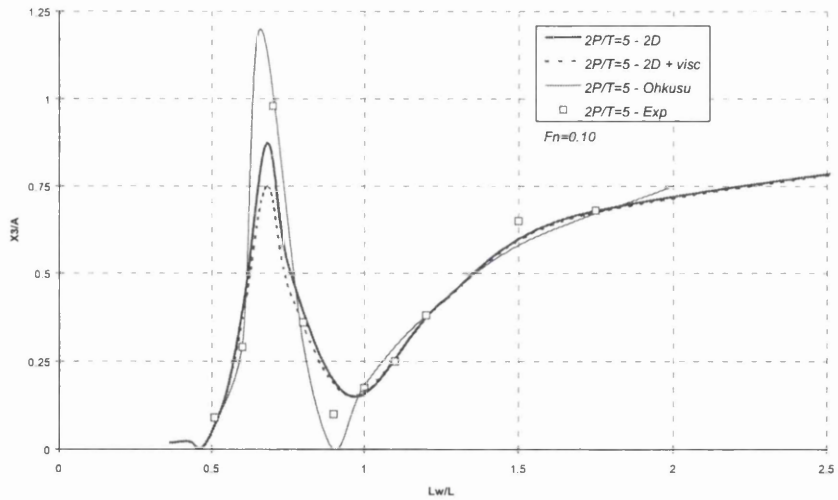

Figure 3.15 – Heave motion at *Fn=0.1* and head waves, *TW2* Ohkusu model.

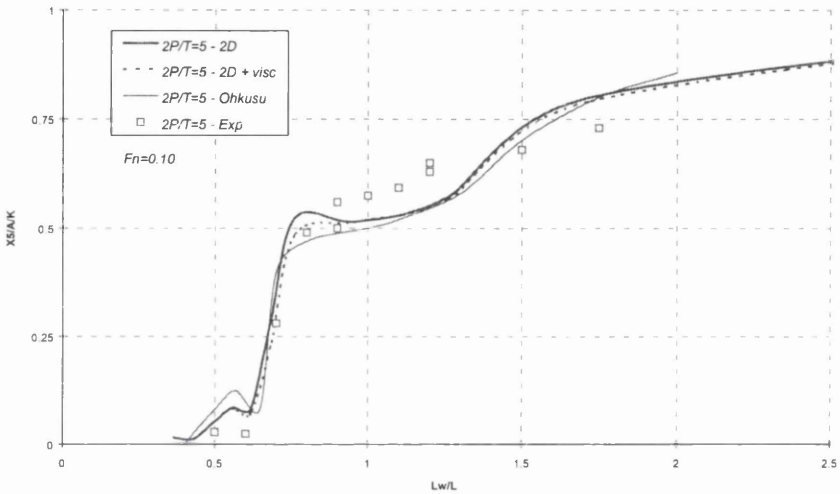

Figure 3.16 – Pitch motion at *Fn=0.1* and head waves, *TW2* Ohkusu model.

3.7 Concluding Remarks

In this chapter the mathematical formulation and the forces that act in the motions of catamarans in waves are presented. All forces including the viscous ones, which are important in the catamaran dynamics, are developed. A flowchart of the numerical algorithm used to solve this problem and some assumptions concerning the numerical implementation is presented.

The present theory is validated with available published results on twin-cylinders and catamarans. In the case of twin-cylinder the study is performed at zero forward speed and in the case of catamaran, finite forward speed is taken into account. The

theoretical cylinder study beside the two-dimensional results from the present theory also included theoretical results from a three-dimensional theory Chan (1990). The theoretical results obtained agree well with published experiments. The twin-cylinder calculations show some interesting features at certain resonance frequencies due to two-dimensional interaction between the hulls. These features will be analysed in more detail in section 5.2.

The theoretical results obtained from the analysed catamarans also show good agreement with the published works. The results show that the viscous effects are more important at the resonance peak and that their effects increase as speed increases.

However, since available published results are not extensive, an experimental program was conducted in order to introduce additional results, and is reported in the next chapter.

Chapter 4

Experimental investigation of two catamaran models in regular waves

4.1 Introduction

The comparisons with existing results reported in section 3.7 are encouraging as regards adequacy of the present approach. However, since the published experimental results are very limited, it was decided to conduct an experimental study in order to have more data available to validate the developed method. The experimental work was carried out at the Towing Tank of the Hydrodynamics Laboratory at the University of Glasgow.

The experiments were conducted using the hull form developed by Vosper International, Incecik et al. (1991). This high-speed catamaran was developed to provide a platform for the transport of passengers and vehicles over short sea routes for a basic 43.5m catamaran design. The form of each demi-hull is of the hard-chine type with low deadrise sections in the after body and high deadrise concave sections in the forward body. The experiments were performed using two different hull separations, four different speeds, head waves, one wave height and a range of wave frequencies.

This chapter presents the data analysis performed to choose the main model characteristics, especially the draught and the distance between the catamaran hulls. The other main characteristics, the length and the demi-hull breadth cannot be changed. Also presented in this chapter is the experimental set-up and the tests carried out. The experimental results of calm water resistance, trim and rise of the centre of gravity are presented. The heave and pitch experimental results in regular waves are compared with theoretical predictions. Just as an example some experimental time series results of the wave, heave and pitch amplitudes are shown.

4.2 Model Characteristics

Two catamaran models (*V40* and *V60*) with the same demi-hull form but with different spacing between the two hulls were tested. The *V40* model has 40 cm between the centre lines of each demi-hull (L/B=3.66) and the *V60* model has 60 cm between the two demi-hulls (L/B=2.70). Both models have the same displacement and the same position of the centre of gravity.

From the results of the review of the main dimensions of existing catamarans (Table 4.1), a limited statistical analysis of typical main characteristics and ratios of catamaran ships and models is performed.

Ship or Model	L [m]	B_m [m]	B [m]	D [m]	T [m]	L/B	L/B_m	$D/(Bm/2)$	D/B	B_m/T	B/B_m	D/T
V1	2	0.175	0.6	0.425	0.067	3.33	11.43	4.86	0.71	2.604	3.429	6.3
Lewis	1.5	0.25			0.125		6.00			2.00		
TW1	4	0.36	0.9	0.54	0.18	4.44	11.11	3.00	0.60	2.00	2.50	3
TW2	4	0.36	1.26	0.9	0.18	3.17	11.11	5.00	0.71	2.00	3.50	5
ASR	64	7.32	24.95	17.63	5.49	2.57	8.74	4.82	0.71	1.33	3.41	3.2
HS900	88		30		3.7	2.93						
45M	40		12.7		1.75	3.15						
100M	90	6	36.2	30.2	3.5	2.49	15.00	10.07	0.83	1.71	6.03	
Marintek	3.778	0.267	0.918	0.651	0.24	4.12	14.15	4.88	0.71	1.14	3.44	2.8
Adamant	30.8		7.8		1.1	3.95						
Lindsay	16	2.33	6.7	4.37	0.67	2.39	6.87	3.75	0.65	3.48	2.88	6.5
Discovery	13.1		5.5			2.38						
AIN DAR	36		11.8		1.85	3.05						
TT	44.25	2.68	11.8	9.12	1.35	3.75	16.51	6.81	0.77	1.99	4.40	6.76
V40	2.05	0.158	0.558	0.4	0.085	3.66	12.81	5.00	0.71	1.88	3.50	4.71
V60	2.05	0.158	0.758	0.6	0.085	2.70	12.81	7.50	0.79	1.88	4.75	7.06
					Average	3.2	11.2	5.4	0.7	2.0	3.7	4.8
					Std.Deviation	0.7	3.6	2.2	0.1	0.7	1.1	1.8

Table 4.1 – Catamarans statistical data

The analysis made with the available data has allowed the choice of the draught and hull spacing to be used in the experimental work, in order to be within realistic dimensional values. The data was collected from the available literature and include models and full scale ship information.

In Table 4.1, L is the length at $z=0$, B_m is the demi-hull breadth, B is the breadth over all, D is the distance between hulls center lines and T is the ship draught.

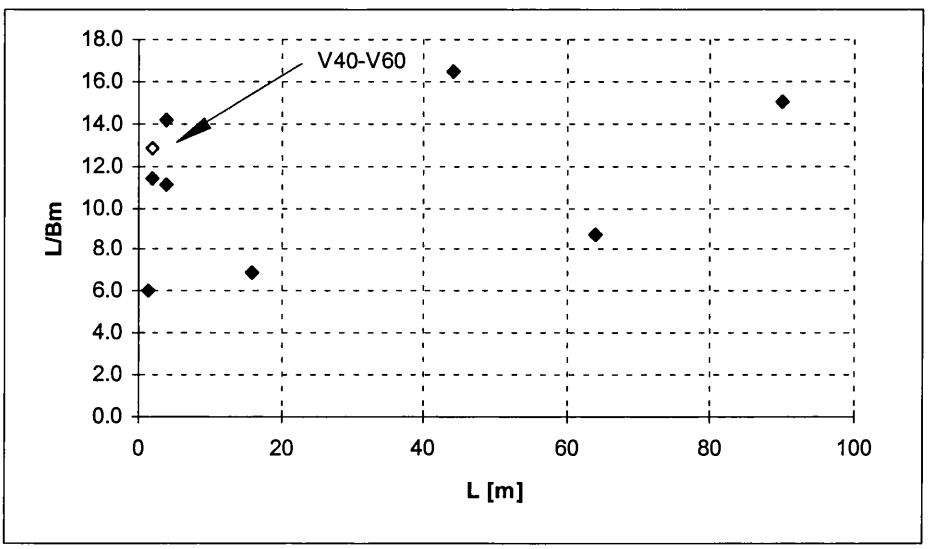

Figure 4.1 – Plot of the relations L vs L/B_m in different hulls

The first figure shows the relation between the demi-hull breadth and the catamaran length. These two main characteristics are unaltered because the hull is a designed Vosper International hull. Since the two models have the same demi-hulls, the L/B_m ratio is the same for both models.

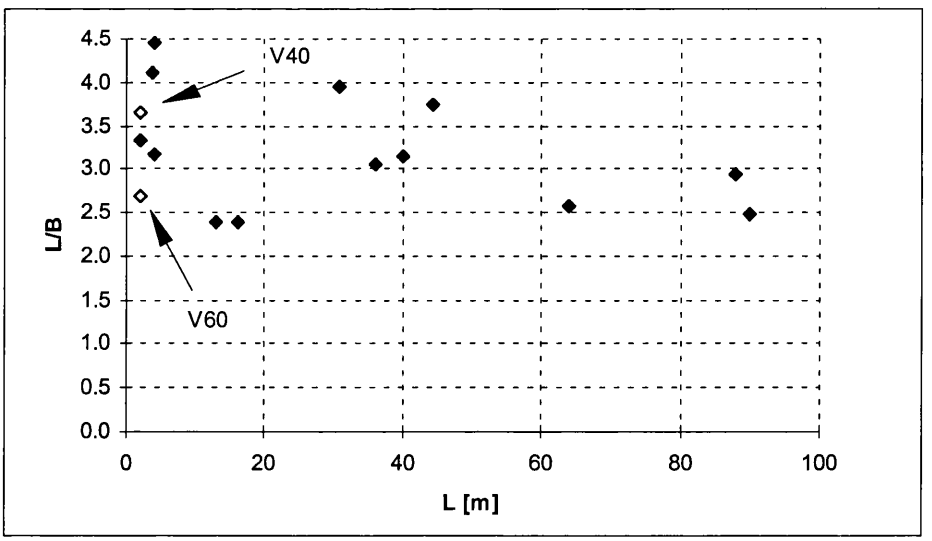

Figure 4.2 – Plot of the relation L vs L/B in different hulls

Figure 4.2 shows the relation between the catamaran length and breadth overall. The breadth overall is related to the distance between hulls and this is varied. The *V60* model breadth was chosen near the lowest *L/B* ratio while the *V40* model breadth was chosen near the largest *L/B* ratio.

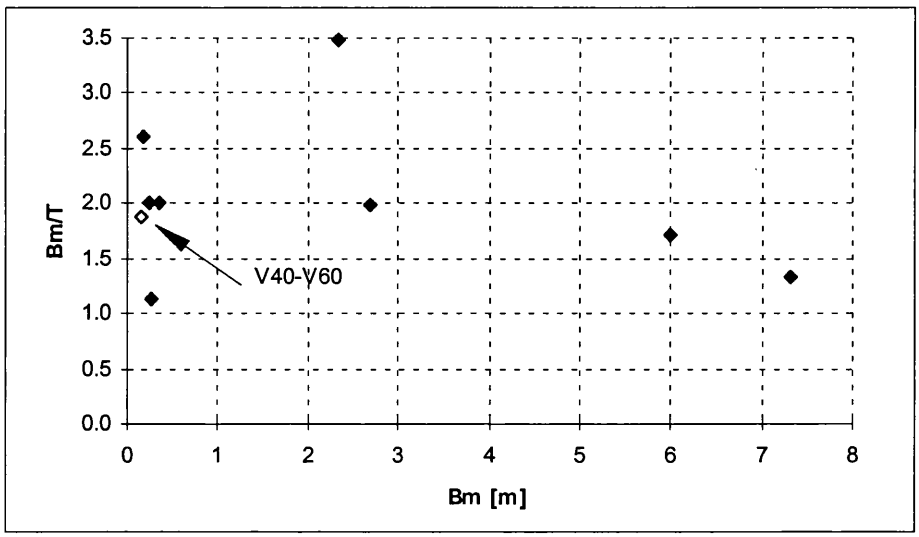

Figure 4.3 – Plot of the relation B_m vs B_m/T in different hulls

The same draught was set for both models. The choise was made considering a value near the statistical average of the B_m/T ratio, Figure 4.3.

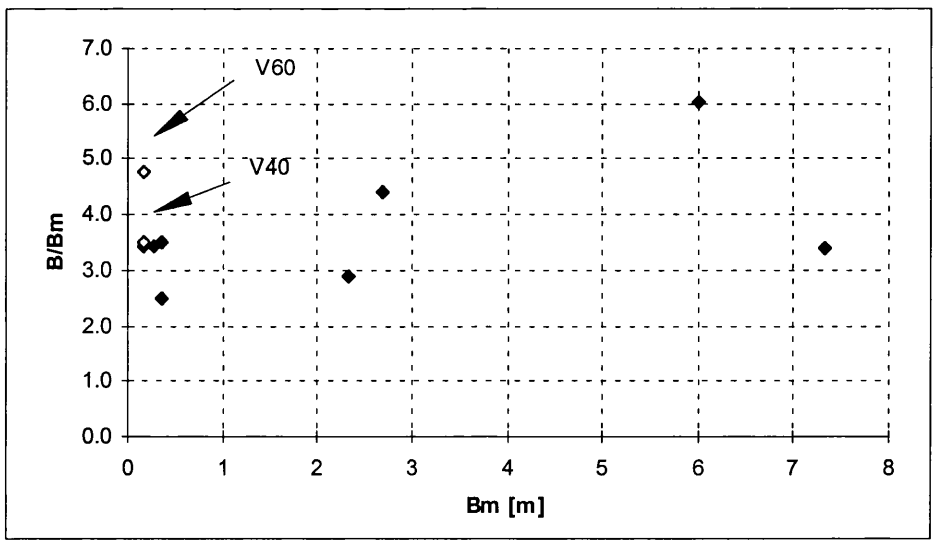

Figure 4.4 – Plot of the relation B_m vs B/B_m in different hulls

The last figure shows that the chosen breadths for both models are within typical B/B_m ratios according to available data.

The main characteristics of the two models are shown in the next table

Main Characteristics	***V40***	***V60***
Length at waterline	2.050 m	2.050 m
Beam at waterline midship	0.558 m	0.758 m
Draught	0.085 m	0.085 m
Breadth of demi-hull	0.158 m	0.158 m
Distance between centre of hulls	0.400 m	0.600 m
Displacement	0.0385 m^3	0.0385 m^3
LCG aft midship	0.207 m	0.207 m
VCG from waterline	-0.030 m	-0.030 m
Block Coefficient	0.695	0.695
Trim	0 degree	0 degree

Table 4.2 – *V40* and *V60* Main characteristics

The hull form shown in Figure 4.5 is of the hard-chine type, low deadrise sections in the after body with a cut-off transom stern and high deadrise concave sections in the forward body.

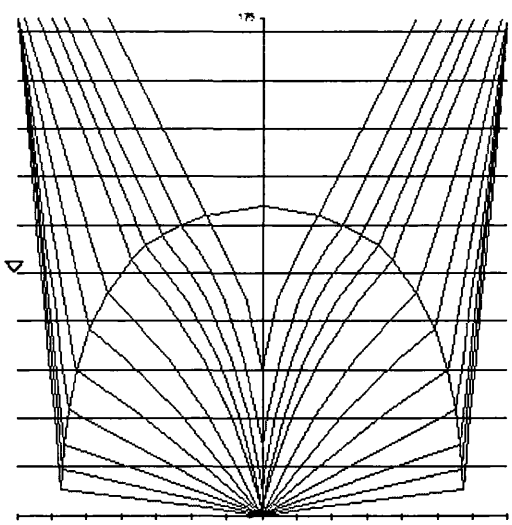

Figure 4.5 – Vosper Body Plan

The model was made of glass-reinforced plastic (GRP) in a 1:20 scale. The scale is dependent of the dimensions of the towing tank. A pair of aluminium bars was used to provide a rigid coupling between the hulls. Studs of 3 mm diameter and 3 mm height at a spacing of 25 mm were fit near the bow in order to make turbulence simulation. No other underwater appendages were attached to the models.

4.3 The Instrumentation Set-up and the Towing Tank

The instrumentation set-up installed for these experiments is similar to a previous system, designed, tested and used before in this Laboratory. The heave and pitch motion were measured as well as the accelerations at the bow and stern, the total resistance and the wave height at different points.

The models were towed by a vertical post that allowed freedom in pitch and heave motion but restrained the roll and yaw motions. The towing point was positioned at the centre of gravity and a hinge pin allowed the free pitch. The yaw motion was restrained by two vertical rods mounted in the stern and the bow of the models and passing between two pairs of horizontal rollers mounted longitudinally on the carriage. The set-up of the equipment used is represented in Figure 4.6.

The devices used to make all measurements are described in the next sub-sections. All devices were properly calibrated before they were used.

4.3.1 The Towing Tank

The Towing Tank of the Hydrodynamics Laboratory at the University of Glasgow is 77 m long, 4.6 m wide and 2.7 m deep. The tank is equipped with a wave maker fitted across the width at one top end of the tank and at the other top end the tank has a beach to absorb the generated waves. The generated wave frequencies range from 0.4 to 1.4 Hz. The electronically controlled towing carriage enables any towed model to run with a maximum speed of 6.4 m/s

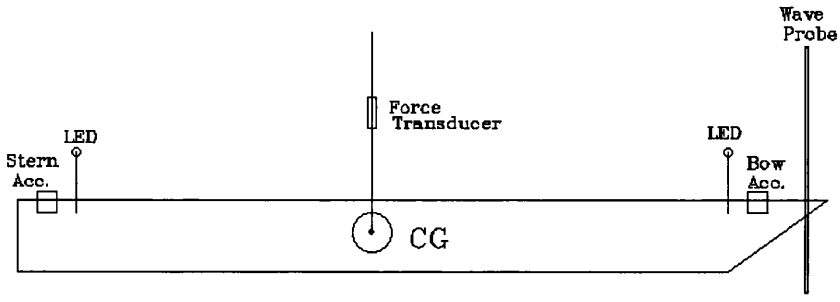

Figure 4.6 - Instrumentation set-up

4.3.2 Wave Probes

To measure the wave height, four resistance type wave probes were used in these experiments.

The resistance type wave probe induces electrical signals whose strength varies with the varying wave height. The electrical signal is then amplified and recorded in a chart recorder. The calibration process was carried out by lifting the wave probes by 5 cm and recording the corresponding analogue signal in the chart recorder.

One wave probe was located on the carriage and parallel to the bow line. This wave probe was used to measure the phase difference between the wave and the model motion response. The three other wave probes were placed across the tank width and approximately at 5 m from the wave maker. These wave probes were placed there to accurately measure the incident wave amplitude because the carriage wave probe suffers a significant deformation at high forward speeds and the results may be affected (Fang 1996).

The incident wave amplitude was calculated through the average value of the three wave probe measurements. Every run was analysed even when the wave maker input was repeated. At the end of this chapter in the error analysis sub section 4.6, a small analysis of the wave amplitude results is performed.

4.3.3 Selspot System

The heave and pitch motions of the models were measured using a Selspot system with two light-emitting diodes (LED) positioned on the deck, one at the bow and the other at the stern. The Selspot system is designed to measure the coordinates of multiple points. A versatile optoelectronic camera detects the position of small light-emitting diodes (LED) for registration and analysis of static as well as dynamic processes in real time as described by the Selspot System (1997). The device is a specially developed photodetector with four electrodes, and when the infrared light from a LED is focused on the detector surface, a phtotocurrent will occur. The current can be used to obtain two signals linearly related to the vertical and horizontal coordinates of the LED without any contact with the model.

4.3.4 Force Gauge Transducer and Accelerometer

To measure the total resistance, a designed force gauge transducer was installed at the middle of the towing post frame.

Two gravity type accelerometers were used to measure the vertical bow and stern accelerations.

4.3.5 Data Acquisition and Data Analysis

The electronic signals from the instrumentation were collected through an amplifier data collecting system and an analogue to digital converter. The digital signals were recorded by a Macintosh-IIci computer in real time and displayed graphically to ensure that the acquisition and measuring system was working properly during the tests. The data collected during each test was automatically converted into the corresponding unit of any measured mode.

On the carriage seven acquisition channels were set to record the wave height, the resistance, the bow and stern motions, the bow and stern accelerations and the model speed. Outside the carriage a chart recorder was used to record the incident wave height from the three wave probes set in front of the wave maker.

The data was collected at a rate of fifty samples per second on every channel and the length of each run was approximately between 6 and 15 seconds depending on the running forward speed.

The data from the bow and stern motions had to be processed in order to find the heave and pitch motion. These motions were calculated using the following expressions:

$$heave = \frac{z_{bow} + z_{stern}}{2}$$

$$pitch = \tan^{-1} \frac{z_{stern} - z_{bow}}{l}$$

where l is the longitudinal distance between the bow and stern measurement points.

The model speed and the total resistance were calculated by determining the corresponding mean series values. The phase angle between the motion and the incident wave measured with the wave probe installed in the carriage had to be calculated. The shift between the wave probe position and the model centre of gravity had to be considered. The phase angle is positive when the ship motion reaches his positive peak before the peak of the incoming wave crosses the origin of the coordinate system.

4.4 Performed Experiments

The experimental work was performed using two models (model *V40* and *V60*). The experiments were performed at four different speeds corresponding to the following Froude numbers (*Fn=0, Fn=0.25, Fn=0.625, Fn=0.75)*. At the real ship scale (43.5 m long) these Froude numbers correspond to 0, 10, 25 and 30 knots. Head waves were tested with approximately 1 cm of amplitude and a wave frequency range from *0.3 Hz* up to *1.4 Hz*. These wave frequencies correspond to wave lengths approximately between half of the model length and four times the model length.

Fn	0.0	0.25	0.625	0.75
Model speed [m/s]	0.0	1.12	2.80	3.36
Ship speed [knots]	0.0	10	25	30

Table 4.3 - Test speeds

After the set of tests were finished, some tests were repeated in order to have more data to perform an error analysis.

Calm water tests were performed at the three forward speeds. The total resistance, trim and the rise of the centre of gravity were measured and analysed. Some video recordings were also made, particularly for the runs near the expected resonance frequencies, where the ship motions are higher.

As explained in section 5.2, after a certain speed and frequency, theoretically the hull interference is expected to be small. Table 4.4 shows for both models the speed and frequency where theoretically the interference between the hulls starts to be small.

V40			***V60***		
U [m/s]	*Fn*	ω_e [rad/s]	*U* [m/s]	*Fn*	ω_e [rad/s]
0.0	0.0	-	0.0	0.0	-
1.12	0.25	73.9	1.12	0.25	41.0
2.80	0.625	29.6	2.80	0.625	16.4
3.36	0.75	24.6	3.36	0.75	13.7

Table 4.4 - Theoretical hull interference

Table 4.5 and Table 4.6 show the planned experiments and in bold and underlined are the expected conditions (model-speed-frequency) where the interference between the hulls are expected to be small.

	Model V40		*Fn*	0.00	0.25	0.625	0.75
fo [Hz]	wo [rad/s]	Lw/L	wo.sqrt(L/g)	ω_e [rad/s]	ω_e [rad/s]	ω_e [rad/s]	ω_e [rad/s]
0.4	2.51	4.76	1.15	2.51	3.24	4.32	4.68
0.5	3.14	3.05	1.44	3.14	4.27	5.96	6.53
0.6	3.77	2.12	1.72	3.77	5.39	7.83	8.64
0.7	4.40	1.55	2.01	4.40	6.61	9.93	11.03
0.8	5.03	1.19	2.30	5.03	7.91	12.25	13.69
0.9	5.65	0.94	2.59	5.65	9.31	14.79	16.62
1	6.28	0.76	2.87	6.28	10.79	17.56	19.82
1.1	6.91	0.63	3.16	6.91	12.37	20.56	23.29
1.2	7.54	0.53	3.45	7.54	14.04	23.78	***27.03***
1.3	8.17	0.45	3.73	8.17	15.79	27.23	***31.04***
1.4	8.80	0.39	4.02	8.80	17.64	***30.90***	***35.33***

Table 4.5 – Set of tests of the *V40* model

	Model V60		*Fn*	0.00	0.25	0.625	0.75
fo [Hz]	wo [rad/s]	Lw/L	wo.sqrt(L/g)	ω_e [rad/s]	ω_e [rad/s]	ω_e [rad/s]	ω_e [rad/s]
0.4	2.51	4.76	1.15	2.51	3.24	4.32	4.68
0.5	3.14	3.05	1.44	3.14	4.27	5.96	6.53
0.6	3.77	2.12	1.72	3.77	5.39	7.83	8.64
0.7	4.40	1.55	2.01	4.40	6.61	9.93	11.03
0.8	5.03	1.19	2.30	5.03	7.91	12.25	***13.69***
0.9	5.65	0.94	2.59	5.65	9.31	14.79	***16.62***
1	6.28	0.76	2.87	6.28	10.79	***17.56***	***19.82***
1.1	6.91	0.63	3.16	6.91	12.37	***20.56***	***23.29***
1.2	7.54	0.53	3.45	7.54	14.04	***23.78***	***27.03***
1.3	8.17	0.45	3.73	8.17	15.79	***27.23***	***31.04***
1.4	8.80	0.39	4.02	8.80	17.64	***30.90***	***35.33***

Table 4.6 – Set of tests of the *V60* model

4.5 Experimental Results

This section presents the experimental results. First the calm water tests for resistance, trim and rise of the centre of gravity are presented. The heave and pitch results are then compared with theoretical results. To conclude some time series results for heave, pitch and wave amplitude are shown.

As can be seen in Figure 4.7 the calm water resistance of the *V40* and *V60* models are very similar.

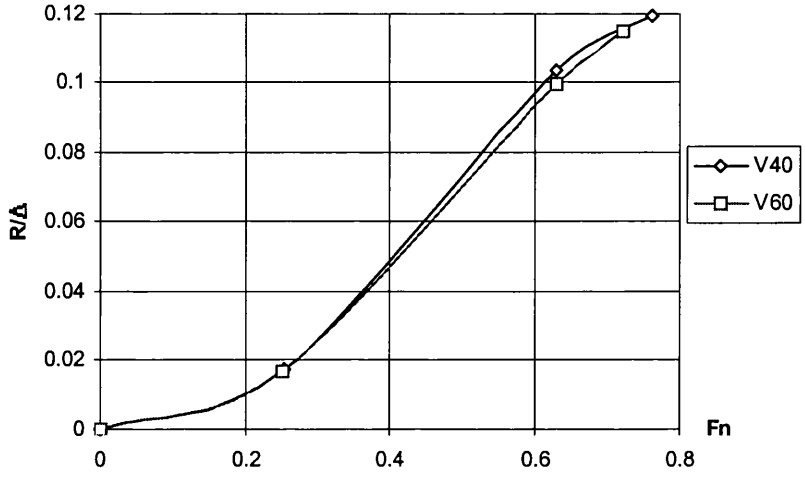

Figure 4.7 - Model Resistance

The main difference is around $Fn = 0.625$ where the *V40* model resistance is 4.4% higher than the *V60* resistance. The difference is not unexpected since the rise of the centre of gravity (Figure 4.8) is bigger in the *V60* model.

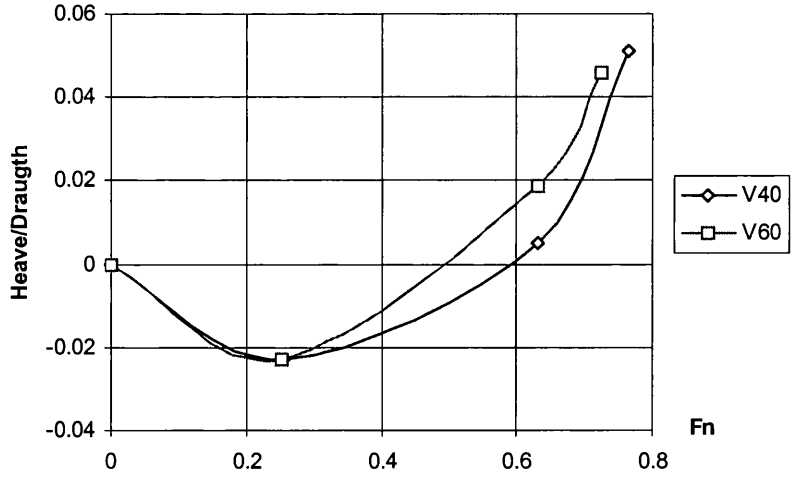

Figure 4.8 - Rise of the centre of gravity

The non-dimensional resistance is obtained using the model displacement in Kg and the rise of the centre of gravity using the still water draught.

Figure 4.9 shows the trim angle versus non-dimensional Froude number for both models in calm water.

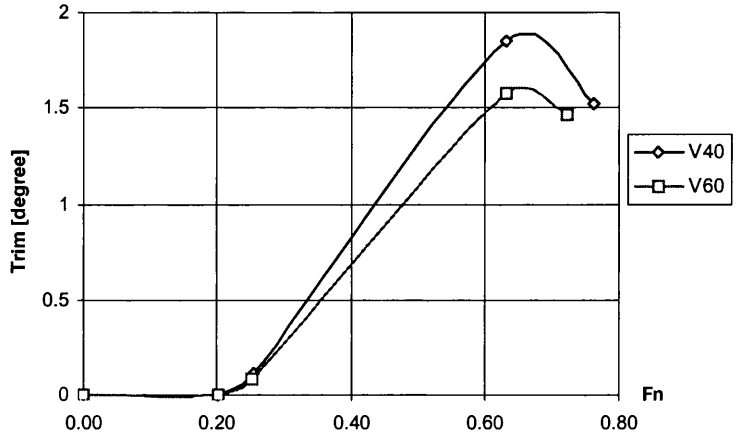

Figure 4.9 - Trim angle

4.5.1 Heave and Pitch Experimental Results

Figure 4.10 to Figure 4.41 compare the experimental and the theoretical results. The experimental response amplitude operator (RAO) for heave and pitch as well as the phase angles are compared with 2-dimensional theoretical results for cases with and without the viscous force terms. The heave response is normalised against the wave amplitude A and the pitch response against the product wave amplitude and wave number k.

The lift and the cross flow drag coefficients used in the present calculations are a_l =0.07 and C_D = 0.01 respectively. The lift coefficient according to Thwaites (1960) and Lee (1976) does not vary much and is considered almost constant for these applications. The cross flow drag coefficient does vary more than the lift coefficient and for the present application it is set as 0.01, following a previous study performed by Fang et al (1996). For the moment these coefficients in most cases have to be set empirically. Rathje and Schellin (1997) performed a comparison study of the influence of these coefficients in the ship motion responses using a viscous approach similar to the one presented in this work. From the study they concluded that at low speeds the variation of lift coefficient has almost no effect on motion responses, but

on the other hand the drag coefficient influences the responses near the resonance frequencies. At high speeds the choice of drag coefficients hardly influences the ship motion and the lift coefficient for stabilising fins becomes more important.

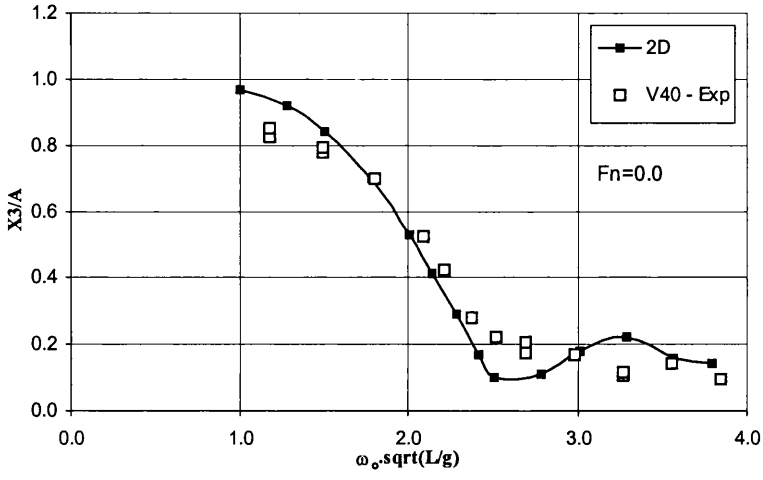

Figure 4.10 - Heave motion at *Fn*=0.0 in head waves, *V40* model

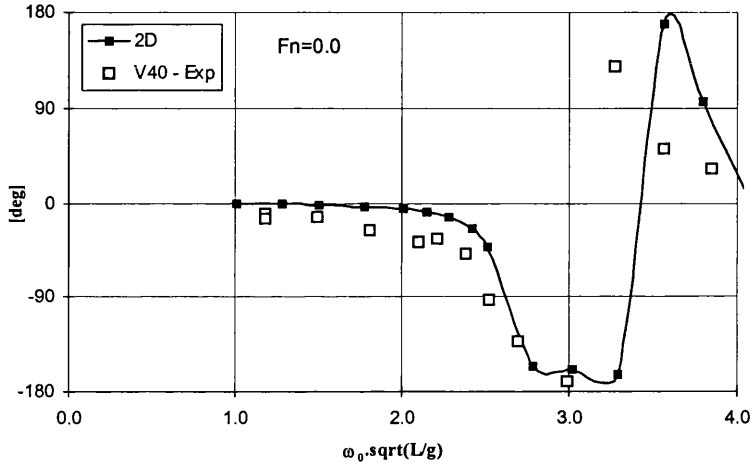

Figure 4.11 – Phase angle of the heave motion at *Fn*=0.0 in head waves, *V40* model

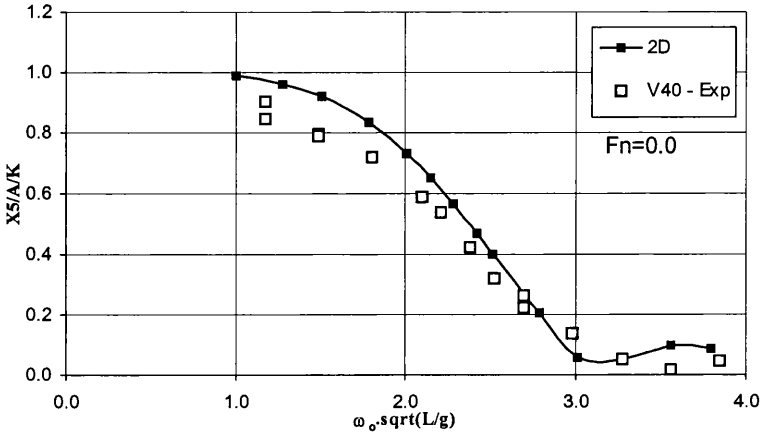

Figure 4.12 - Pitch motion at *Fn*=0.0 in head waves, *V40* model

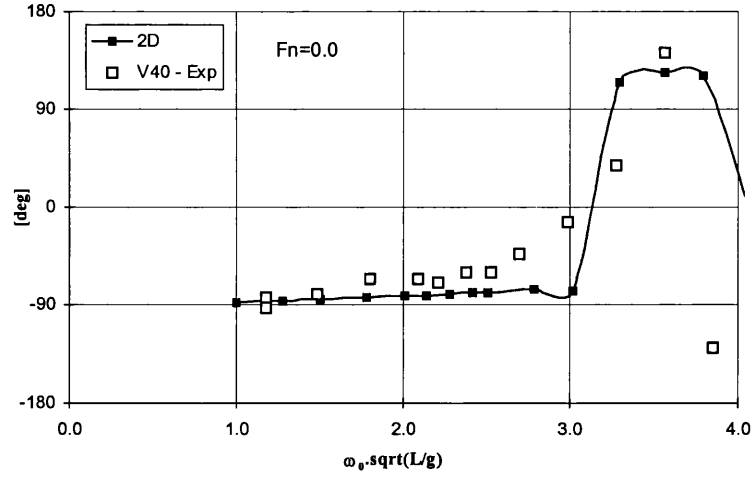

Figure 4.13 – Phase angle of the pitch motion at *Fn*=0.0 in head waves, *V40* model

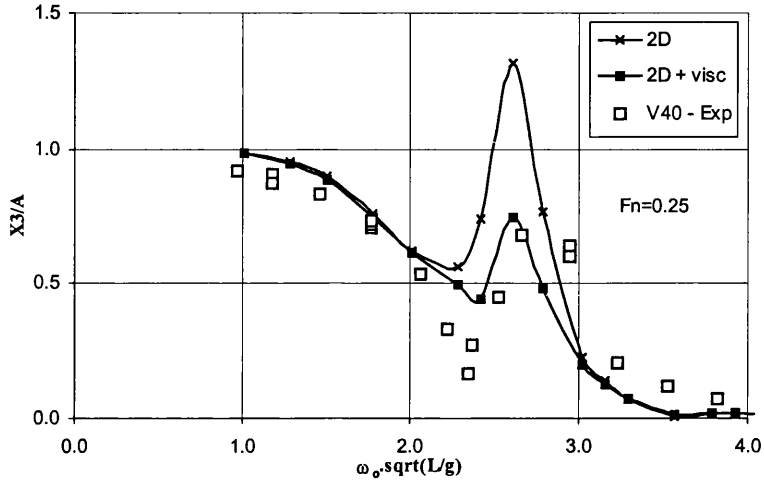

Figure 4.14 - Heave motion at *Fn*=0.25 in head waves, V40 model

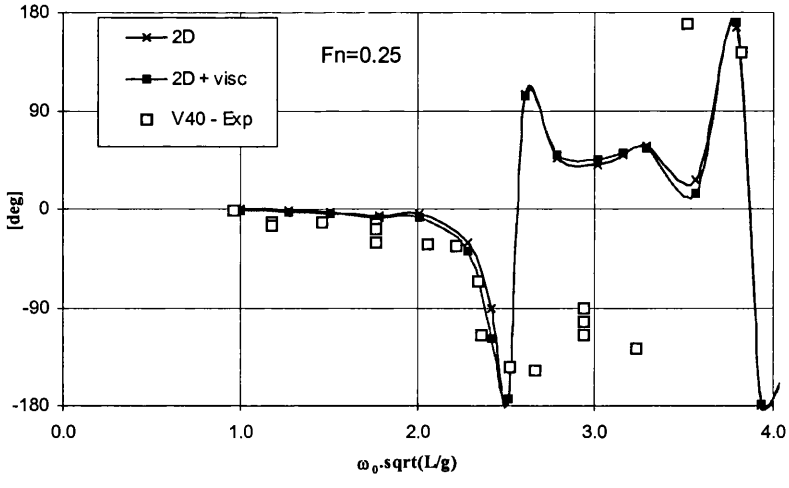

Figure 4.15 – Phase angle of the heave motion at *Fn*=0.25 in head waves, *V40* model

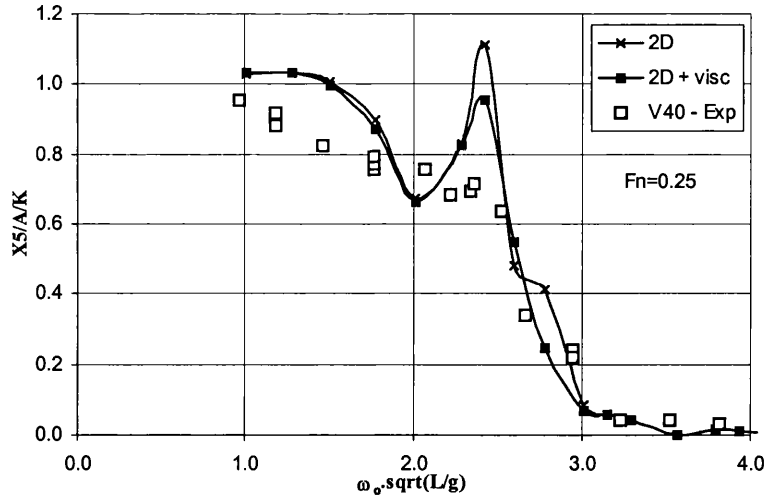

Figure 4.16 - Pitch motion at *Fn*=0.25 in head waves, *V40* model

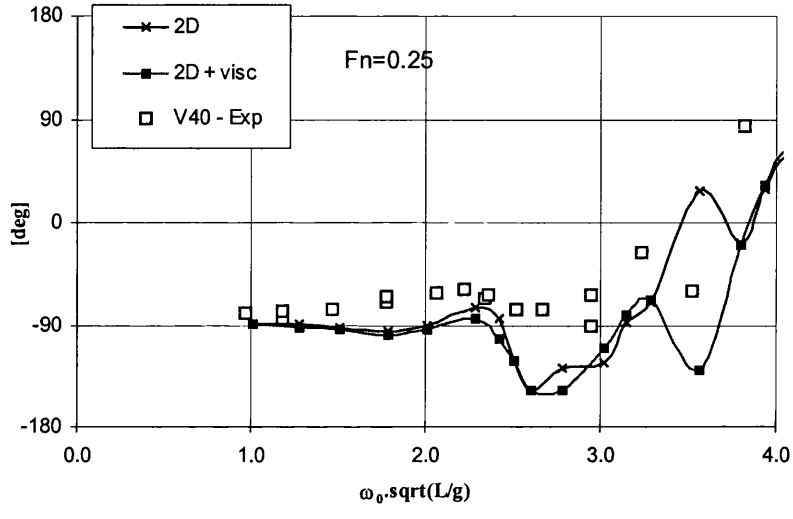

Figure 4.17 – Phase angle of the pitch motion at *Fn*=0.25 in head waves, *V40* model

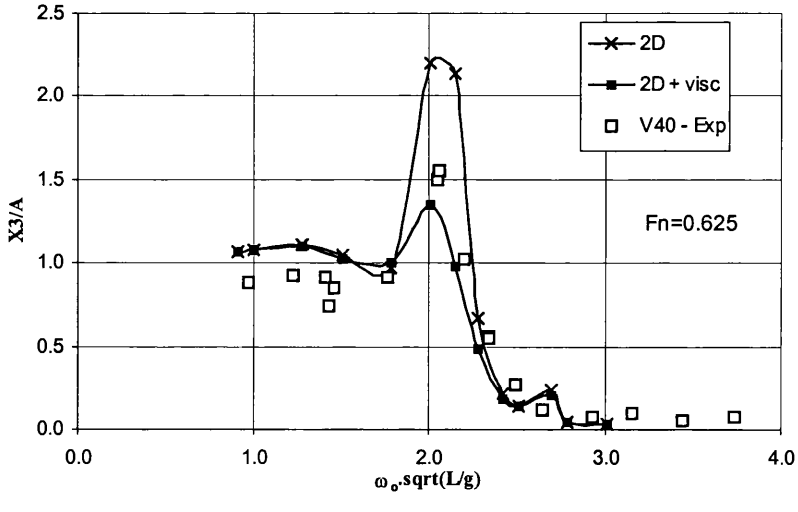

Figure 4.18 - Heave motion at *Fn*=0.625 in head waves, *V40* model

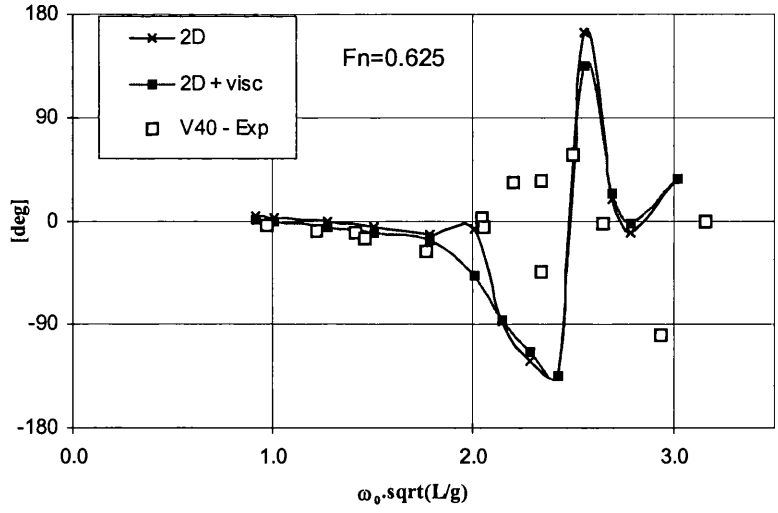

Figure 4.19 – Phase angle of the heave motion at *Fn*=0.625 in head waves, *V40* model

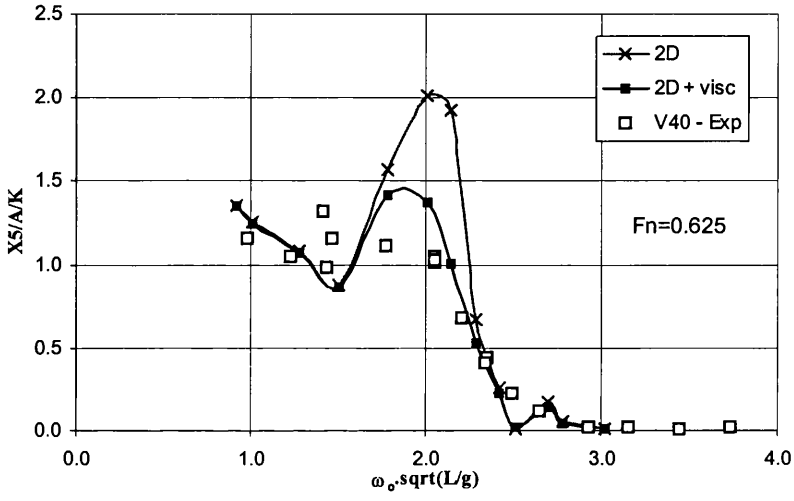

Figure 4.20 - Pitch motion at *Fn*=0.625 in head waves, *V40* model

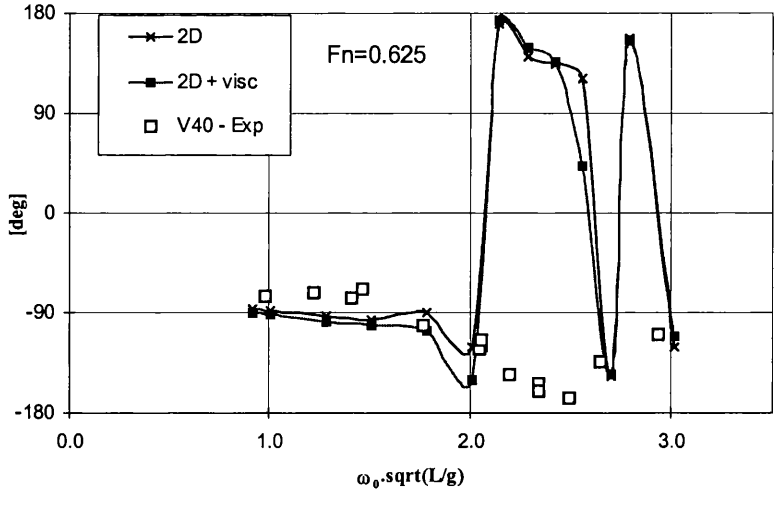

Figure 4.21 – Phase angle of the pitch motion at *Fn*=0.625 in head waves, *V40* model

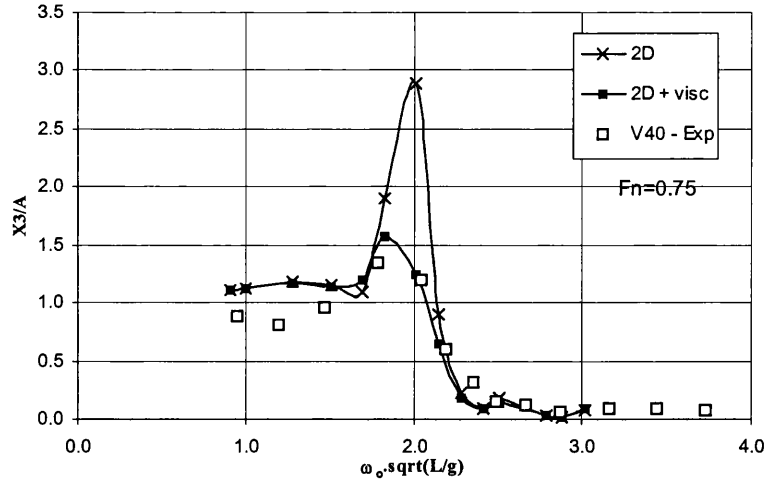

Figure 4.22 - Heave motion at *Fn*=0.75 in head waves, *V40* model

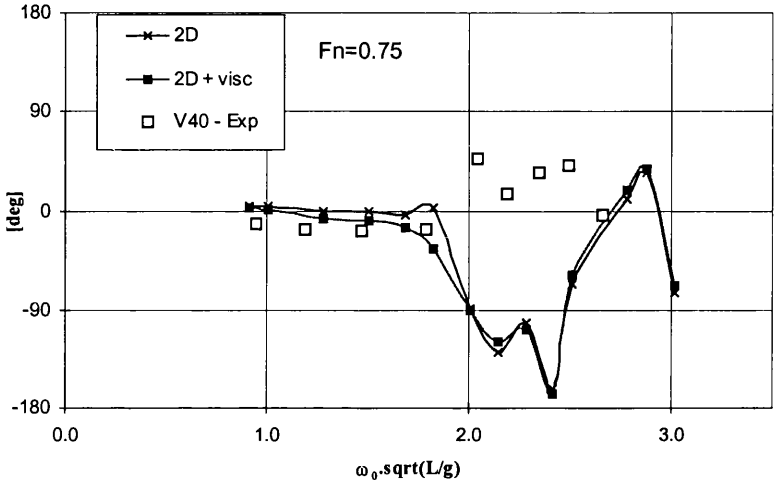

Figure 4.23 – Phase angle of the heave motion at *Fn*=0.75 in head waves, *V40* model

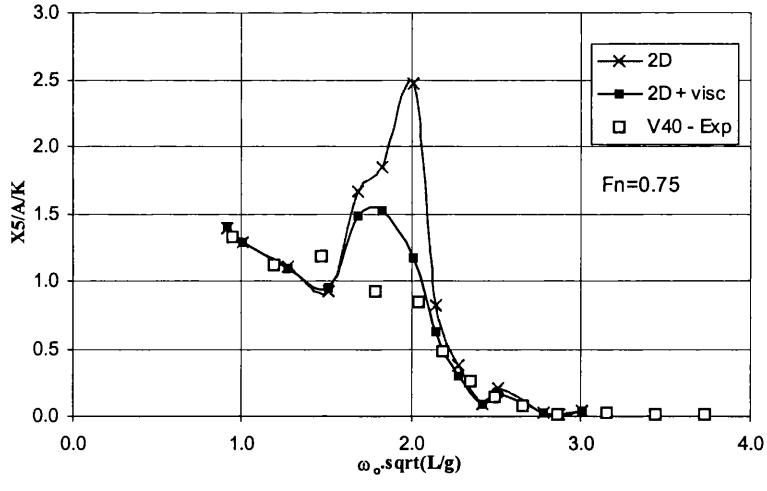

Figure 4.24 - Pitch motion at *Fn*=0.75 in head waves, *V40* model

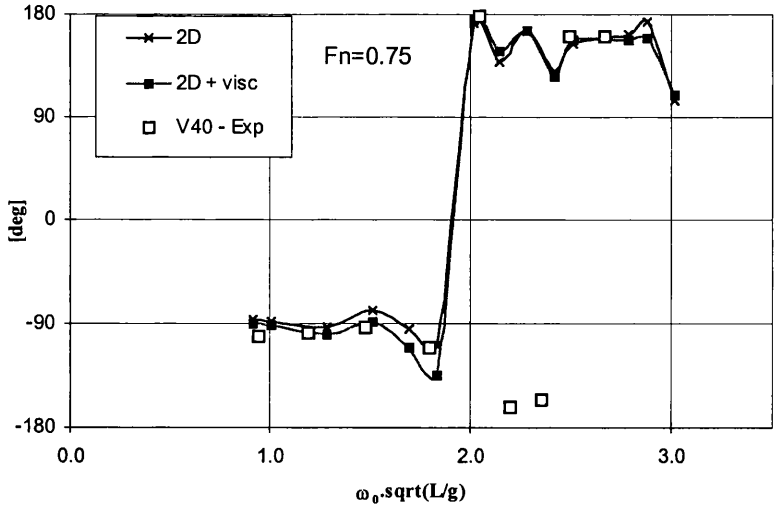

Figure 4.25 – Phase angle of the pitch motion at *Fn*=0.75 in head waves, *V40* model

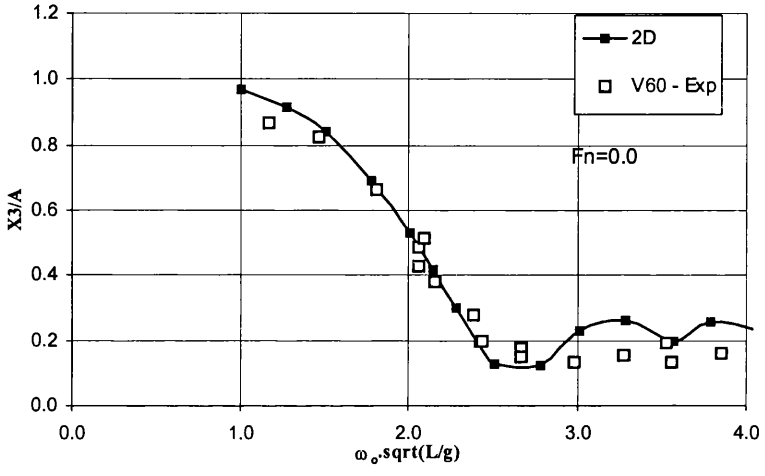

Figure 4.26 - Heave motion at *Fn*=0.0 in head waves, *V60* model

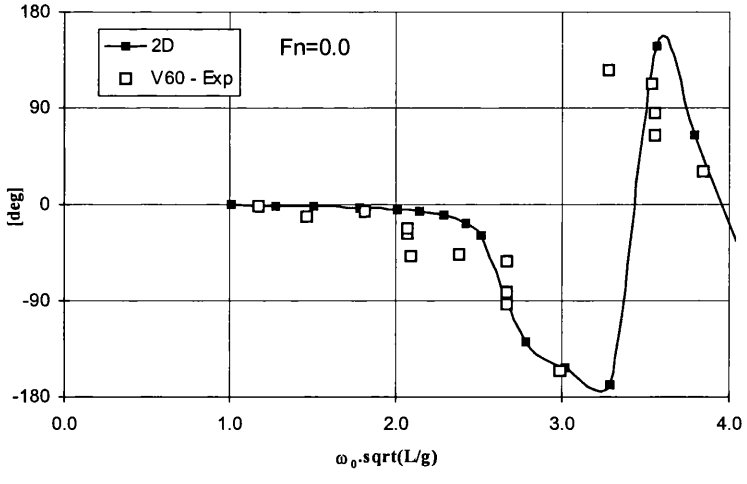

Figure 4.27 – Phase angle of the heave motion at *Fn*=0.00 in head waves, *V60* model

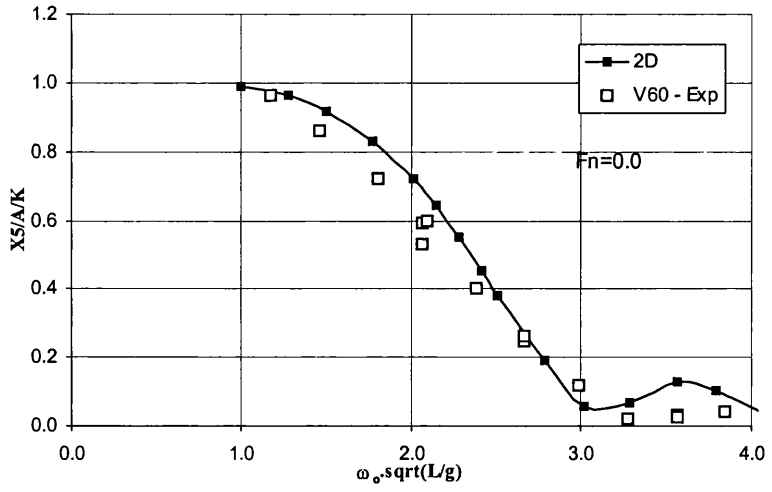

Figure 4.28 - Pitch motion at *Fn*=0.0 in head waves, *V60* model

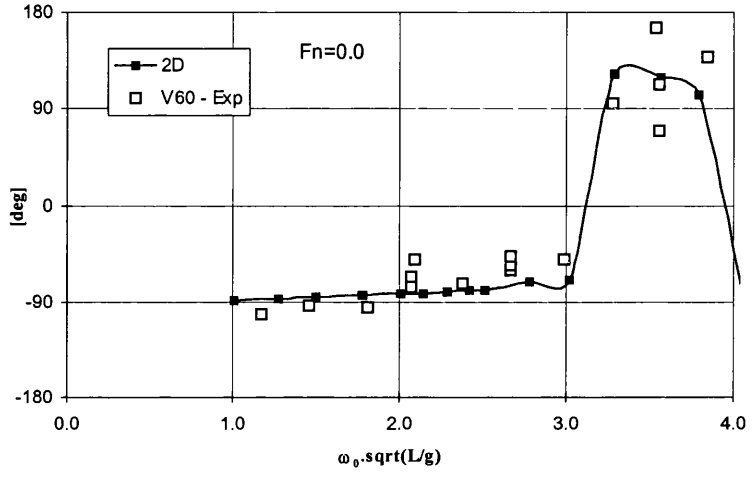

Figure 4.29 – Phase angle of the pitch motion at *Fn*=0.00 in head waves, *V60* model

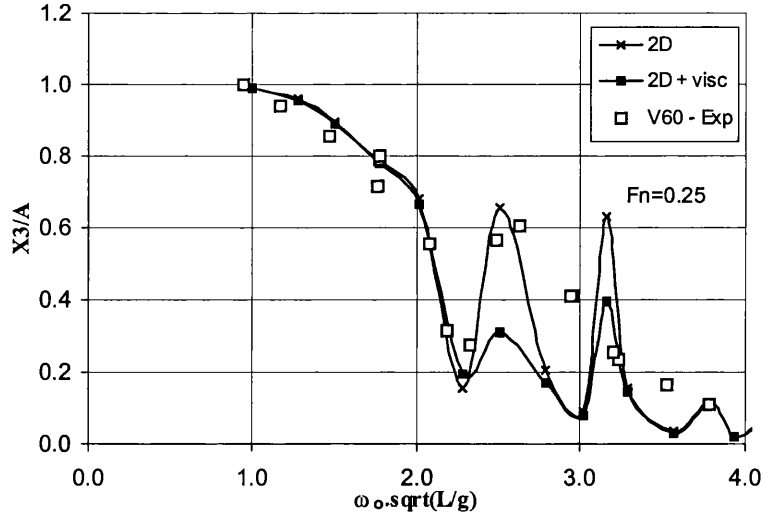

Figure 4.30 - Heave motion at *Fn*=0.25 in head waves, *V60* model

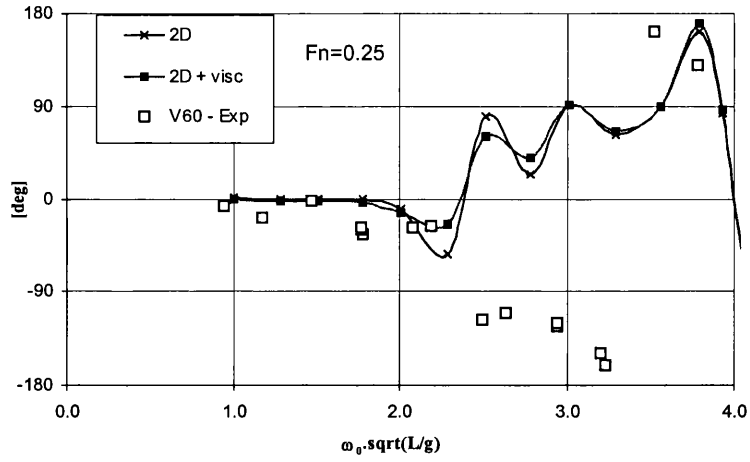

Figure 4.31 – Phase angle of the heave motion at *Fn*=0.25 in head waves, *V60* model

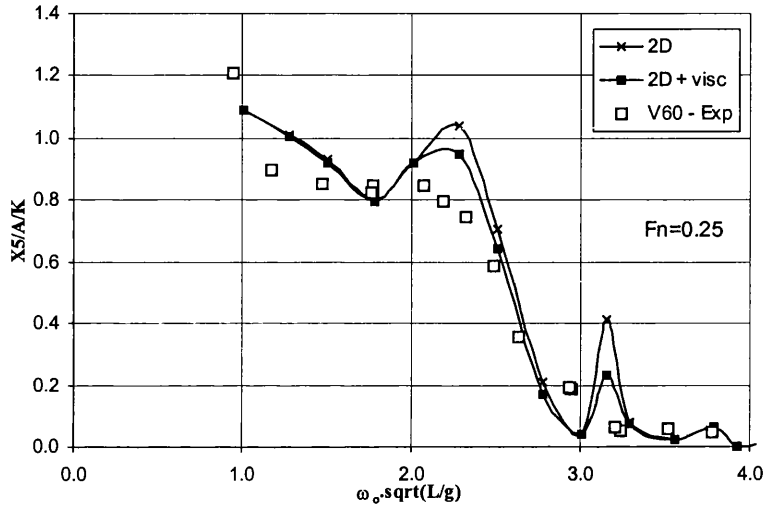

Figure 4.32 - Pitch motion at Fn=0.25 in head waves, V60 model

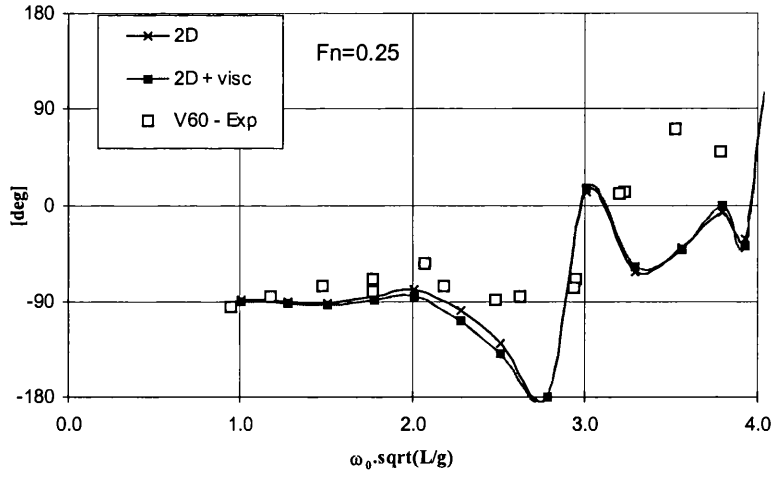

Figure 4.33 – Phase angle of the pitch motion at *Fn*=0.25 in head waves, *V60* model

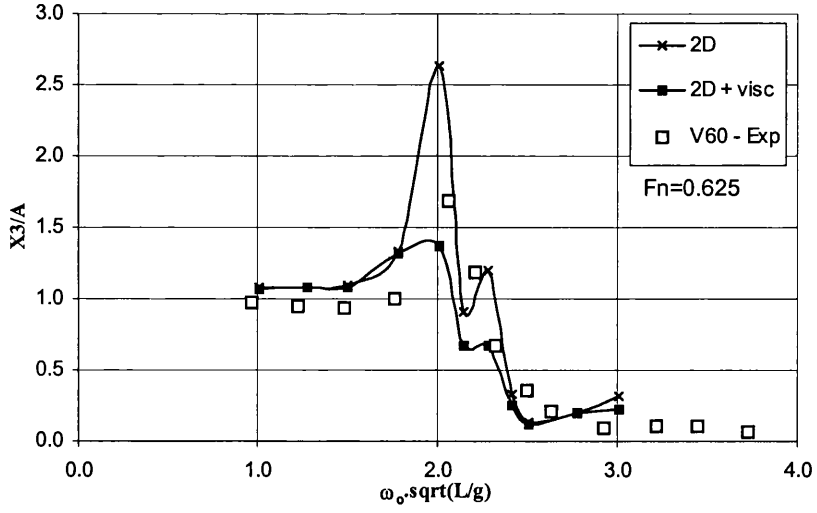

Figure 4.34 - Heave motion at *Fn*=0.625 in head waves, *V60* model

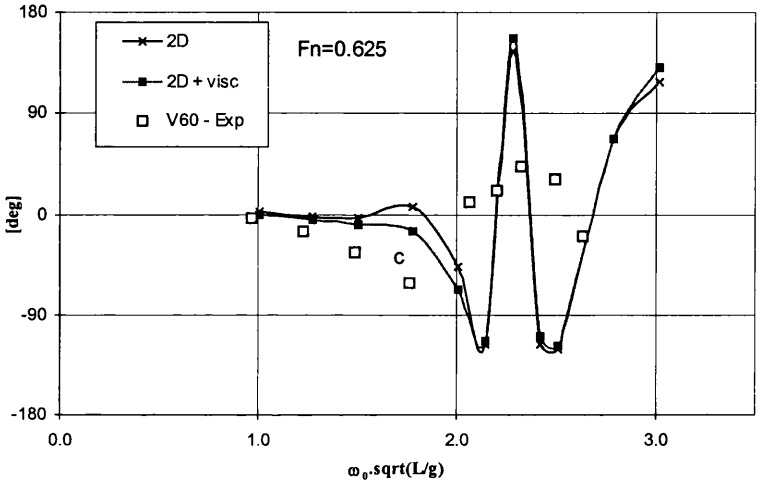

Figure 4.35 – Phase angle of the heave motion at *Fn*=0.625 in head waves, *V60* model

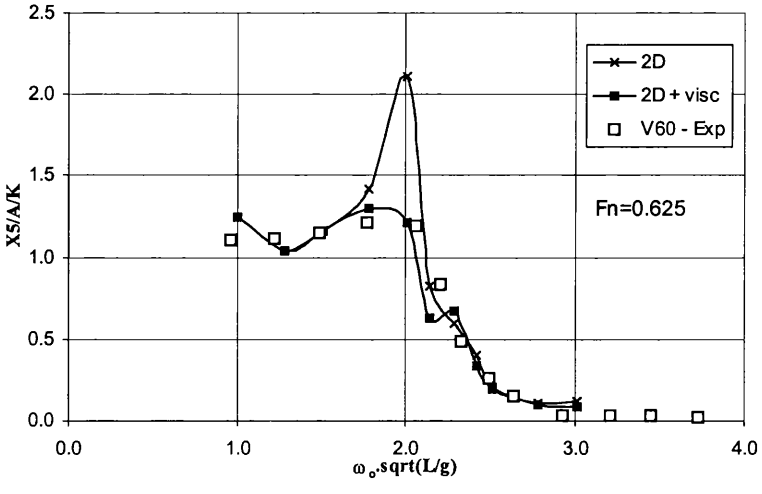

Figure 4.36 - Pitch motion at *Fn*=0.625 in head waves, *V60* model

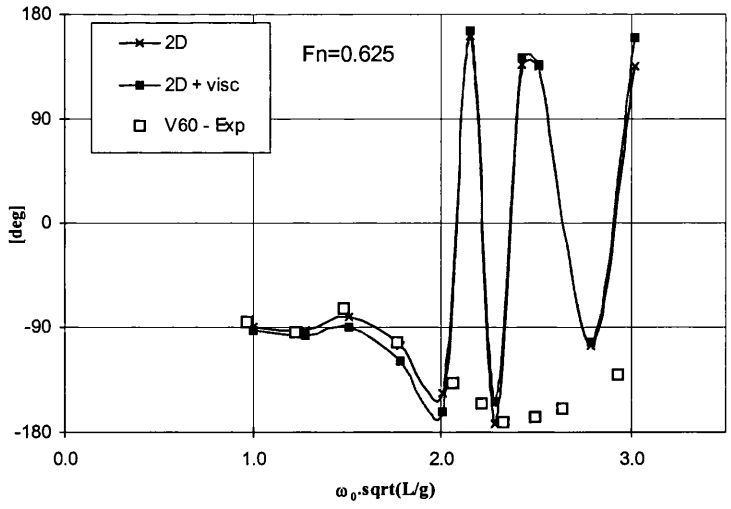

Figure 4.37 – Phase angle of the pitch motion at *Fn*=0.625 in head waves, *V60* model

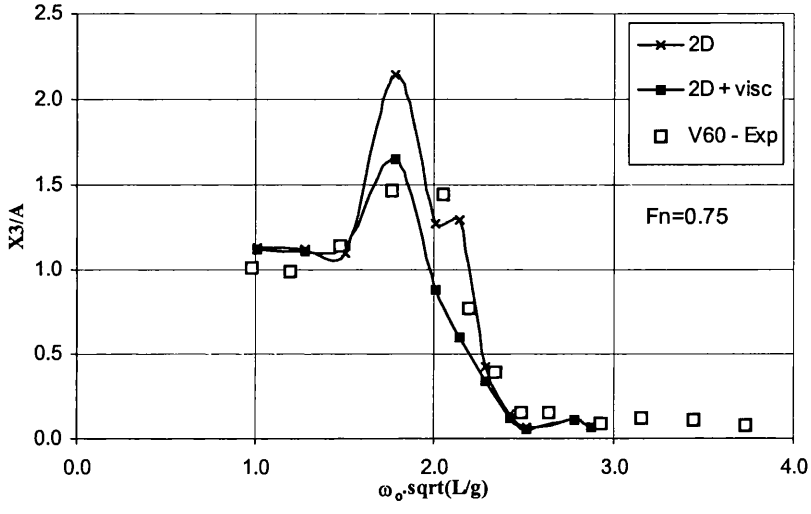

Figure 4.38 - Heave motion at *Fn*=0.75 in head waves, *V60* model

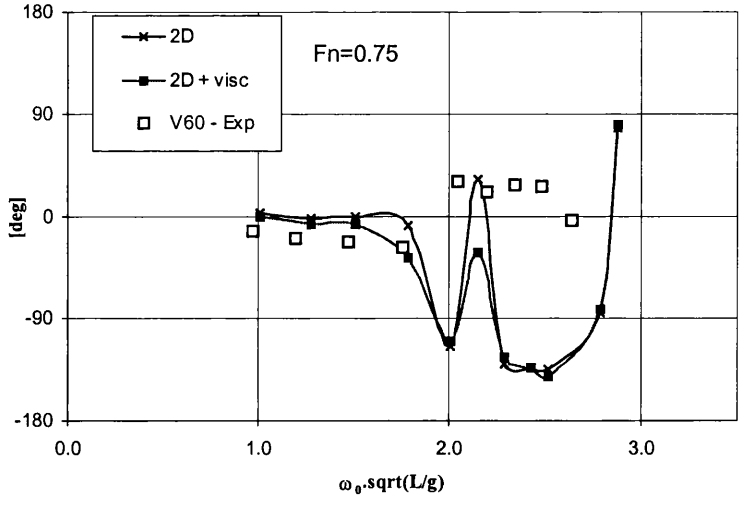

Figure 4.39 – Phase angle of the heave motion at *Fn*=0.75 in head waves, *V60* model

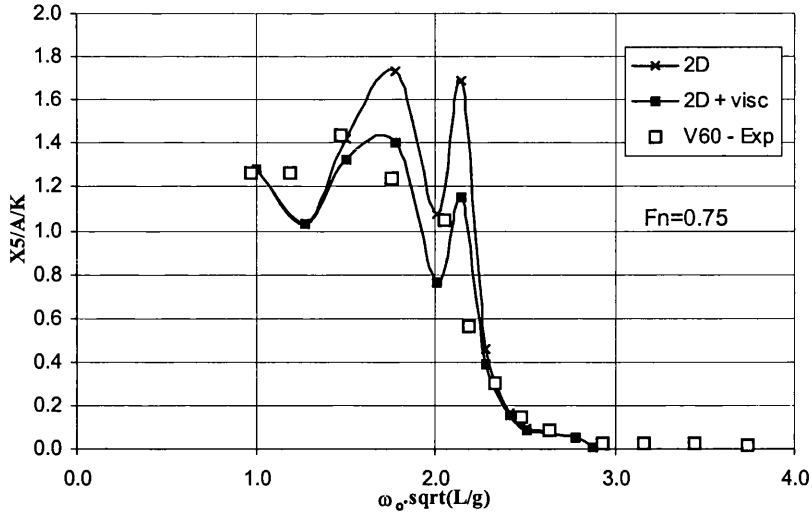

Figure 4.40 - Pitch motion at *Fn*=0.75 in head waves, *V60* model

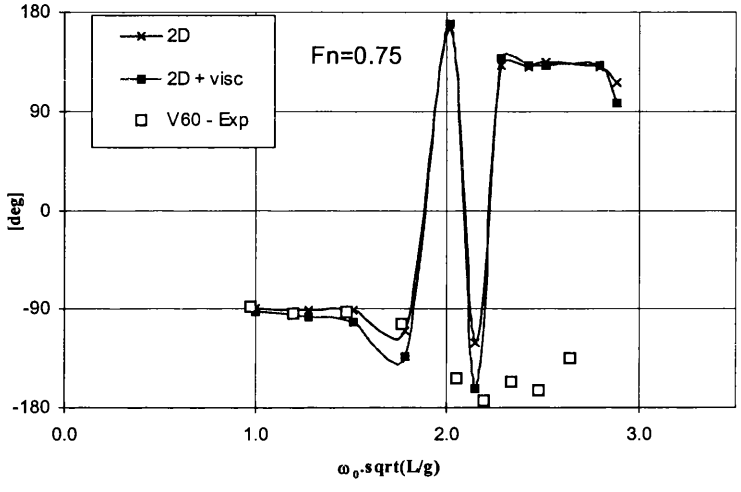

Figure 4.41 – Phase angle of the pitch motion at *Fn*=0.75 in head waves, *V60* model

As is seen in the foregoing figures, the two-dimensional heave and pitch RAOs calculated with the viscous forces are in good agreement with the experimental results, in most cases. At zero speed (Figure 4.10 to Figure 4.13 and Figure 4.26 to Figure 4.29) both heave and pitch experimental results are very well predicted by the theory at the full wave frequency range. This good agreement between the results show that the two dimensional effects are very well modelled by the theory when there is no forward speed effects. Since the viscous formulation depends on the ship forward speed, the figures at *Fn=0.0* only present one theoretical curve.

With forward speed the experimental heave responses at the resonance frequencies are generally over-predicted by the theoretical results when the viscous forces are not

considered. The agreement between theoretical and experimental results is much better when the viscous terms are added to the theory. The amplitude of the peaks in the theoretical results when the viscous terms are not included increases with the forward speed increase. Generally at forward speed there is a better agreement between the heave results than the pitch results. In Figure 4.14 (*V40* model, *Fn=0.25*) the theoretical heave amplitude at the resonance peak ($\omega_0\sqrt{L/g}$ =2.6) is very good. In Figure 4.18 (*V40* model, *Fn=0.625*) the difference between the theoretical and the experimental results at peak resonance frequency is 15%. In Figure 4.22 (*V40* model, *Fn=0.75*) the agreement between the results is very good again. Most of the *V60* model results at forward speed present a second peak at high wave frequencies. These second peaks are due to the symmetric interaction explained in chapter 5.2.2 but this phenomenon is analysed in the next chapter, where a more detailed analysis of the results are performed. These peaks make the comparisons difficult as in for example Figure 4.30 where the symmetric resonance frequency is near $\omega_0\sqrt{L/g}$ =3.1. In Figure 4.34 (*V60* model, *Fn=0.625*) the peak differences is 18% and again the symmetric resonance frequency is very evident.

Pitch theoretical results of the *V40* model generally show a pronounced peak near the first natural frequency but in the experimental results that peak is not so pronounced. As shown in Figure 4.16 near the resonance peak ($\omega_0\sqrt{L/g}$ =2.4) the difference between theoretical and experimental results is 20% and in Figure 4.24 at the resonance peak the difference is even bigger, 40%. The pitch responses are better predicted for the *V60* model where in the worst case the difference between theoretical and experimental results is less than 16% (Figure 4.32).

The phase angle between the incident wave and the ship motion at zero speed is very well predicted by theory for both heave and pitch motions. When the speed increases the phase angle results do not match very well and there are some discrepancies between theoretical and experimental results. At high speed and high wave frequency, where the encounter frequencies are very high the motion amplitude responses are typically very small, the phase angle results are not so important as in the low and medium range frequencies where in fact the theoretical predictions agree better.

Time series results

The following Figures show an example of typical experimental data (wave, heave and pitch amplitudes) and compare them with a sinusoidal function of the type $A\cos(\omega_e t + \varepsilon)$. In the figures, the line is the cosine function and the small circles are the experimental data.

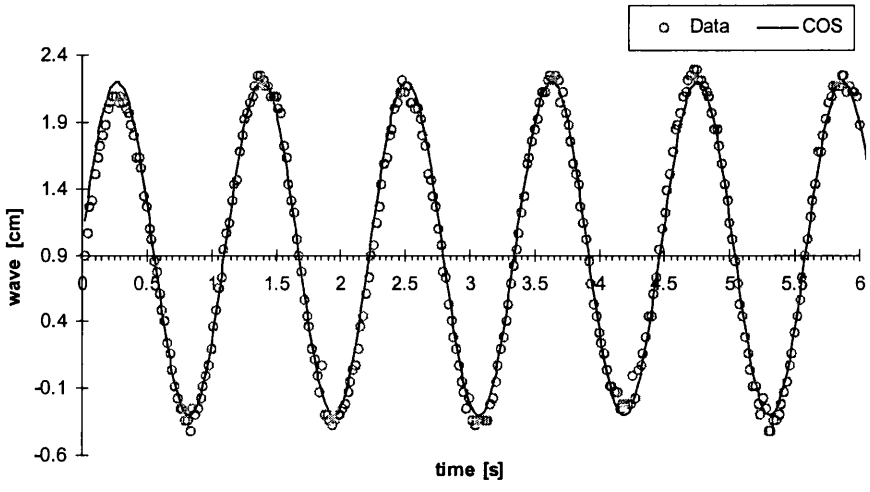

Figure 4.42 – Wave time series, ω_e = 0.893 Hz, Fn=0.25

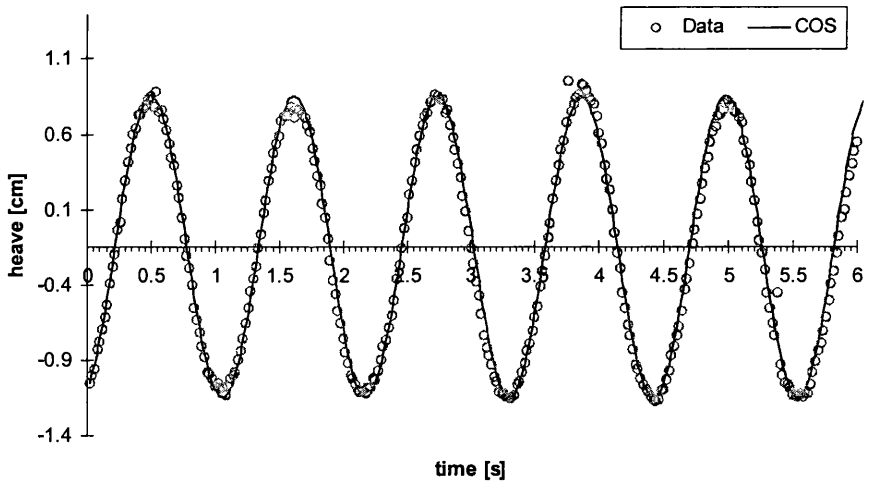

Figure 4.43 – Heave time series, ω_e = 0.893 Hz, Fn=0.25

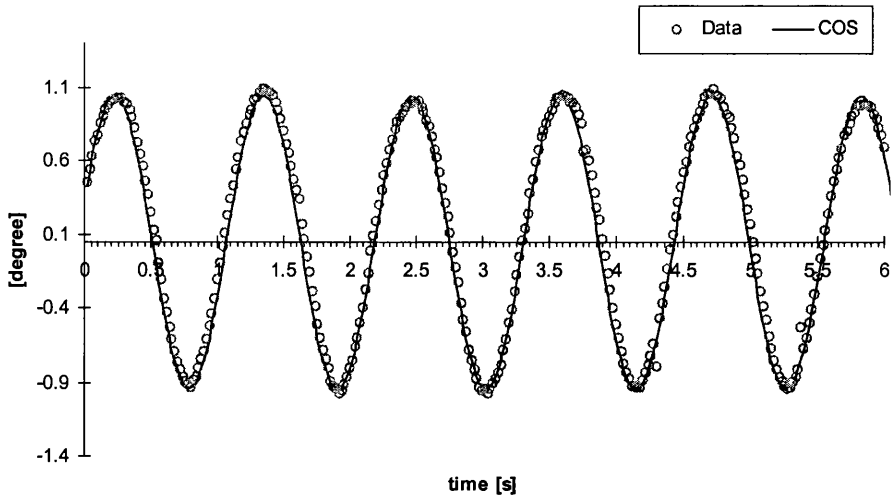

Figure 4.44 – Pitch time series, ω_e = 0.893 Hz, Fn=0.25

4.6 Error Analysis

Every experimental work has an associated error. The errors come from very different sources and are due to a wide range of reasons. Error sources can be classified according to ITTC 1978 as model tests errors (resulting from instrumentation errors, procedures and experiment conditions), prediction method errors (resulting from approximate assumptions) and sea trial errors (including instrumentation errors and errors such as influence of sea water temperature, propeller cavitation and others).

In the present work an error analysis was made in order to assess the confidence of the experimental data and to be conscious of the quality of the results. The main experimental errors are attributed to the asymmetric wave sent by the wave maker and the model restrictions in some degree of freedom.

The heave and pitch motion responses are the most important results in this study and this analysis is focused on these results. Nevertheless a wave amplitude analysis is also made.

To perform the motion responses error analysis several runs were repeated three times and a few runs were repeated twice using both models (*V40* and *V60*). The heave and pitch errors (dispersion from the mean value) were calculated as follows. Consider X the test variable and the mean value of the test $E[X]$ given by

$$E[X] = \frac{\sum_{i}^{n} X_i}{n}$$

then the error is

$$Error_i = \frac{E[X] - X_i}{E[X]}$$

and the mean error is

$$E[Error] = \frac{\sum_{i}^{n} Error_i}{n} \tag{4.16}$$

The coefficient of variation was also calculated and the results are not much different from the mean error Eq.(4.16) as can be seen in the following tables.

Heave Amplitude – V40 model							
Fn	ω_0[Hz]	X_1	X_2	X_3	*E[X]*	*E[Error]*	*St.Dev[X]*
0.0	0.4	0.822	0.852	-	0.837	1.8%	1.8%
0.0	0.5	0.779	0.795	-	0.787	1.1%	1.1%
0.0	0.9	0.175	0.204	0.205	0.195	6.8%	7.3%
0.0	1.1	0.106	0.114	0.115	0.112	3.2%	3.4%
0.25	0.4	0.902	0.874	-	0.888	1.6%	1.6%
0.25	0.6	0.708	0.719	0.734	0.721	1.3%	1.5%
0.625	1.0	0.612	0.641	0.604	0.619	2.3%	2.5%
0.625	0.5	0.911	0.742	0.846	0.833	7.3%	8.4%
0.625	0.7	1.550	1.500	1.553	1.534	1.5%	1.6%
0.625	0.8	0.565	0.547	-	0.556	1.6%	1.6%

Table 4.7 – Error Analysis for Heave Amplitude – *V40*

Heave Amplitude – V60 model							
Fn	ω_o[Hz]	X_1	X_2	X_3	*E[X]*	*E[Error]*	*St.Dev[X]*
0.0	0.7	0.429	0.488	0.514	0.477	6.7%	7.5%
0.0	0.9	0.168	0.178	0.150	0.165	6.2%	7.0%
0.0	1.2	0.135	0.135	0.190	0.153	16.1%	17.1%
0.25	0.6	0.788	0.801	0.713	0.768	4.7%	5.0%
0.25	1.0	0.411	0.408	-	0.410	0.4%	0.4%
0.25	1.1	0.253	0.233	-	0.243	4.0%	4.0%

Table 4.8 – Error Analysis for Heave Amplitude – *V60*

The maximum error for heave amplitude using the *V40* model is 6.8%, while the minimum error is 1.1%. For the *V60* model the maximum error is 16.1% and the minimum is 0.4%. The mean of the mean errors for heave amplitude is 4.2% (using both models results) which is a small error.

Pitch Amplitude – V40 model							
Fn	ω_o[Hz]	X_1	X_2	X_3	*E[X]*	*E[Error]*	*St.Dev[X]*
0.0	0.4	0.808	0.863	-	0.835	3.2%	3.2%
0.0	0.5	0.764	0.757	-	0.760	0.4%	0.4%
0.0	0.9	0.239	0.282	0.283	0.268	7.1%	7.6%
0.0	1.1	0.052	0.056	0.054	0.054	2.3%	2.8%
0.25	0.4	0.916	0.880	-	0.898	2.0%	2.0%
0.25	0.6	0.754	0.771	0.791	0.772	1.6%	1.9%
0.625	1	0.227	0.237	0.221	0.228	2.6%	3.0%
0.625	0.5	1.318	0.983	1.153	1.151	9.7%	11.9%
0.625	0.7	1.047	1.019	1.031	1.032	1.0%	1.1%
0.625	0.8	0.439	0.410	-	0.424	3.4%	3.4%

Table 4.9 – Error Analysis for Pitch Amplitude – *V40*

Pitch Amplitude – V60 model							
Fn	ω_o[Hz]	X_1	X_2	X_3	*E[X]*	*E[Error]*	*St.Dev[X]*
0.0	0.7	0.531	0.594	0.598	0.574	5.0%	5.3%
0.0	0.9	0.253	0.245	0.260	0.253	2.0%	2.5%
0.0	1.2	0.031	0.026	0.040	0.032	16.5%	18.7%
0.25	0.6	0.817	0.846	0.824	0.829	1.4%	1.5%
0.25	1.0	0.192	0.186	-	0.189	1.6%	1.6%
0.25	1.1	0.060	0.051	-	0.056	8.7%	8.7%

Table 4.10 – Error Analysis for Pitch Amplitude – *V60*

The maximum error for pitch amplitude using the *V40* model is 9.7%, while the minimum error is 0.4%. For the *V60* model the maximum error is 16.5% and the minimum is 1.4%. The mean of the mean errors for pitch amplitude is 4.3% (using both model results) which is a small error.

Both heave and pitch maximum errors occurred in the same trial and since all the other errors are quite below that maximum, it can be said that the experimental results have about 4% of confidence, for the heave and pitch amplitudes.

Incident wave error analysis

All waves were analysed even when the input to the wave maker was repeated. Table 4.11 shows the wave amplitudes recorded.

In Table 4.11, X_i is the mean of the three wave probes measurements for each different *i* run. From the table it can be seen that the deviations of the wave amplitudes from the mean value are very small (less than 3%), with the exception of frequency 1.0 Hz and 1.2 Hz where the variations are higher.

Another important aspect is the mean value of the standard deviation of each three wave probe measurements. The mean value is 10% and this shows a small asymmetry in the wave form which means the wave crest is not a perfect line from one tank wall to the other wall.

Wave frequency wo[Hz]	X_1	X_2	X_3	X_4	X_5	X_6	X_7	X_8	Average wave amplitude [cm]	Std.Dev.
0.30	0.97	0.98	0.91	0.95	0.97	0.96	-	-	0.96	3%
0.40	1.33	1.37	1.35	1.35	1.34	1.59	1.40	1.38	1.39	6%
0.50	1.54	1.54	1.42	1.49	1.42	1.49	1.49	1.49	1.49	3%
0.60	1.34	1.33	1.29	1.32	1.30	1.33	1.31	1.31	1.32	1%
0.70	1.42	1.44	1.35	1.40	1.35	1.38	1.41	1.40	1.39	2%
0.75	1.54	1.53	1.43	1.53	1.48	1.53	-	-	1.51	3%
0.80	1.65	1.65	1.57	1.65	1.52	1.57	1.55	1.58	1.59	3%
0.85	1.63	1.77	1.60	1.56	1.59	1.62	-	-	1.63	5%
0.90	1.34	1.25	1.27	1.30	1.24	1.27	1.29	1.28	1.28	2%
1.00	1.43	1.33	1.33	1.36	1.32	1.78	1.37	1.36	1.41	11%
1.10	1.77	1.68	1.69	1.70	1.67	1.66	1.68	1.68	1.69	2%
1.20	1.93	1.87	1.88	1.90	1.45	1.45	1.47	-	1.71	14%
1.30	1.85	1.79	1.79	1.83	1.77	1.77	-	-	1.80	2%

Table 4.11 – Wave amplitude error analysis

4.7 Conclusions

A statistical analysis of the main dimensions and ratios of catamarans was performed. This analysis provided a basis to choose the dimensions of the tested models. This analysis was important because the main dimensions of catamarans change a lot and there are no typical dimensions. In a catamaran beside the demi-hull main dimensions, there are also other very important dimension to be considered like the distance between the hulls. After the statistical analysis, two models configuration were decided, i.e. one with 40 cm between the two hulls centre lines (*V40*) and the other with a distance of 60 cm between hulls (*V60)*.

An experimental set-up was designed and installed at the Hydrodynamic Laboratory of the University of Glasgow to investigate the motions of the models in waves.

The resistance tests in calm water show that the two models at certain speeds have different resistance. The *V40* model has higher resistance than the *V60* model (about

4.4% at Fn=0.6). This difference is because their behaviour in terms of trim and rise of the centre of gravity is different. The *V60* model rises more from the water than the *V40* model.

The heave and pitch experimental results were compared with 2D theoretical results. Two different theoretical calculations were performed, one including viscous forces and another without viscous forces. At forward speed, the experimental heave responses near the resonance peaks are generally over predicted by the theoretical calculations when the viscous force terms are not considered. The first natural resonance peak increases its magnitude when the speed increases. The results when the viscous forces are included agree better than the results of the cases without viscous forces.

At forward speed the theoretical heave and pitch response amplitude operators present a second small resonance peak due to theoretical symmetric resonance frequency. This peak is not present in the experimental results. The reason for its appearance in the theoretical results is because of the simplified way the forward speed effects are added to the theory. Both heave and pitch theoretical results with the viscous effects agree well with the experimental results but the agreement is more precise for the heave calculations.

An error analysis of the heave and pitch results, as well as the incident wave amplitude was performed. This analysis shows that the mean motion response errors are around 4%, which is a perfectly acceptable error. Two points are concluded from the incident wave analysis. The first conclusion is that there is 10% of asymmetry in the waveform, which means the wave crest is not a straight line from one tank wall to the other. The second is that the mean wave error is about 4%, which is also an acceptable value.

Chapter 5

Features of Catamaran Motions

5.1 Introduction

In this chapter several calculations and comparisons between theoretical and experimental results are performed. Some special features such as hull interference and resonance frequencies, strictly related to twin hulls, are presented and discussed. A parametric study is also performed comparing different hull configurations in which the hull main characteristics are varied.

Some calculations made in this chapter use results from two different theories: the two-dimensional theory with viscous effects developed in the present work, and the three-dimensional theory developed by Chan (1990), whose software is available at the University of Glasgow. The theoretical results from the two theories are compared between each other and also with the experimental results. These comparisons use calculations of the *V40* and *V60* models running at the same forward speeds as those tested in the experimental work (Chapter 4).

Beside the comparison made between experimental and theoretical results, other comparisons are made between experimental results of the two models tested and also between experimental and theoretical mono-hull results. In addition the following comparisons are also performed in order to assess the validity of the suggested hull interference.

A parametric study is performed by changing the distance between the Vosper catamaran hulls and the catamaran draught. In this parametric study three different hull spacings and two different draughts are used. The calculations made in this study are based on the two-dimensional theory with viscous effects. The results are analysed and compared with the experimental results performed with the models tested at the laboratory.

Another parametric study is performed using a different type of catamaran, a round hull displacement catamaran instead of the hard-chine Vosper hull. In this study the

catamaran displacement is kept constant and the variations are in terms of the ship length, breadth and draught. The speed and the distance between the hulls are also varied parameters.

5.2 Catamaran Hull Interaction and Resonance Frequencies

5.2.1 Introduction

The twin-hull interaction is an interesting and difficult problem that has been discussed before by other authors Wang and Wahab (1971), Ohkusu and Faltinsen (1990), Faltinsen et al (1992), Van't Veer and Siregar (1995) and Hudson et al (1995).

Ohkusu and Faltinsen (1990) presented a method to predict three-dimensional hydrodynamic forces between two hulls of a catamaran oscillating and with forward speed. The predicted hydrodynamic forces agree generally well at high speed with the model test results and they concluded that hydrodynamic interaction between hulls is weak at high speeds. Faltinsen et al (1992) extended a strip theory model with a full linearised free surface boundary condition with the forward speed effect terms to calculate motions and loads of catamarans in waves. They also stated that at high speeds if the hulls are not too close to each other and the waves generated on one hull do not influence the pressure distribution on the other hull, it could be assumed that the hulls are hydrodynamically independent of each other.

Van't Veer and Siregar (1995) also studied the interaction effects on a catamaran travelling with forward speed in waves. They used a strip theory and considered three different kinds of interference between hulls depending on the ship speed and hull spacing. For very low speeds the hull interaction is considered two-dimensional and is well predicted by strip-theory as proved by the twin-cylinder results and also by experimental results. At very high speed the authors say that there is no wave interaction between the hulls because at high speed the waves generated by one hull do not reach the other hull and as a result there is no interaction between the hulls. It is only at medium speed that there is a longitudinal wave interaction.

As can be seen in Figure 5.1, by simple kinematic analysis it is possible to determine when the waves generated by one hull reach the other just considering the ship length L, the distance between the inner sides of the two hulls H, the ship speed U and the wave frequency ω_0. The relation is given by

$$\sigma = \frac{U}{V_p} = \frac{U}{L\omega_e/T_e} = \frac{U.k_e}{\omega_e} = \frac{U.\omega_e}{g} \tag{5.17}$$

where V_p is the propagated wave velocity, Lw_e and T_e are the propagated wave length and period and k_e is the encounter wave number.

When σ is greater than L/H there is no interaction between the waves generated at the bow section of one hull and the stern section of the other hull. Alternatively, expressing the same in a more appropriate way, when

$$\omega_e \rangle \frac{L}{H} \cdot \frac{g}{U} \tag{5.18}$$

there should be no wave interaction.

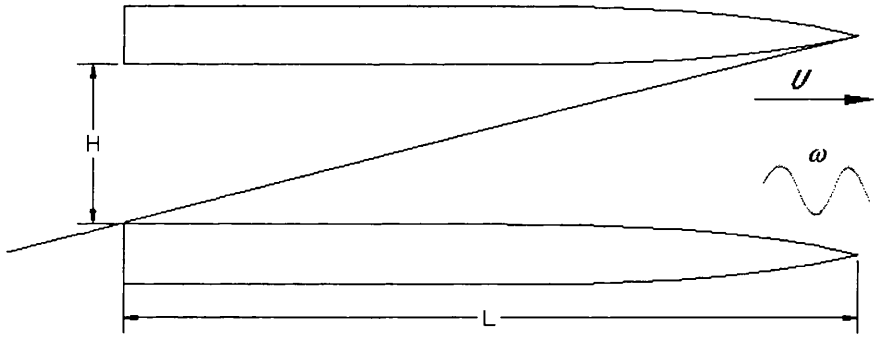

Figure 5.1 – Hull interference

Another study made by Hudson, Price and Temarel (1995) compared catamaran motion responses predicted by different mathematical theories. They concluded that near the resonance frequencies the theories have different responses and that the distance between the hulls has influence on the calculations of the hydrodynamic coefficients and the ship motion responses. On that study they used two and three-dimensional theories and two different catamaran configurations (with D/L ratios of

0.2 and 0.4, where D is the centre line to centre line separation and L is the ship length).

5.2.2 Resonance Frequencies

Several ways of estimating the resonance frequencies were studied in order to analyse and understand some of the peaks in the calculated response operators.

The first natural frequencies ω_{nh}, ω_{np}, ω_{nr} for the heave, pitch and roll motions respectively, are easily estimated as the natural frequencies of a spring-damping-mass system and given by the following equations

$$\omega_{nh} = \sqrt{\frac{C_{33}}{M + A_{33}}}$$

$$\omega_{np} = \sqrt{\frac{C_{55}}{I_{55} + A_{55}}} \tag{5.19}$$

$$\omega_{nr} = \sqrt{\frac{C_{44}}{I_{44} + A_{44}}}$$

where M is the mass of the catamaran, A_{ij} are the added mass coefficients, C_{ij} are the restoring coefficients and I_{jk} are the mass moment of inertia. These approximations can only predict one natural frequency assuming a constant added mass. In order to predict other resonance frequencies, Hudson et al (1995) rewrote equations (5.19) and presented a frequency dependent function

$$A_{jk}(\omega_e) = \frac{C_{jk}}{\omega_e^2} - M_{jk} \tag{5.20}$$

where M_{ij} and the restoring coefficients are constants with the frequency. M_{ij} is the mass or the inertia depending upon j and k.

The added mass curve calculated from the radiation forces is also a frequency dependent function. Hence, each time the curve generated by equation (5.20) intersects the added mass curve calculated from the radiation forces, there is a resonance frequency. The curve generated by Equation (5.20) may intersect the added mass curve more than once because the calculated added mass curve for catamarans

have pronounced troughs that can even result in negative values, as seen in the twin-cylinders added mass results presented in section 3.6.1 (Figure 3.5 and Figure 3.7).

Another approximate way to determine theoretical resonance frequencies is given by Wang and Wahab (1971) and was found through the study of the heaving oscillations of twin cylinders in a free surface. The troughs in the twin cylinders added mass curves (Figure 3.5 and Figure 3.7) are due to the fluid interaction between the hulls which is essentially of two forms, symmetric and anti-symmetric. The symmetric waves generated inside the two hulls usually take the form indicated in Figure 5.2.

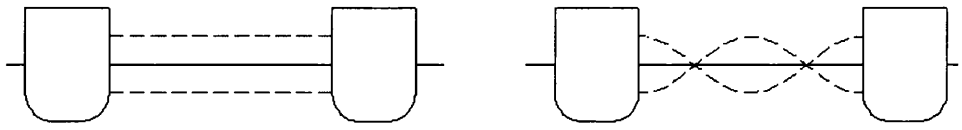

Figure 5.2 – Interaction wave inside the hulls

The first wave form in Figure 5.2 is simply a vertical motion of the fluid. The second wave form is like a standing wave with a wavelength equal to the distance between the hulls. This symmetric frequency is the same phenomenon studied by Wang and Wahab (1971) and is given by

$$\omega_{n3} = \sqrt{\frac{2 \cdot \pi \cdot g \cdot n}{H}} \qquad n = 1,2,\ldots \tag{5.21}$$

where H is the inner distance between the hulls.

Faltinsen (1990) points out another resonance frequency when he says that the natural frequencies of oscillation due to the sloshing effect between the two hulls of the catamaran, is estimated by assuming that resonance occurs when there is a half wavelength between the inner sides of the two hulls.

$$\omega_s \left(\frac{B_m/2}{g} \right)^{1/2} = \left(\frac{\pi}{\frac{D}{B_m/2} - 2} \right)^{1/2}$$

$$\omega_s = \sqrt{\frac{\pi \cdot g}{D - B_m}}$$

where D is the distance between the two hulls, B_m is the breadth of one single hull, and g is the gravitational constant. This resonance frequency expresses the anti-symmetric fluid interaction between the hulls, which affects mainly the horizontal plane motions. In a general form this frequency is given by

$$\omega_s = \sqrt{\frac{\pi \cdot g(2n-1)}{H}} \qquad n = 1,2,\ldots$$

The symmetric resonance frequency at zero forward speed is well identified experimentally and well predicted theoretically as shown by the twin-cylinder results in section 3.6.1. At zero forward speed and at this frequency a trough and a hump in the added mass and damping coefficients is observed. At zero speed the experimental results match with the theoretical results, but at forward speed the resonance frequency is not experimentally observed which suggest that because of the two-dimensional approach the added mass and damping coefficients are not properly calculated in the forward speed case. Theoretically the three-dimensional approach should be more appropriate but as seen in the next sections, this approach also presents small peaks in the catamaran motion responses near that frequency.

The purpose of the twin-cylinder calculations (section 3.6.1) is to validate the two-dimensional results and also to show that the symmetric resonance frequency is well predicted in the zero speed case. This frequency is dependent on the inverse of the distance between the hulls, eq (5.21), which implies that wider the distance between the hulls, the lower the resonance frequency (as shown before by the twin-cylinder results).

5.3 Analysis of the Motion Responses of Two Catamarans

In section 4.5 the experimental results were compared with results calculated by the two-dimensional theoretical model with and without the viscous forces terms. From these comparisons it is concluded that the theory is appropriate to simulate the physical reality when the viscous forces are added to the formulation. In this chapter the two-dimensional results with the viscous effects and the experimental results are compared with the three-dimensional theory developed by Chan (1990). The calculations and comparisons are made for both *V40* and *V60* models. The

comparisons focus on the quality of the results and the influence of the hull distance on the motion responses.

5.3.1 *V40* and *V60* Catamaran Motion Responses

Number of panels = 634

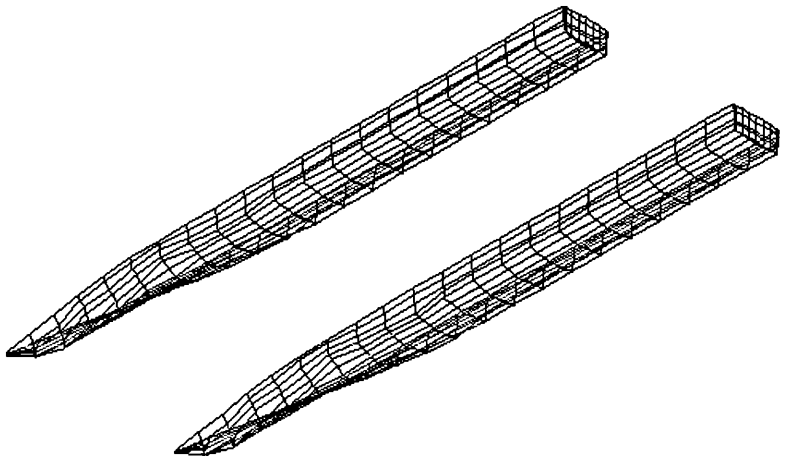

Figure 5.3 – Discretisation of the *V60* model

The discretisation of the catamaran hulls to enter as an input in the three-dimensional software is presented in Figure 5.3.

The number of panels of the twin hulls is 634. Both models (*V40* and *V60*) use the same number of panels and the only difference between them is the separation of the hulls.

2D, 3D Results vs Experimental Results

The following figures compare two and three-dimensional results with experimental results. The *V40* results are presented in Figure 5.4 to Figure 5.11 while the *V60* results are presented from Figure 5.12 to Figure 5.19.

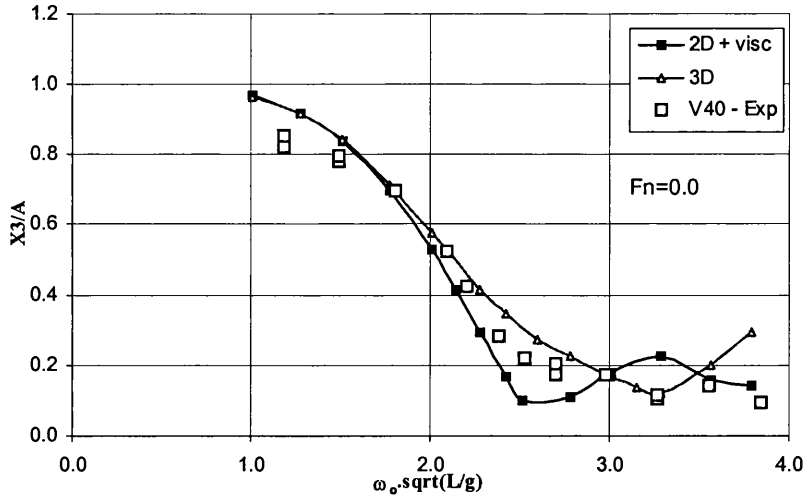

Figure 5.4 – 2D, 3D and Experimental Heave motion at *Fn*=0.0, *V40* model

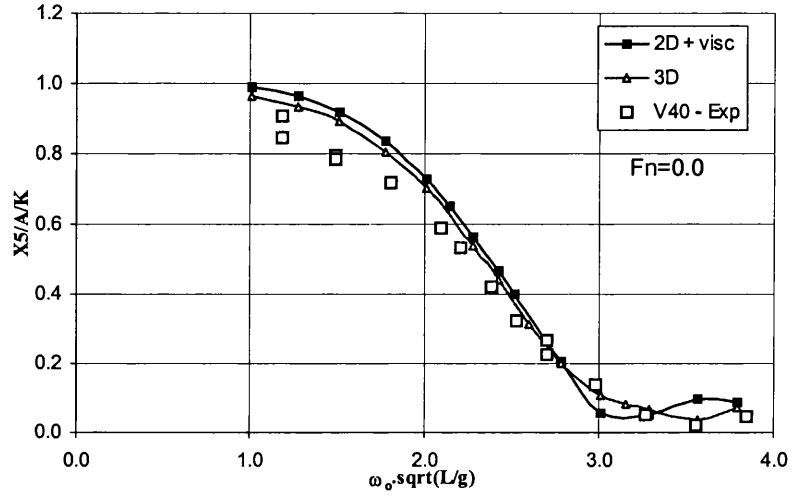

Figure 5.5 – 2D, 3D and Experimental Pitch motion at *Fn*=0.0, *V40* model

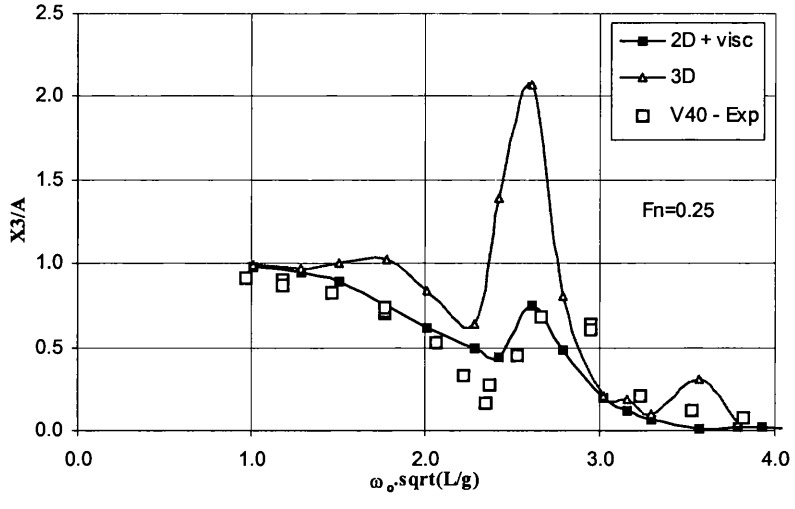

Figure 5.6 – 2D, 3D and Experimental Heave motion at *Fn*=0.25, *V40* model

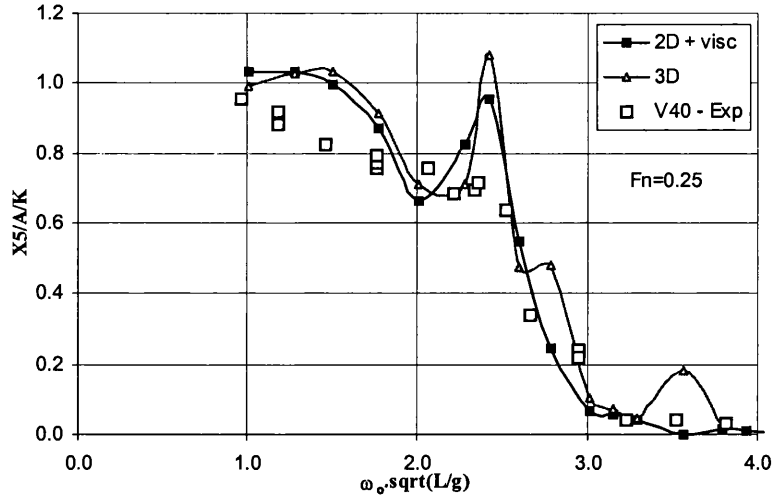

Figure 5.7 – 2D, 3D and Experimental Pitch motion at *Fn*=0.25, *V40* model

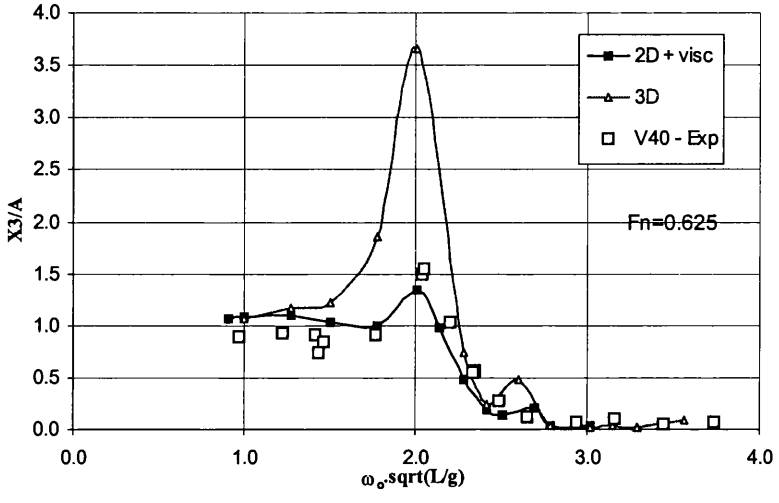

Figure 5.8 – 2D, 3D and Experimental Heave motion at *Fn*=0.625, *V40* model

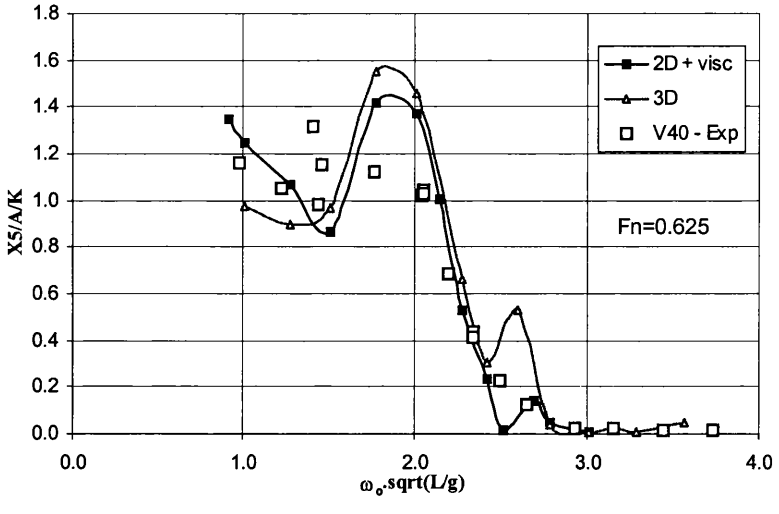

Figure 5.9 – 2D, 3D and Experimental Pitch motion at *Fn*=0.625, *V40* model

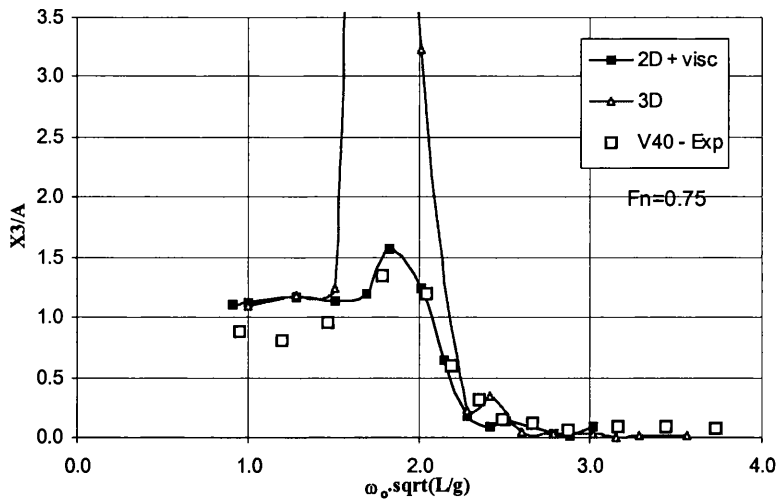

Figure 5.10 – 2D, 3D and Experimental Heave motion at *Fn*=0.75, *V40* model

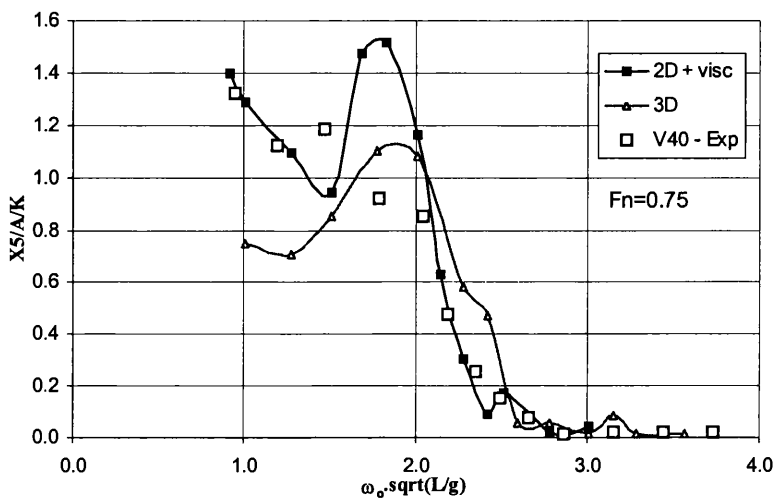

Figure 5.11 – 2D, 3D and Experimental Pitch motion at *Fn*=0.75, *V40* model

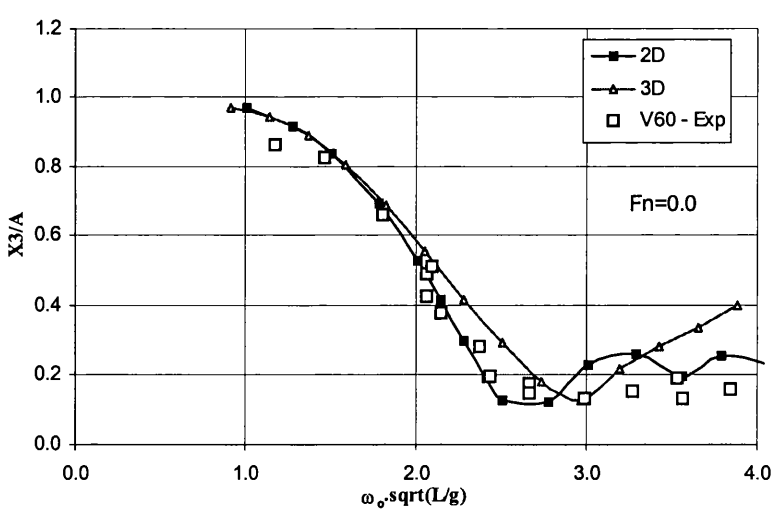

Figure 5.12 – 2D, 3D and Experimental Heave motion at *Fn*=0.0, *V60* model

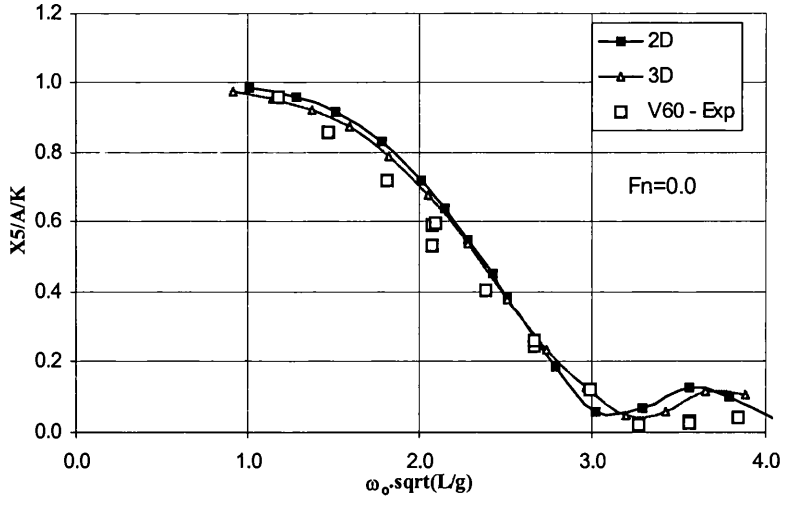

Figure 5.13 – 2D, 3D and Experimental Pitch motion at *Fn*=0.0, *V60* model

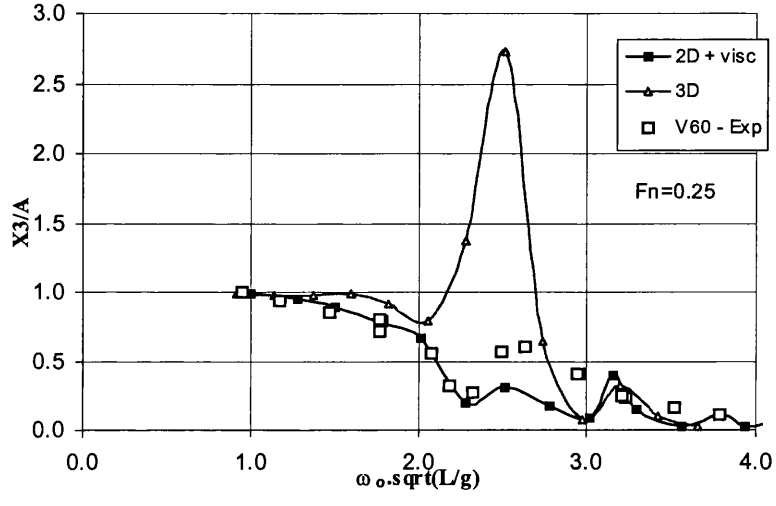

Figure 5.14 – 2D, 3D and Experimental Heave motion at *Fn*=0.25, *V60* model

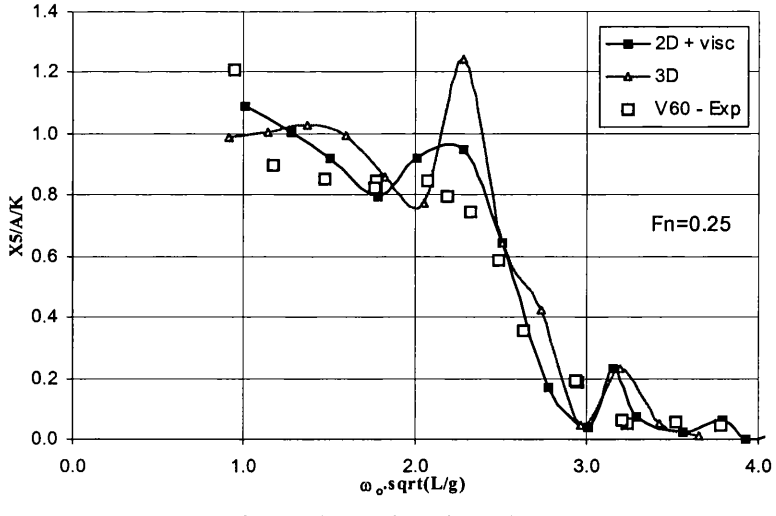

Figure 5.15 – 2D, 3D and Experimental Pitch motion at *Fn*=0.25, *V60* model

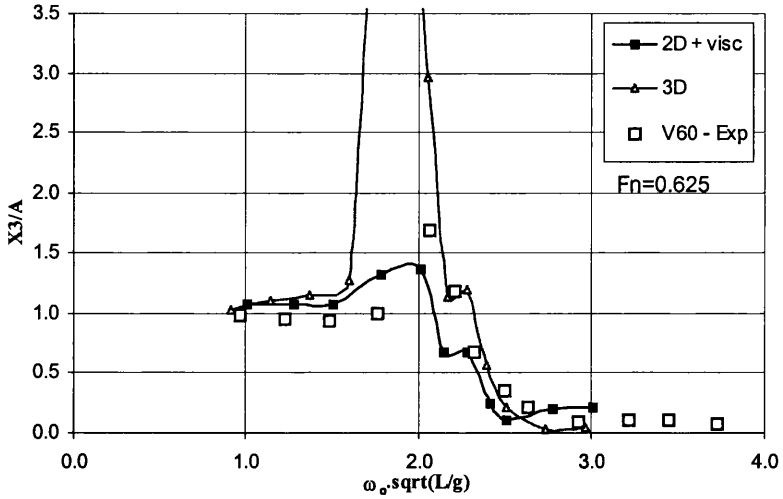

Figure 5.16 – 2D, 3D and Experimental Heave motion at *Fn*=0.625, *V60* model

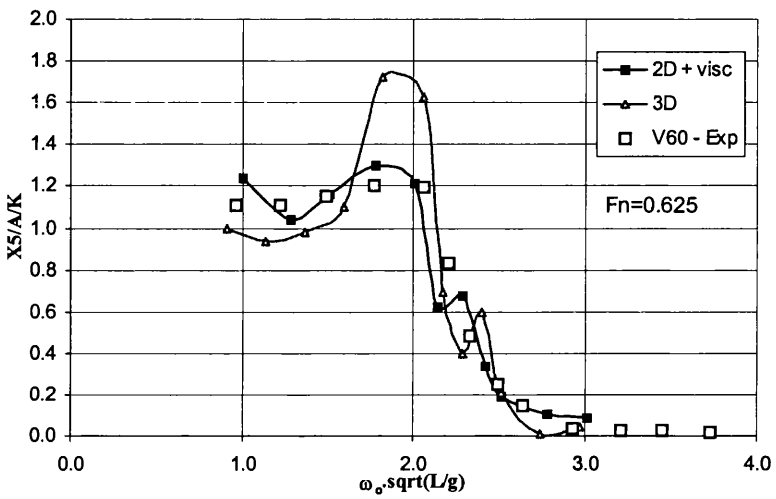

Figure 5.17 – 2D, 3D and Experimental Pitch motion at *Fn*=0.625, *V60* model

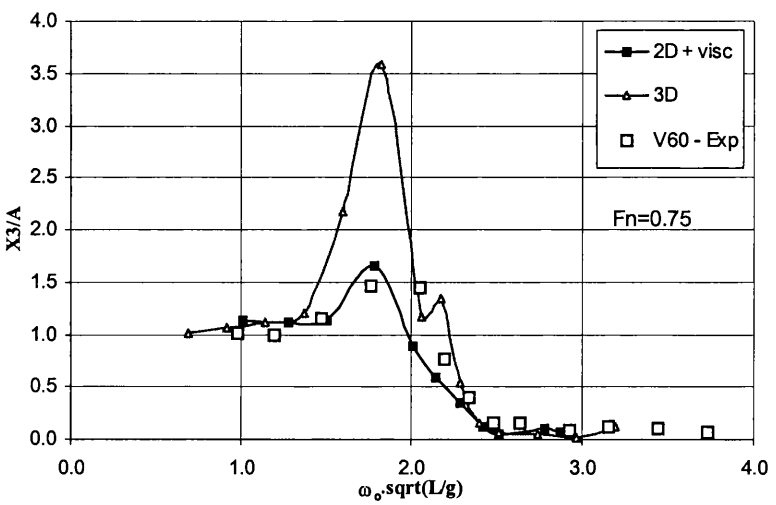

Figure 5.18 – 2D, 3D and Experimental Heave motion at *Fn*=0.75, *V60* model

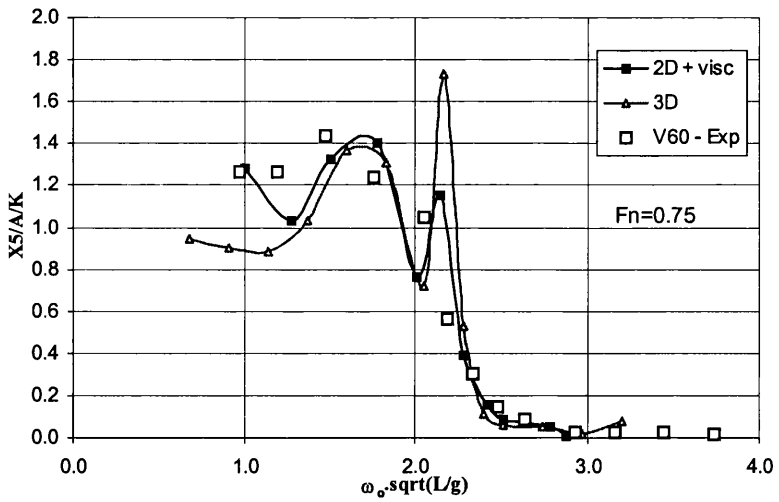

Figure 5.19 – 2D, 3D and Experimental Pitch motion at *Fn*=0.75, *V60* model

The three-dimensional results at zero speed agree very well with the experimental results. In the *V40* model the 3D results agree even better than the two-dimensional results.

At forward speed the 3D heave responses near the first resonance frequency always over-predict the experimental results. The over-prediction of the 3D heave motion calculations near the first natural frequency happens because that theory is also based on potential flow and as explained in section 3.3 the viscous effects are not properly considered in potential flow theory. The over-predicted peaks increase drastically at higher speeds. Curiously, on the other hand the 3D pitch amplitude responses are quite well predicted and in many cases they are very similar to the 2D calculations.

At forward speed, almost every theoretical heave and pitch response amplitude operators show two resonance peaks. The lower frequency peak is due to the first natural frequency and is easily determined by equation (5.19) or by a more precise way through equation (5.20). The second peak is due to the theoretical symmetric interaction as explained in section 5.2.2.

Table 5.1 presents the theoretical non-dimensional symmetric resonance frequencies for both *V40* and *V60* models.

	V40		V60	
Fn	ω_e [rad/s]	ω_o.sqrt(L/g)	ω_e [rad/s	ω_o.sqrt(L/g)
0.00	15.95	7.3	11.80	5.4
0.25	15.95	3.8	11.80	3.1
0.625	15.95	2.7	11.80	2.3
0.75	15.95	2.5	11.80	2.1

Table 5.1 – First symmetric resonance frequencies

Both 2D and 3D theoretical predictions show a peak near the symmetric resonance frequency. In the *V60* model at high speeds (Figure 5.16 to Figure 5.19) the symmetric resonance frequency is close to the first natural frequency and the two peaks in the theoretical curves are sometimes difficult to compare with the experimental results. Nevertheless in the *V40* model where the symmetric resonance frequency is higher, the two peaks are apart and easily identifiable and it is evident that in the experimental results there is no second peak. This is even more obvious in the figures presented in section 4.5 where the theoretical curve without viscous effects is plotted and the theoretical peaks are more pronounced.

As Hudson et al (1995) suggested, the most likely reason for this discrepancy between the symmetric resonance frequency and the experimental results is that the treatment of forward speed effects in the theoretical methods is inadequate.

V40 vs *V60* experimental results

A comparative analysis of the motion responses of both experimental models is performed. The next figures (Figure 5.20 to Figure 5.27) compare the heave and pitch experimental responses of the *V40* and *V60* models at different speeds.

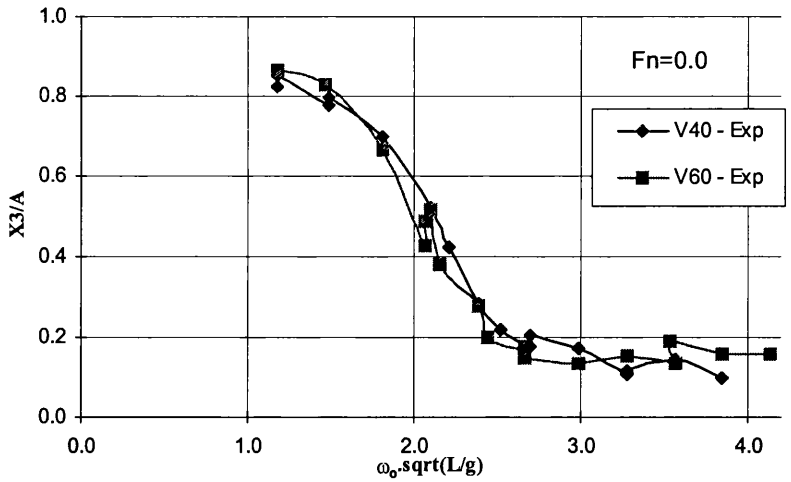

Figure 5.20 –Experimental Heave motion at *Fn*=0.0, *V40* and *V60* models

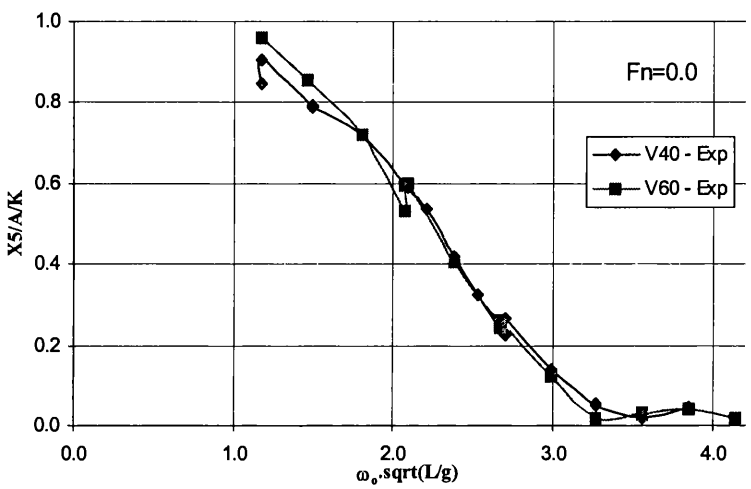

Figure 5.21 –Experimental Pitch motion at *Fn*=0.0, *V40* and *V60* models

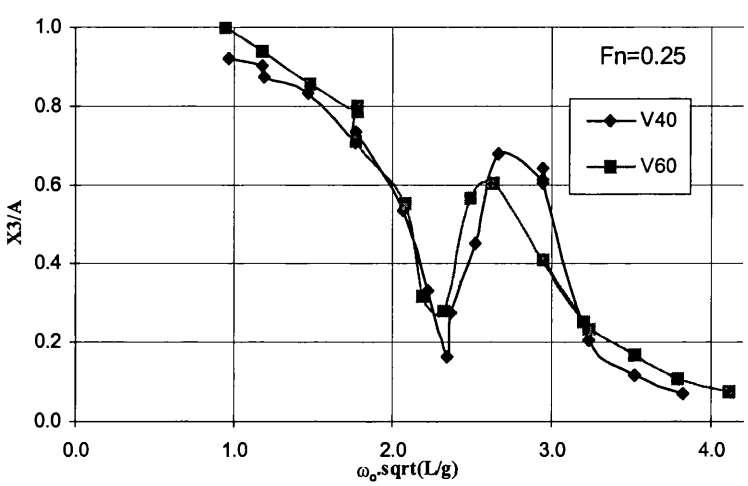

Figure 5.22 –Experimental Heave motion at *Fn*=0.25, *V40* and *V60* models

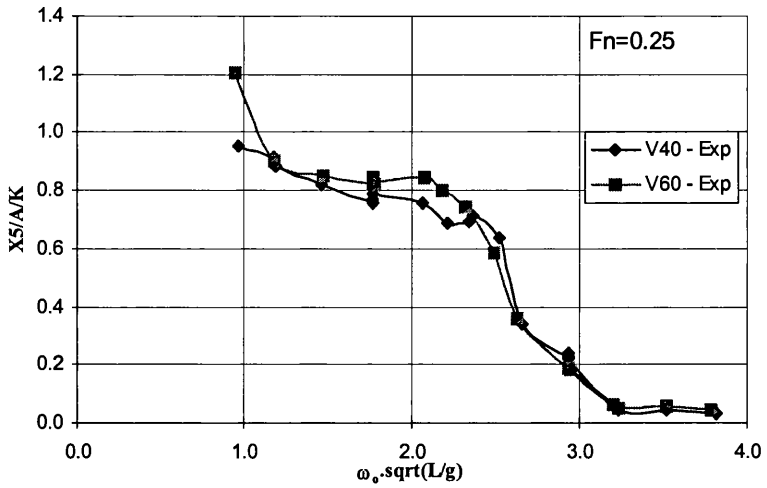

Figure 5.23 –Experimental Pitch motion at *Fn*=0.25, *V40* and *V60* models

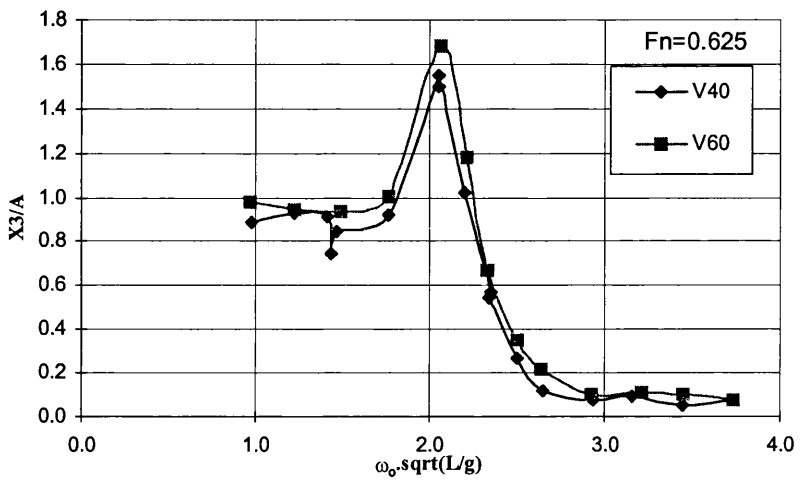

Figure 5.24 –Experimental Heave motion at *Fn*=0.625, *V40* and *V60* models

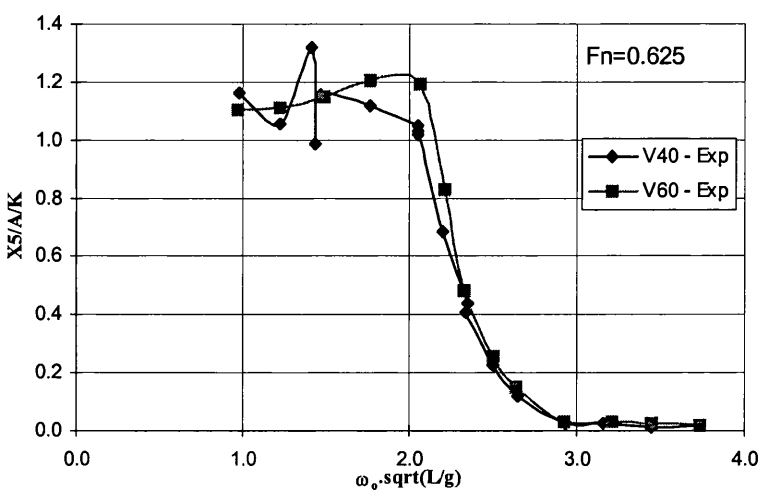

Figure 5.25 –Experimental Pitch motion at *Fn*=0.625, *V40* and *V60* models

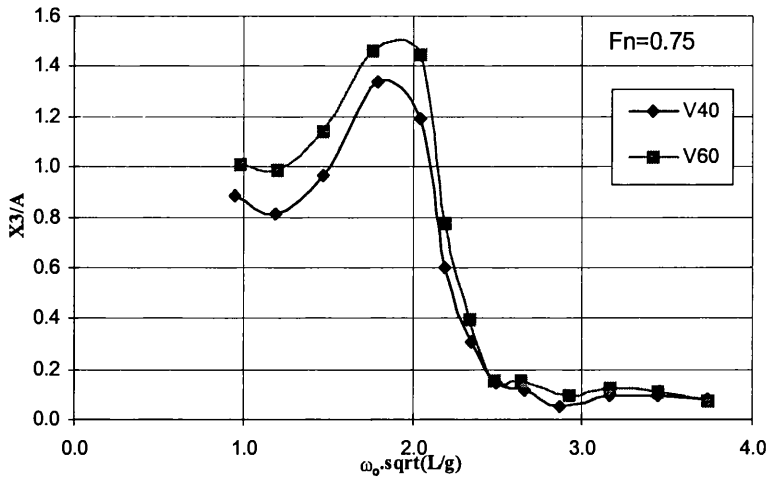

Figure 5.26 –Experimental Heave motion at *Fn*=0.75, *V40* and *V60* models

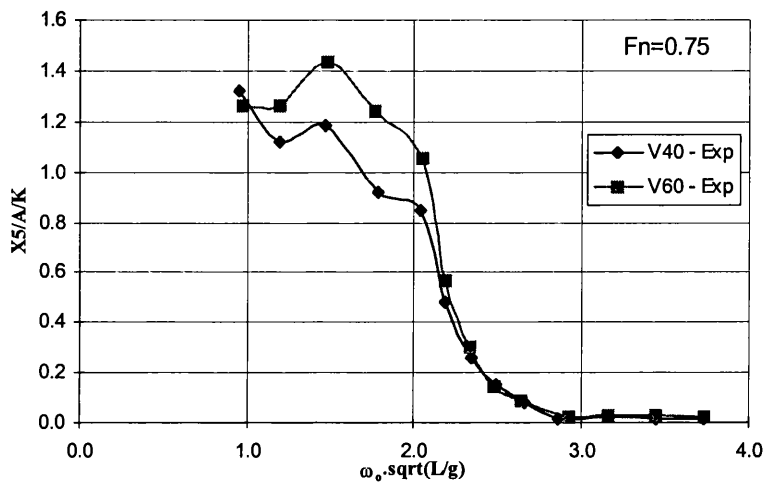

Figure 5.27 –Experimental Pitch motion at *Fn*=0.75, *V40* and *V60* models

The comparison of the experimental results of the two models show that the heave and pitch transfer functions of both models have a similar shape, and that there are no special peaks resulting from the different hull spacing and symmetric resonance frequencies. What the comparison shows is that at the first natural peak and at high speeds (*Fn=0.625* and *Fn=0.75)*, there is a slight tendency to get larger response amplitudes in the *V60* experimental results than in the *V40* results. At *Fn=0.25* the *V60* heave response amplitude at the resonance peak is smaller than the *V40* response.

At *Fn*=0.625 and at the resonance peak the *V60* model heave amplitude is 9% higher than the response amplitude of the *V40* model. At the same speed, the pitch response amplitude is 15% higher than the *V40* response. At *Fn*=0.75 the differences are even

larger, the *V60* heave amplitude is 11% higher than the *V40* and the pitch amplitude is 20% higher.

At high speeds and high frequencies the response amplitudes are small and almost equal for both models. This result agrees with the no interference assumption made in section 5.2. The next section analyses this point in more detail through the comparison made between the experimental results from the catamaran models and some theoretical calculations made with a mono-hull equal to one of the catamaran demi-hull.

At zero speed both models have very similar responses. Since the range of wave frequencies tested $\left(1 < \omega_0\sqrt{L/g} < 4\right)$ do not reach the theoretical symmetric resonance frequency $\left(\omega_0\sqrt{L/g} \approx 5.4\right.$ in the *V40* model and $\omega_0\sqrt{L/g} \approx 7.3$ in the *V60* model) it is difficult to assess and compare with the phenomenon studied and observed in the twin-cylinders configuration (section 3.6). The only conclusion is that at zero speed and for usual catamaran dimensions the so-called symmetric resonance interference is not important because of the extremely high frequency at which the phenomenon occurs.

V40, V60 experimental results vs mono-hull theoretical results

Figure 5.28 to Figure 5.31 present the comparison between the experimental results of both models and the calculated response of a mono-hull with the same body plan of a demi-hull of the catamaran models. The purpose of this comparison is to check the validity of the assumption of no hull interference at high speeds and high frequencies as explained before in section 5.2.

Table 5.2 presents for both models at Fn=0.625 and Fn=0.75 the theoretical encounter frequency where the hull interference starts to vanish according to section 5.2, eq(5.18). The frequencies in Table 5.2 are presented in the dimensional form and also in the non-dimensional form usually used in the figures.

	V40 model		V60 model	
Fn	ω_e [rad/s]	ω_o.sqrt(L/g)	ω_e [rad/s]	ω_o.sqrt(L/g)
0.625	-	-	16.4	2.8
0.75	24.6	3.3	13.7	2.3

Table 5.2 – Hull interference frequency limit.

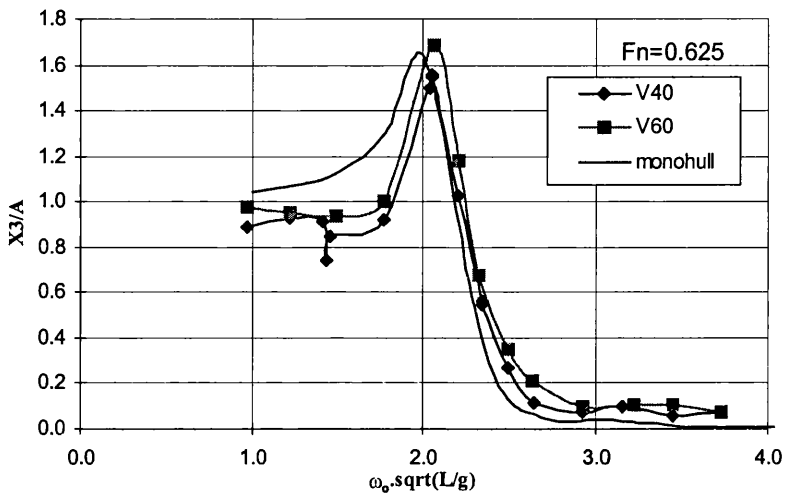

Figure 5.28 –Heave motion at *Fn*=0.625, Mono-hull versus *V40* and *V60* models

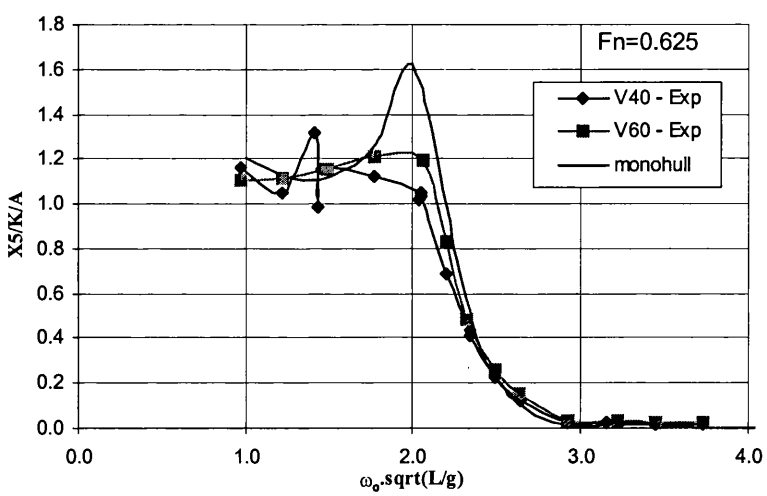

Figure 5.29 –Pitch motion at *Fn*=0.625, Mono-hull versus *V40* and *V60* models

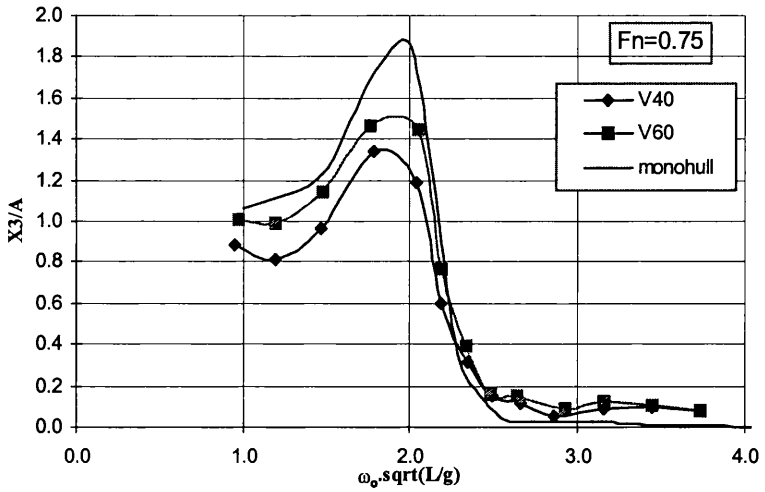

Figure 5.30 –Heave motion at *Fn*=0.75, Mono-hull versus *V40* and *V60* models

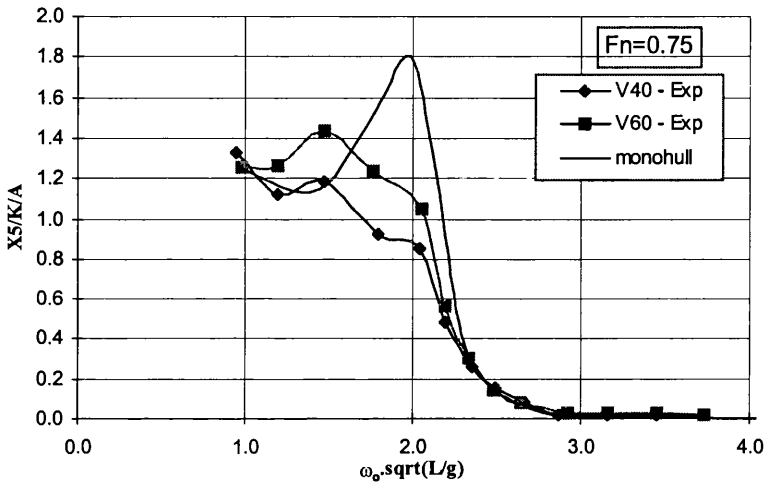

Figure 5.31 –Pitch motion at *Fn*=0.75, Mono-hull versus *V40* and *V60* models

From the foregoing figures at high speeds (*Fn*=0.625 and *Fn*=0.75) it is observed that after a certain frequency (Table 5.2) the heave and pitch response operators are similar to the mono-hull theoretical response. As expected, the frequency at which that occurs decreases with the increase of forward speed. These results give confidence to say that in head waves the interference between the hulls is small after a certain speed, wave frequency and hull spacing and we can also say that under these conditions the catamaran response is similar to a mono-hull.

5.4 *Parametric Study of Vosper Catamaran Motions in Regular Waves*

In this section a parametric study of catamaran motions in regular waves is done. This study is performed after having shown in section 4.5.1 the good agreement between the experimental results and the theoretical results obtained with the two-dimensional theory with the viscous effects incorporated.

The study is performed by changing the distance between the hulls and the ship draught. In this comparison three different hull spacing are used: the already studied *V40* and *V60* models plus a new wider configuration (*V80* model) with 80 cm between the two hulls centre lines. The *V80* model has a *L/B* ratio of 2.14, which is a very small ratio when compared with the other configurations (see Table 4.1).

Besides the different hull spacing, two different draughts were also compared, the experimental draught (*T=0.085 m)* and a smaller one equal to *T=0.075 m.*

5.4.1 Heave and Pitch Theoretical Results of the *V40, V60* and *V80* Models at *T=0.085 m*

Figure 5.32 up to Figure 5.39 show the two dimensional theoretical results with the viscous effects included of the *V40, V60* and *V80* models at draught *T=0.085m.*

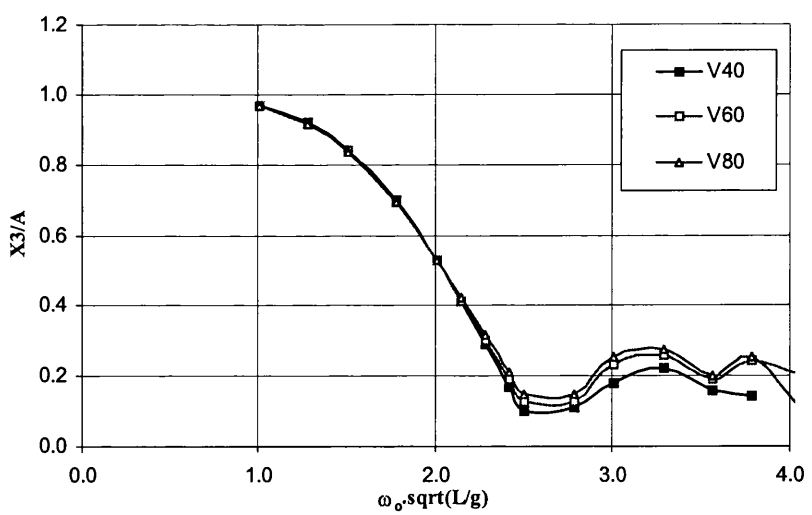

Figure 5.32 –Heave motion at *Fn*=0.0, *V40 V60* and *V80* models (*T=0.085m)*

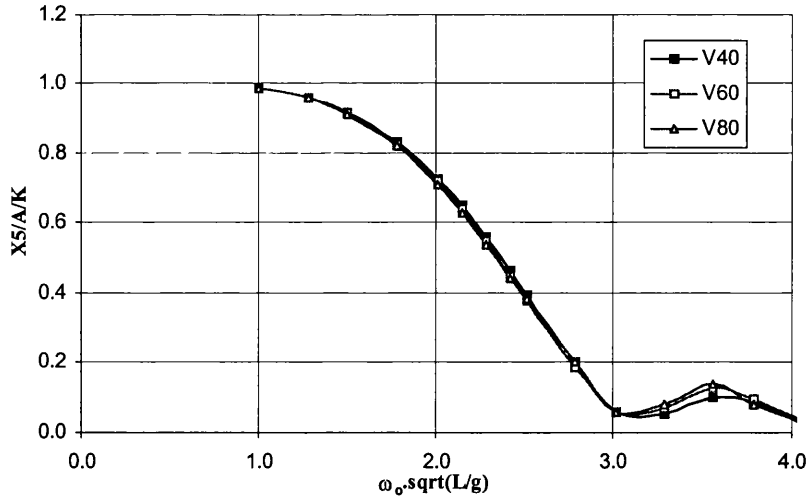

Figure 5.33 –Pitch motion at *Fn*=0.0, *V40 V60* and *V80* models (*T=0.085m)*

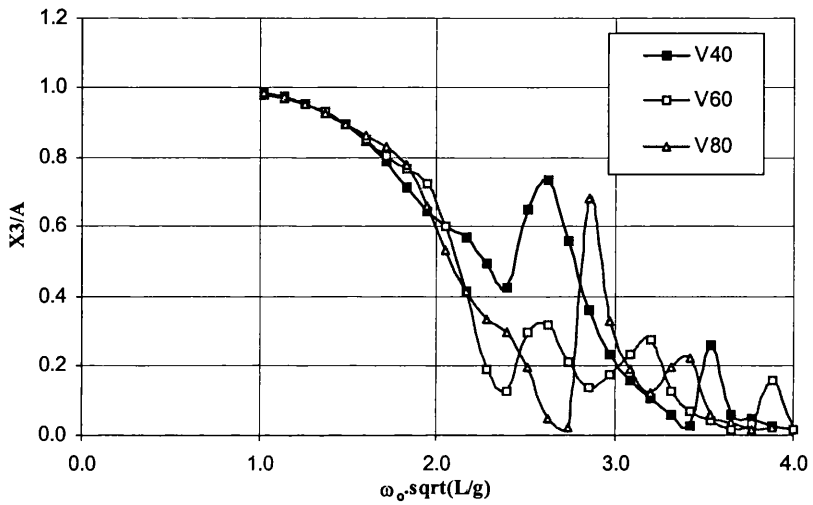

Figure 5.34 –Heave motion at *Fn*=0.25, *V40 V60* and *V80* models (*T=0.085m)*

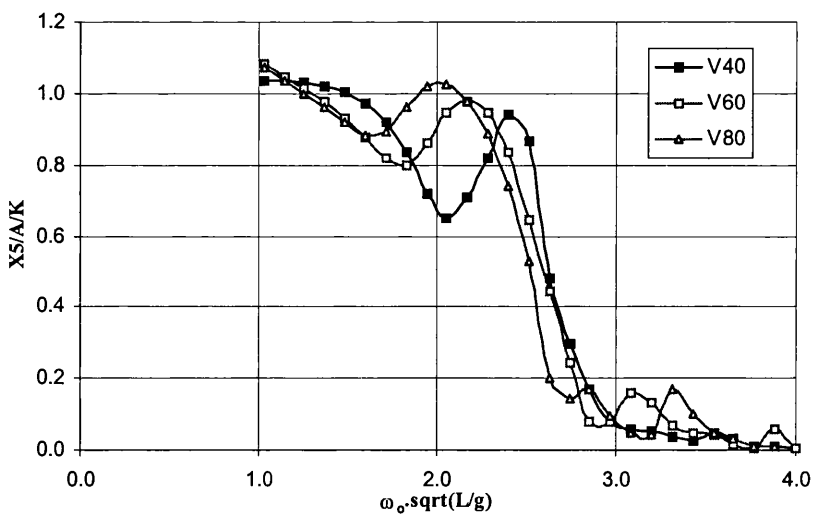

Figure 5.35 –Pitch motion at *Fn*=0.25, *V40 V60* and *V80* models (*T=0.085m)*

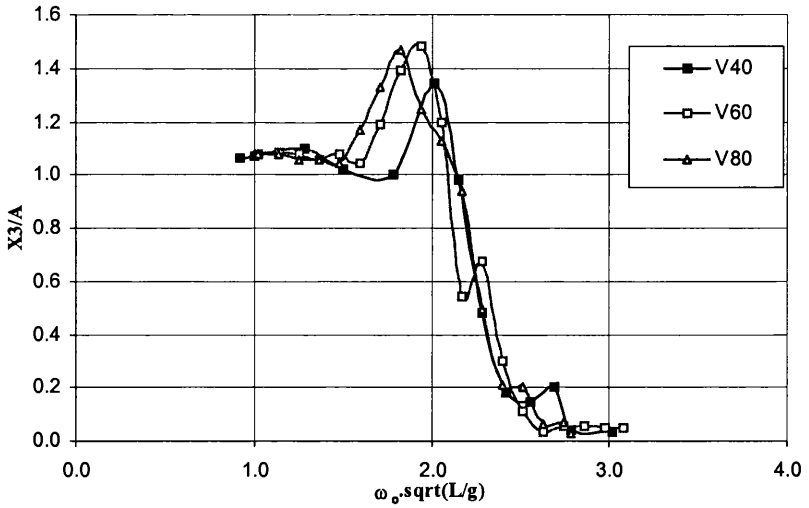

Figure 5.36 –Heave motion at *Fn*=0.625, *V40 V60* and *V80* models (*T=0.085m)*

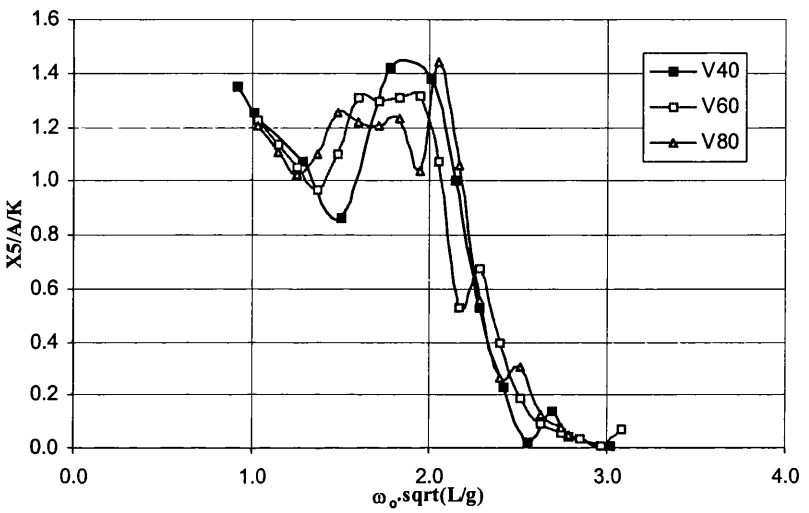

Figure 5.37 –Pitch motion at *Fn*=0.625, *V40 V60* and *V80* models (*T=0.085m)*

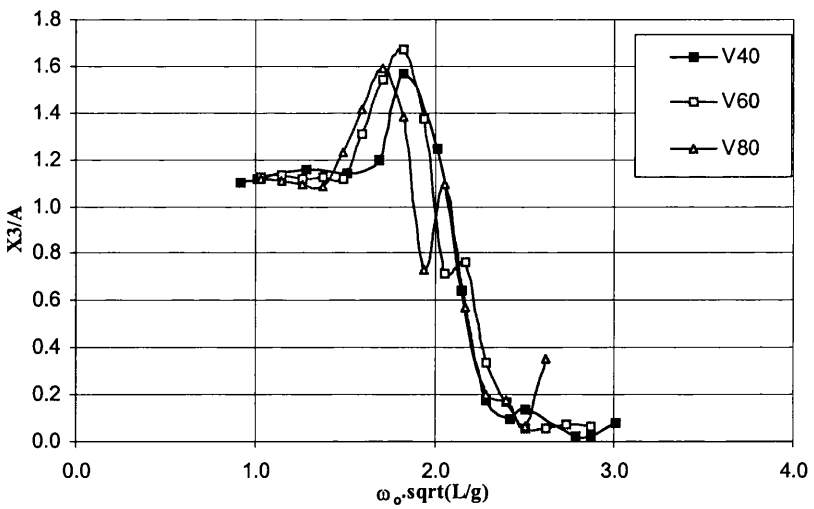

Figure 5.38 –Heave motion at *Fn*=0.75, *V40 V60* and *V80* models (*T=0.085m)*

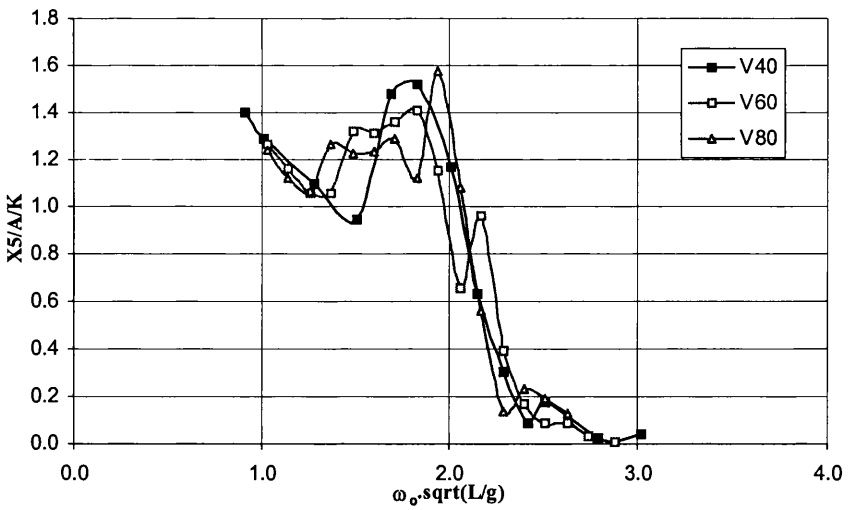

Figure 5.39 –Pitch motion at *Fn*=0.75, *V40, V60* and *V80* models (*T=0.085m)*

The comparison of the theoretical heave responses between the models shows higher responses on the *V60* model, especially at high Froude numbers (*Fn=0.625* and *Fn=0.75*) as in the experimental results. The quantitative differences between the peak amplitudes of the calculated responses of the two models (*V40* and *V60*) are not so high as in the experimental results but the difference still exists. At Fn=0.625 the heave motion difference is 4% and at Fn=0.75 the difference is 6%. This similar tendency between the experimental and theoretical results also shows the good agreement between the theoretical results and the physical reality.

The pitch theoretical results of the *V60* model at high Froude numbers agree very well with the experiments but the *V40* calculations do not agree so well.

At zero speed the differences between the theoretical results are minimum and all responses agree very well with the experimental results (Figure 5.20 and Figure 5.21).

The comparisons between the heave experimental results show that the *V40* model, at Fn=0.25 (Figure 5.22) has higher peak amplitude at the first resonance frequency than the *V60* model. This response is also predicted by the theoretical calculations (Figure 5.34).

The comparison of the theoretical results of all three configurations show that at high speeds the peak amplitudes of the heave motion are higher on the *V60* configuration while the *V40* and *V80* have almost the same peak amplitudes but at slightly different wave frequencies. On the other hand the pitch responses show higher peak amplitudes

on the *V40* configuration and these peaks decrease with the increase of the hull distance.

5.4.2 Heave and Pitch Theoretical Results of the *V40, V60* and *V80* Models at *T=0.075 m*

Figure 5.40 up to Figure 5.47 show the two-dimensional theoretical results of the *V40, V60* and *V80* models with the viscous effects at a lighter condition where *T=0.075m.*

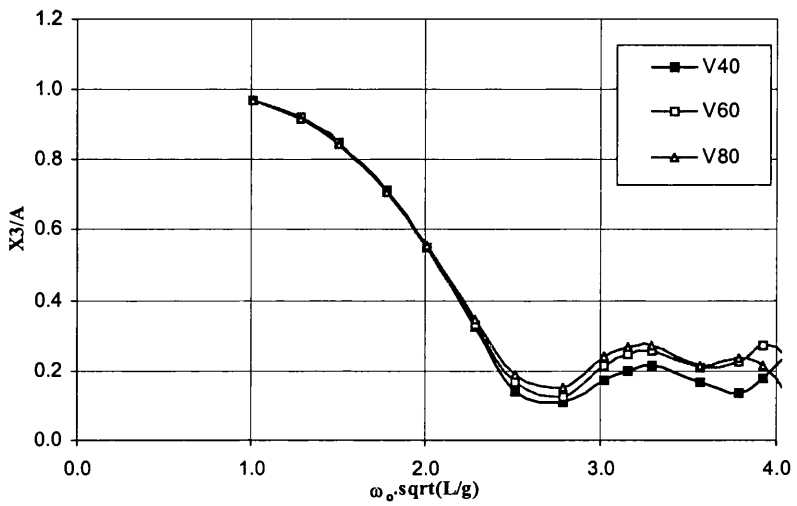

Figure 5.40 –Heave motion at *Fn*=0.0, *V40 V60* and *V80* models (*T=0.075m)*

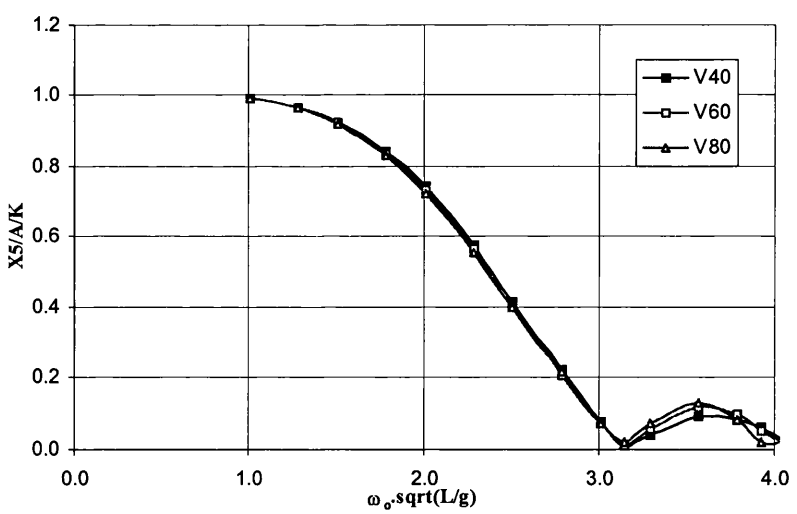

Figure 5.41 –Pitch motion at *Fn*=0.0, *V40 V60* and *V80* models (*T=0.075m)*

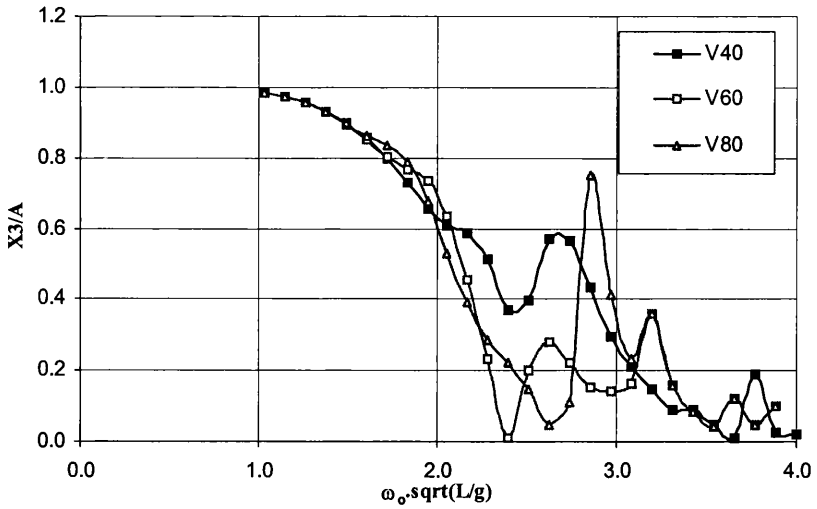

Figure 5.42 –Heave motion at *Fn*=0.25, *V40 V60* and *V80* models (*T=0.075m)*

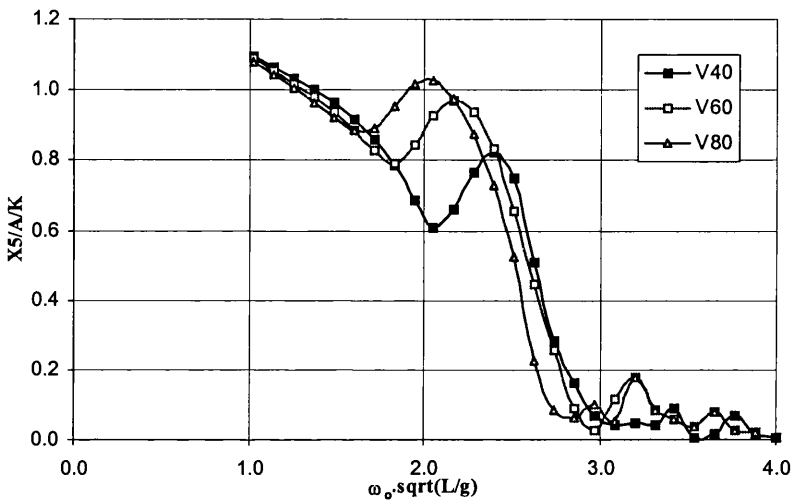

Figure 5.43 –Pitch motion at *Fn*=0.25, *V40 V60* and *V80* models (*T=0.075m)*

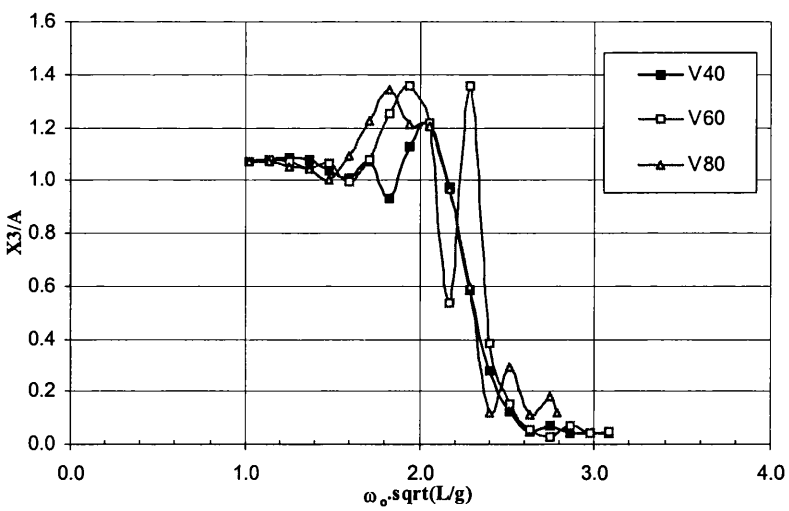

Figure 5.44 –Heave motion at *Fn*=0.625, *V40 V60* and *V80* models (*T=0.075m)*

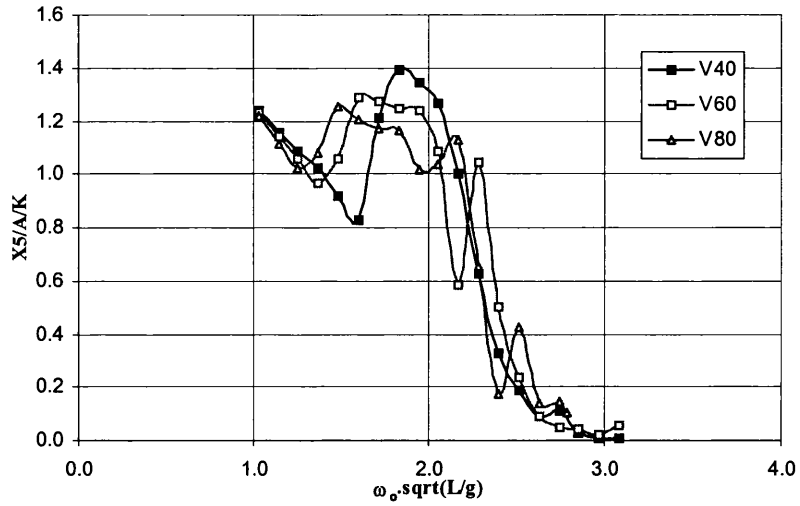

Figure 5.45 –Pitch motion at *Fn*=0.625, *V40 V60* and *V80* models (*T=0.075m)*

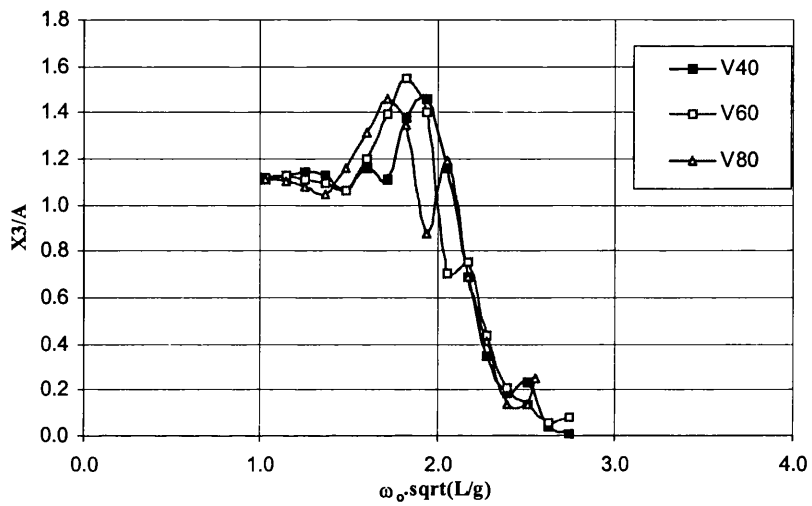

Figure 5.46 –Heave motion at *Fn*=0.75, *V40 V60* and *V80* models (*T=0.075m)*

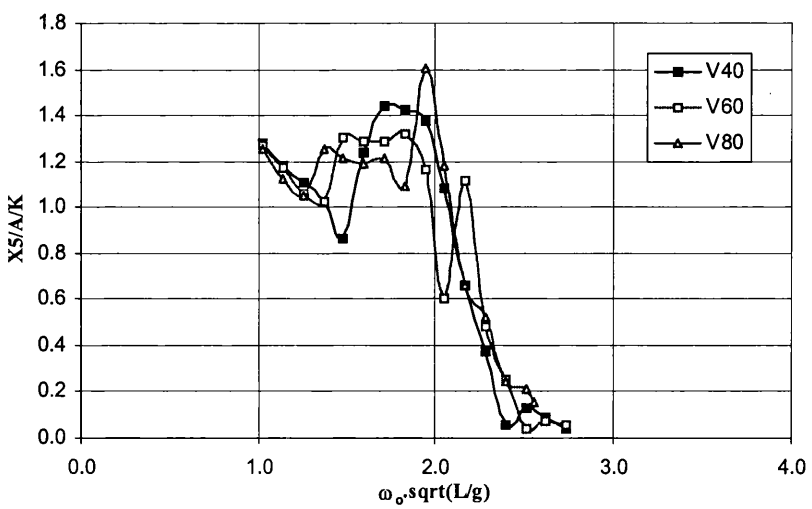

Figure 5.47 –Pitch motion at *Fn*=0.75, *V40 V60* and *V80* models (*T=0.075m)*

Figure 5.40 to Figure 5.47 show that at the lower draught *(T=0.075m)* the ship motion response operators have smaller peak amplitudes than the responses at *T=0.085m* (Figure 5.32 to Figure 5.39). These differences in the peak motion amplitudes are small, and despite the peak differences it is seen that *V40, V60* and *V80* configurations have similar relative results at both draughts.

5.5 Parametric Study of the TransCat Catamaran Motions in Regular Waves

Another parametric study with a different hull was performed. This hull is not a hard-chine type hull like the Vosper catamaran but a round displacement hull. This catamaran is a 45 meters long passenger catamaran operating at Tejo River. The hull form is presented in the figure below.

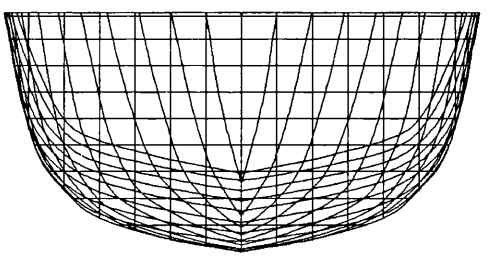

Figure 5. 48 – TransCat body plan

The seakeeping parametric study was performed considering the parent hull at the following condition:

Main Characteristics	
Length overall	45.0 m
Waterline Length	44.25 m
Displacement	175 t
Inter-axis separation	9.0 m
Demi-hull breadth	2.8 m
Draught	1.33 m
Trim	0 deg

Table 5.3 – TransCat main characteristics

The following main design parameters were selected for the parametric study on the seakeeping characteristics:

- main proportion parameters L, B_m and T of the demi-hulls;
- inter-axis separation between the demi-hulls (D);
- ship speed, given by the Froude number

It was further decided to keep the displacement constant at 175 t through this analysis.

In order to efficiently generate in an automatic way the model for each parametric variation the ship dimension were changed in *affinity* relation, that is the co-ordinates x, y, z of the offset of the Parent Hull were uniformly stretched by a proper scale factor along the three directions:

$$x' = \alpha \cdot x$$
$$y' = \beta \cdot y$$
$$z' = \gamma \cdot z$$

This means that global form parameters such as C_B, C_p, and C_M are not changed by these variations. The requirement of constant displacement implies that:

$$\alpha \cdot \beta \cdot \gamma = 1$$

It was thus decided to consider α and β as independent parameters and let γ vary consequently as $\gamma = 1/(\alpha \cdot \beta)$.

The parametric variations were considered according to Table 5.4 shown below.

Parameter	***Value***		
α	0.8	1.0	1.2
β	0.8	1.0	1.2
D	7m	9m	11m
Fn	0.0	0.25	0.62

Table 5.4 – TransCat Parametric variations

The results of the seakeeping calculations are presented in terms of XY graphs of the non-dimensional heave response operator $X_3/WaveAmpl$ and non-dimensional pitch

response operator $X_5/WaveAmpl/K$ versus the non-dimensional wave frequency $\omega_0 sqrt(L/g)$.

The legends on the figures indicate the ship variant. The following table presents all the ships variants with the distance between the hulls and their α and β values:

D=9m			D=7m			D=11m		
Ship	α	β	**Ship**	α	β	**Ship**	α	β
11	0.8	0.8	21	0.8	0.8	31	0.8	0.8
12	0.8	1.0	22	0.8	1.0	32	0.8	1.0
13	0.8	1.2	23	0.8	1.2	33	0.8	1.2
14	1.0	0.8	24	1.0	0.8	34	1.0	0.8
15-Parent hull	1.0	1.0	25	1.0	1.0	35	1.0	1.0
16	1.0	1.2	26	1.0	1.2	36	1.0	1.2
17	1.2	0.8	27	1.2	0.8	37	1.2	0.8
18	1.2	1.0	28	1.2	1.0	38	1.2	1.0
19	1.2	1.2	29	1.2	1.2	39	1.2	1.2

Table 5.5 – TransCat ship variant legend

Only the results that are important to make some conclusions are presented in this section in the following figures.

The way L, B_m and T parameters influence the ship responses do not change with the distance between the hulls i.e. the same effect is observed even if is magnitude is different. So to study the influence of those parameters only the original hull separation results will be analysed, which means D = 9.0m (Ship *15*).

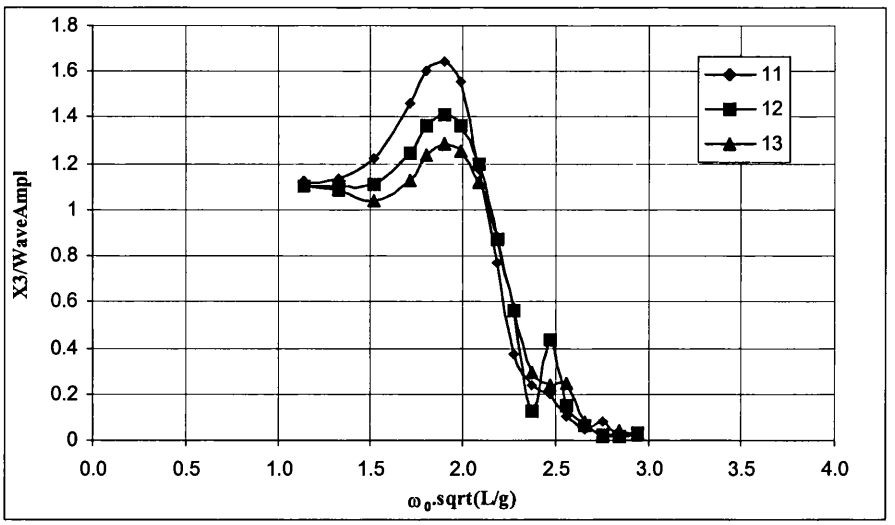

Figure 5.49 - Heave motion; α=0.8 at Fn=0.62 in head waves

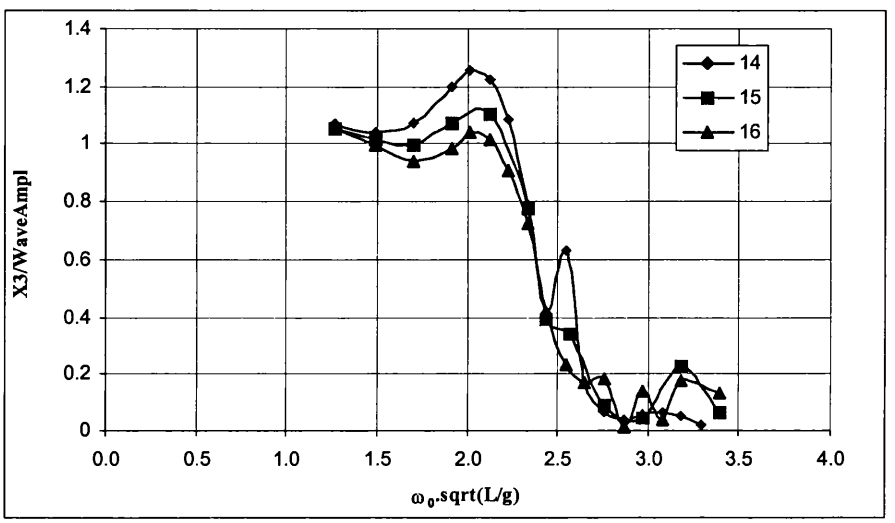

Figure 5.50 - Heave motion; α=1.0 at Fn=0.62 in head waves

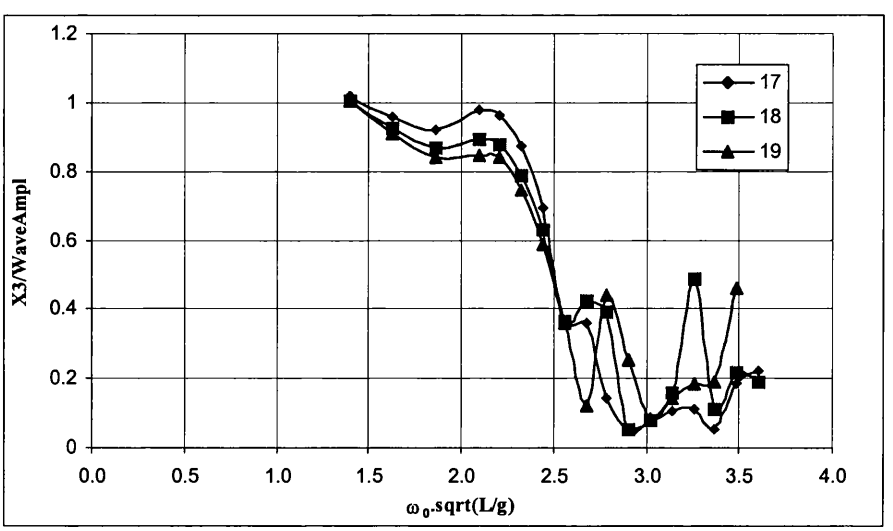

Figure 5.51 - Heave motion; α=1.2 at Fn=0.62 in head waves

From Figure 5.49 to Figure 5.51 the ship length was kept constant in each figure but changed from figure to figure (α=0.8 in Figure 5.49, α=1.0 in Figure 5.50 and α=1.2 in Figure 5.51). Analysing these figures, it is seen that when the demi-hull breadth increases and as the draught decreases at constant length, the heave response amplitude at the first resonance peak decreases. This effect is also observed at the other speeds and hull separations but with different strengths.

Comparing Figure 5.49 up to Figure 5.51 it is seen that an increase of ship length, decreases the heave responses at the resonance peaks. This effect is also observed independently of the speed and hull separation.

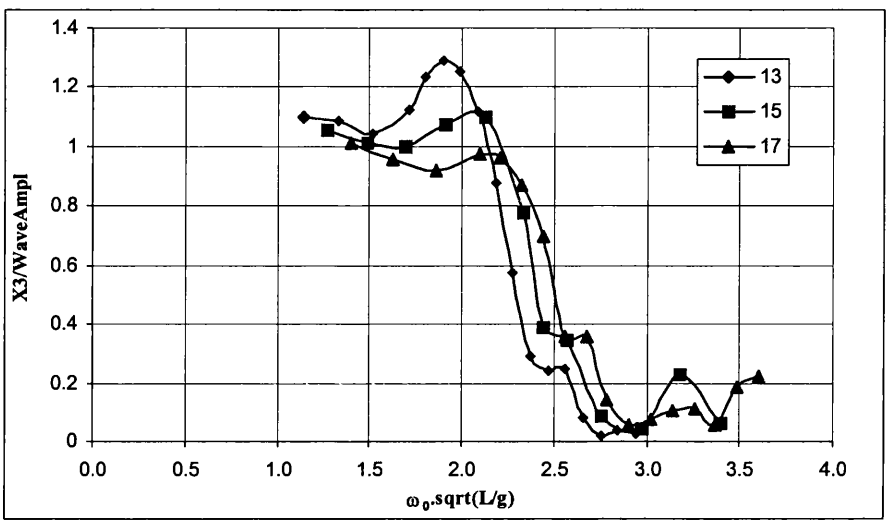

Figure 5.52 - Heave motion; (α=0.8; β=1.2) (α=1.0; β=1.0) (α=1.2; β=0.8) at Fn=0.62 in head waves

The previous Figure 5.52 compares two different aspects: ship length and demi-hull breadth. It shows as before that as ship length increases the heave motion response amplitudes decrease but at the same time the higher the demi-hull breadth the higher the ship response at the first resonance frequency. This means that in these conditions the length is more important than the hull breadth in what concerns heave amplitude responses.

As in the heave motion response case, the following Figure 5.53 to Figure 5.55 show the same kind of relations between the main dimensions and the ship motion amplitudes in pitch motion responses.

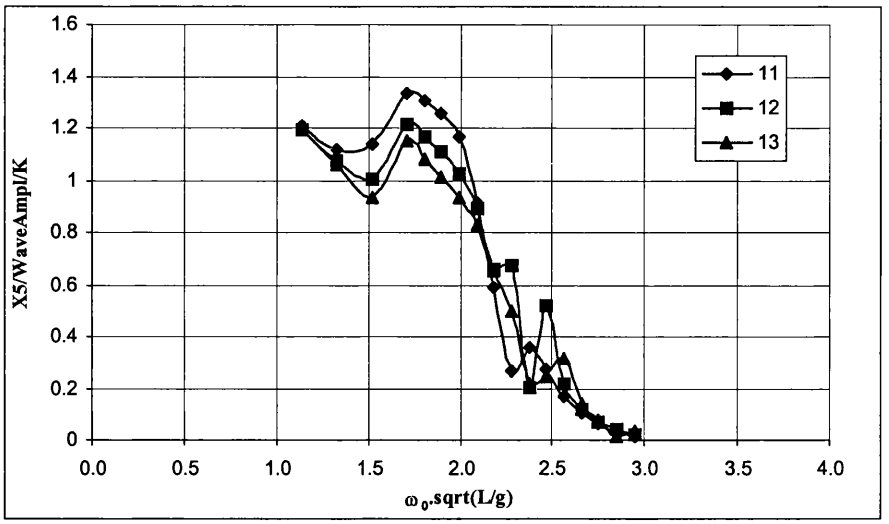

Figure 5.53 - Pitch motion; α=0.8 at Fn=0.62 in head waves

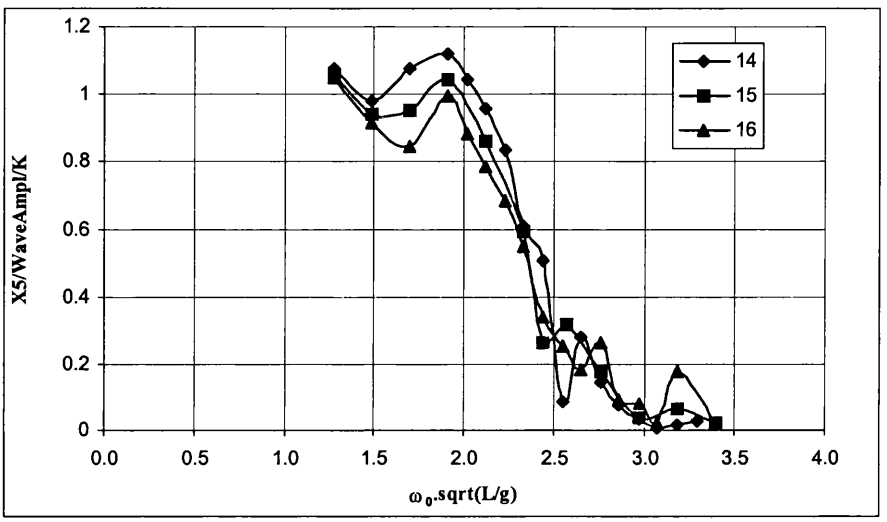

Figure 5.54 - Pitch motion; α=1.0 at Fn=0.62 in head waves

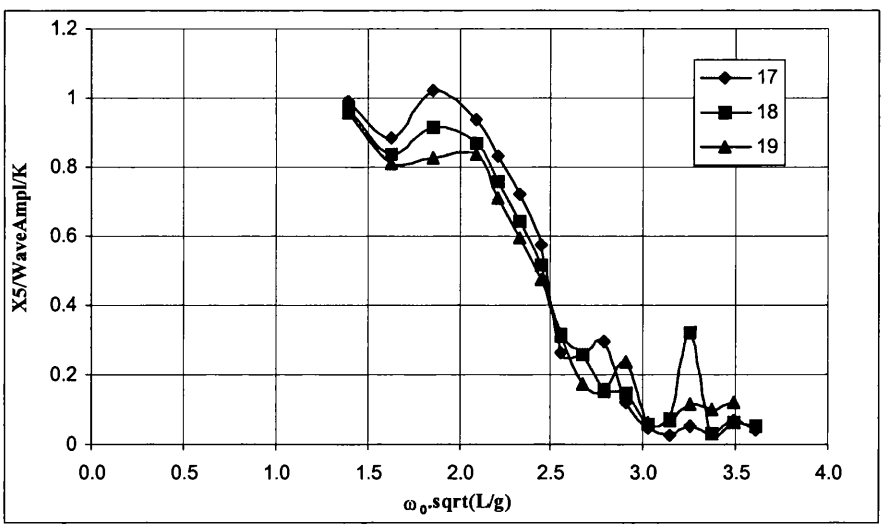

Figure 5.55 - Pitch motion; α=1.2 at Fn=0.62 in head waves

As in the heave case, from Figure 5.53 to Figure 5.55 the length was kept constant in each figure (α=0.8 in Figure 5.53, α=1.0 in Figure 5.54 and α=1.2 in Figure 5.55). Analysing those figures, it can be seen that when the demi-hull breadth increases and the draught decreases, the pitch response amplitude at the first resonance peak decreases. Again, this effect is observed independently of the speed and hull separation.

Comparing Figure 5.53 to Figure 5.55 it can be seen that the increase of the ship length decreases the pitch responses. This effect is also observed independently of the speed and hull separation.

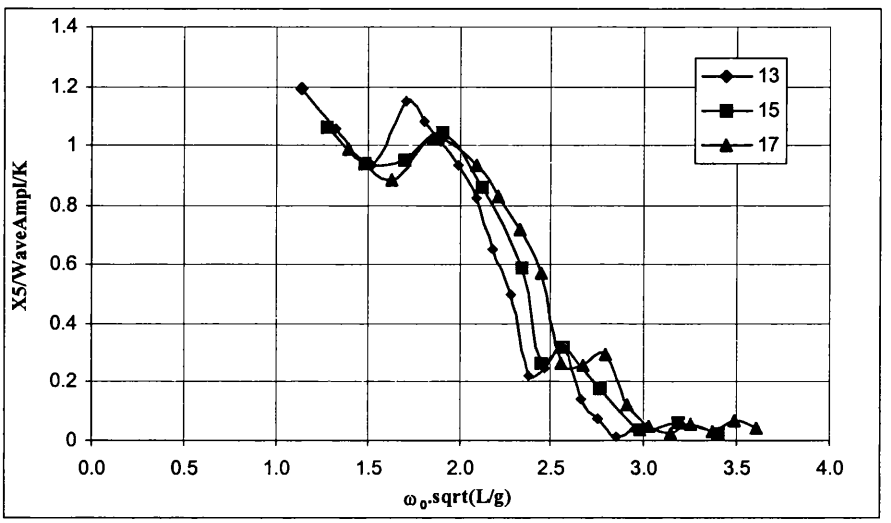

Figure 5.56 - Pitch motion; (α=0.8; β=1.2) (α=1.0; β=1.0) (α=1.2; β=0.8) at Fn=0.62 in head waves

As in the heave analysis, Figure 5.56 shows that the influence of the length is higher than the influence of the demi-hull breath in the pitch response at the resonance frequency.

At zero speed the changes in the responses are small when the main dimensions are changed and the displacement is kept constant. Figure 5.57 shows the heave results at $Fn=0.0$, keeping the same breadth and changing the ship length.

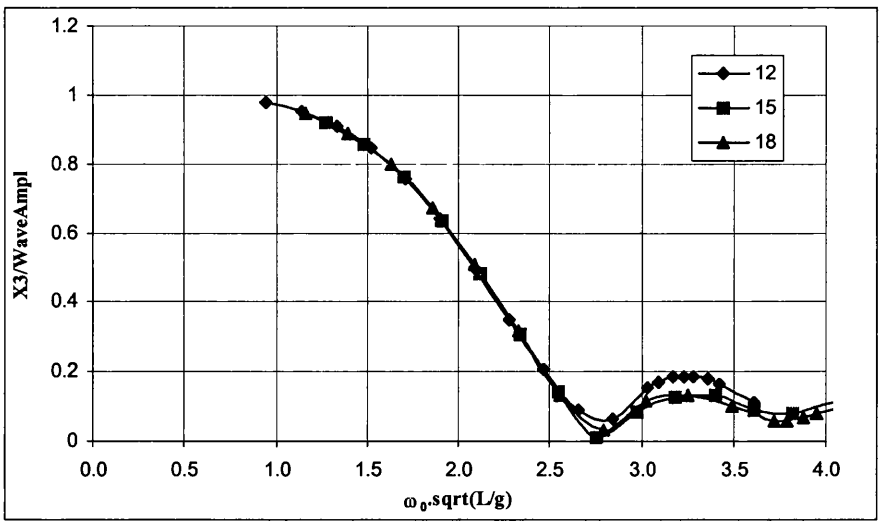

Figure 5.57 - Heave motion; (α=0.8; β=1.0) (α=1.0; β=1.0) (α=1.2; β=1.0) at Fn=0.0 in head waves

Regarding the hull separation effects, three different hull configurations are considered where the *L/B* ratio ranges from 3.2 to 4.5 which is well above the range of ratios considered in Vosper catamaran study (between 2.14 and 3.66). As seen in Figure 5.58 and Figure 5.59, at the TransCat range of ratio, the results have the same nature of the Vosper results at the same range, which in this case includes the *V40* and the *V60* models, because the *V80* model is completely out of the range.

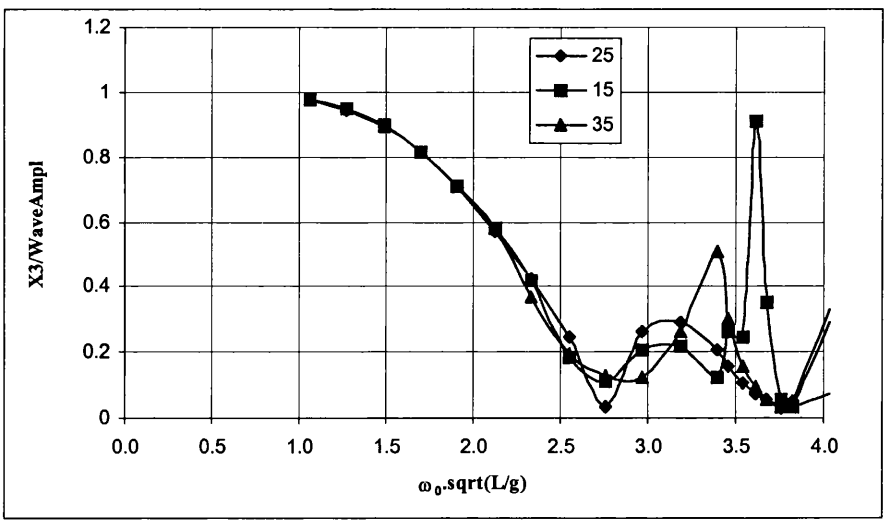

Figure 5.58 - Heave motion; *D=7m*; *D=9m*; *D=11m* (α=1.0; β=1.0) at Fn=0.25 in head waves

Analysing the results it is seen that the wider configuration has slightly higher peak responses at high speed (*Fn=0.62*) while at an intermediate speed (*Fn=0.25*) this is not true. At *Fn=0.25* the ship 35, which is the wider one, and ship 15, the intermediate one, they both have pronounced peaks at the symmetric resonance frequencies but as

explained before these peaks do not happen in the experimental model results so they should not be taken into consideration.

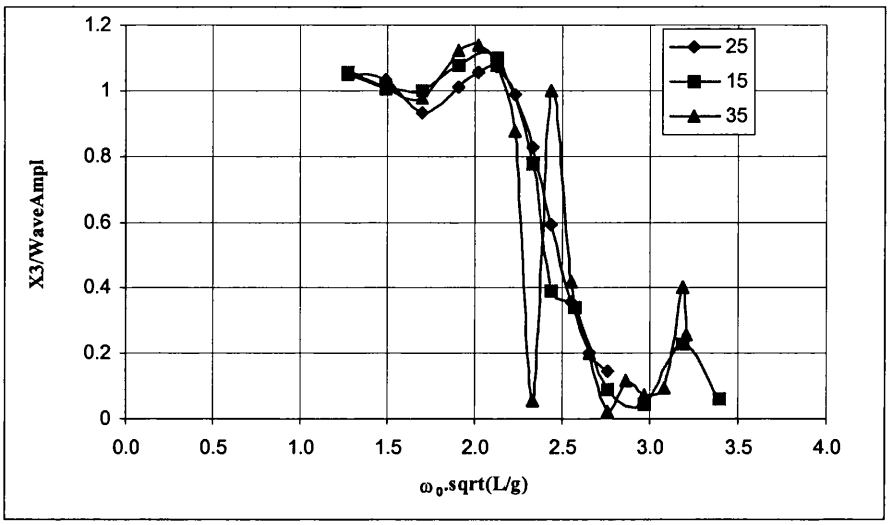

Figure 5.59 - Heave motion; $D=7m$; $D=9m$; $D=11m$ (α=1.0; β=1.0) at Fn=0.62 in head waves

5.6 Conclusions

The results from the two-dimensional theoretical model with viscous effects and the three-dimensional mathematical model based on Chan (1990) work were compared with the experimental results. The two-dimensional results agree well with the experimental results as shown and analysed in the previous chapter. At zero speed both theories give good and similar results to the experimental. At high Froude numbers the three-dimensional results have an over-predicted peak at the first natural frequency. As explained in section 3.3 the potential flow theory used in the three-dimensional approach does not consider the important viscous effects present in the motion of twin-hull ships. This explains the over-prediction of the results in the three dimensional theory.

The experimental and theoretical work performed and analysed in this chapter agrees with the theoretical assumptions presented in section 5.2 concerning the type of interactions that exist between the catamaran hulls. First at zero and very low speeds the interaction between the two hulls is mainly two-dimensional. As speed increases the interference between the hulls becomes three-dimensional because there is a

translation of the waves generated in the forward sections to the aft sections. At high forward speeds the interference vanishes because the waves no longer have time to reach the other hull. This last kind of interaction was confirmed when the two models experimental results were compared with the theoretical calculations of a mono-hull with the same hull form. At the intermediate speed where the three-dimensional effects are bigger, both 2D and 3D theoretical results present a second resonance peak near the first symmetric resonance frequency, but this peak is not present in the experimental results. This leads to the conclusion that the speed effects are not properly modelled by the two-dimensional theory neither by Chan's three-dimensional theory.

The *V40* and the *V60* experimental motion responses were compared this time to show which configuration has lower response amplitudes. At zero speed the experimental heave and pitch response amplitude operators for both models are very similar so in this case the response is independent of the hull distance. At high Froude numbers the *V60* response amplitudes at the natural frequency peaks are slightly higher than the *V40* response amplitudes for both heave and pitch motions. At the intermediate speed ($Fn=0.25$) there are an opposite response and the wider model has lower peak responses than the narrow one. So in this two last cases the response operators are dependent on the hull distance and ship speed.

The parametric study with the Vosper Catamaran was done considering three different hull configurations (*V40, V60* and *V80*) at two different draughts and four different speeds. The theoretical calculations were performed using the two-dimensional mathematical model with the viscous effects. The study showed that the theoretical predictions follow the experimental results. Both experimental and theoretical results show similar relative responses when comparing the *V40* and *V60* models at all speeds. At high forward speeds the peak amplitude of the heave response increase from the *V40* to the *V60* models but at the wider configuration (*V80*) there are a slight decrease of the peak response. On the other hand the pitch theoretical results do not follow this tendency and the responses decrease with the increase of the hull distance. The symmetric resonance peak has a considerable effect on the *V80* pitch result but under the previous considerations made from the experimental results this symmetric peak at forward speed should be ignored.

The comparison between the two draughts showed that the smaller draught ($T=0.075m$) has lower amplitude responses than the higher draught ($T=0.085m$) but the response amplitude functions have the same shape and the same behaviour.

The TransCat parametric study analysed the effect of the main ship dimensions (L, B_m and T) in the motion response operators when the ship displacement was kept constant. It was shown that the ship length is the dominant parameter and the higher the length, the lower is the response peak amplitude. On the other hand at constant length the higher the breadth (lower draught) the lower is the response peak. Comparing at the same range of L/B ratio, the TransCat hull separation results agree with the Vosper catamaran results. It is observed a certain tendency to have at high speeds slightly higher responses at the wider configurations while at lower speeds the opposite is observed.

The TransCat results are qualitative because while in the Vosper catamaran the theoretical results were confirmed by the experiments and so the viscous coefficients were in that case properly set, in the TransCat case there are no experimental results so there is no certainty about the amplitude of the theoretical results obtained.

Chapter 6

Conclusions and Recommendations

The aim of this study was to investigate the hull separation effects and other main characteristics on the catamaran motions through an experimental investigation and also through theoretical calculations. The importance of this study is more and more relevant since the use of catamaran vessels for passenger transportation is increasing every day. The seakeeping characteristics of passenger ships are very important because people nowadays demand for fast, comfortable and safe travels.

The theoretical formulations used in this study are based in a two and three-dimensional potential flow theories.

In the twin-hull vessel configurations the viscous effects are more important than in mono-hull vessels (Lee 1976 and Schellin 1995). In the mono-hull vessels the wave making damping plays a dominant role while in the twin-hull configuration the wave making damping is no longer so dominant and the viscous damping increases its relative importance. When the viscous damping is not considered in the catamaran motion theory the result is an over-prediction of the motion amplitude at the natural frequency peak. To take this into account, the viscous effects were added to the two-dimensional theory through a cross-flow drag approach from aerodynamics theories (Thwaites 1960) and further developed by Lee (1976). After the introduction of these effects the results are much better predicted as shown in chapter 4 where the experimental results were compared with theoretical calculations.

The three-dimensional potential flow theory is based on the work developed by Chan (1990) where the viscous effects were not included in the theory. The three-dimensional calculations were made to analyse how a better three-dimensional model would influence the ship motion results, but in fact the 3D results were not improved the way it was expected especially concerning the forward speed effects.

Two models with different distances between the hulls were tested at the Hydrodynamic Laboratory at the University of Glasgow. The experimental work was

performed to validate the two-dimensional theory with the viscous effects included and also to analyse the influence of the distance between the catamaran hulls in the catamaran motion responses.

Calculations were performed for twin-cylinders and compared with experimental results to show the good quality of the theories used in this work and also to show the symmetric resonance frequencies that exists at zero speed. It is shown that this frequency depends on the inner distance between the hulls. Both two and three-dimensional theoretical results, at forward speed, presented a second resonance peak at the so-called symmetric resonance frequency but the experimental results made in this work did not show any of these peaks. It is believed that this difference between the experimental and the theoretical results is due to an incorrect theoretical characterisation of the forward speed effects. As said before, it was expected that the three-dimensional theory could model these effects but in fact, the 3D results also showed the resonance peak at the symmetric frequency as in the two-dimensional calculations.

The performed experimental and theoretical work agrees with the theoretical assumptions made about the kind of interactions that exist between the catamaran hulls. First at zero and very low speeds the interaction between the two hulls is mainly two-dimensional and is very well predicted by both theories. As speed increases the interference between the hulls becomes three-dimensional because there is a translation of the waves generated in the forward sections to the aft sections. At high forward speeds and high wave frequencies the interference vanishes because the waves no longer have time to reach the other hull. This last kind of interaction was confirmed by comparing the two models experimental results with the theoretical responses of a mono-hull with the same hull form.

The comparison between the experimental results of the two models showed that at high speed there is a slightly higher amplitude of response in the wider catamaran (*V60* model). The differences between the responses of the two models increases as speed increases. On the other hand, at low or intermediate speed *(Fn=0.25)*, the opposite was observed, the higher peak occurs with the narrow model (*V40*). At zero speed both models showed very similar responses.

The symmetric resonance peaks in the theoretical results are not very big and the general behaviour of the calculated heave and pitch RAO match the experimental results, so it can be said that the two-dimensional theory with viscous effects is a good tool to predict catamaran motion responses in waves.

The first parametric study was performed with the Vosper catamaran and the distance between the hulls, the models draught and speed were the changing parameters. Three different hull spacings were considered (*V40, V60* and *V80*) at two different draughts (*T=0.075m* and *T=0.085m*) and four different speeds. From the parametric study some comments regarding the dependence on speed can be formulated. The results showed that at zero speed the responses are similar independently of the hull distance. At moderate speeds the narrow model has higher peak responses at the resonance frequency. At high speeds, it is the intermediate model (*V60*) that has higher responses near the resonance frequency. The decrease of the response amplitude at the wider model can indicate that this model is almost responding as a mono-hull (in fact the *V80* model with the ratio *L/B=2.14* is really a very wide catamaran). From these results it can be said that maybe there is a hull separation that maximise the motion responses at high speeds. However this should be further investigated.

The comparison between the two draughts showed that the smaller one has lower amplitude responses at the resonance peaks than the higher draught but the shape of the response amplitude functions does not change much from one draught to the other.

The second parametric study was performed with a different hull, the TransCat hull. In this study the displacement was kept constant and the variants were the ship main dimensions, such as length, breadth and draught. It was shown that the dominant parameter was the ship length. It was observed that the larger the length, the lower the ship response amplitude at the resonance frequencies. At constant length it was observed that the higher the breadth (which implies lower draught), the lower was the motion response amplitude.

Regarding the hull separation the results agree with the Vosper catamaran results when the comparison is made inside the same range of *L/B* ratio. It was observed under these conditions a certain tendency to have at high speeds slightly higher responses at the wider configurations while at intermediate speeds the opposite was observed.

Recommendations for future work

The viscous effect coefficients (viscous lift and cross-flow drag coefficients) should be studied in more detail in order to find an accurate way to determine these coefficients. In this work the coefficients are assumed constant through all the ship length, but in fact they are a function of ship section, mode of motion, frequency and Reynolds number.

Another aspect that could be improved is the calculation of the relative velocity used in the determination of the viscous forces. The relative velocity is calculated using the incident wave potential but it could be calculated with greater accuracy using other components of the velocity potential.

Some further investigation should be made to clarify the suggestion made concerning the possibility of an intermediate hull distance that would maximise the catamaran motion amplitudes at the resonance frequencies.

References

Abkowitz, M. A., (1969), "Stability and Control of Ocean Vehicles", MIT Press, Cambridge, Massachusetts.

Chan, H. S., (1993), "Prediction of Motion and Wave Loads of Twin-Hull Ships", Marine Structures, Vol. 6, pp. 75-102.

Chan, H. S., (1990),"Three-dimensional Technique for Predicting First and Second Order Hydrodynamic Forces on a Marine Vehicle Advancing in Waves", PhD Thesis, Department of Naval Architecture and Ocean Engineering, University of Glasgow.

Chapman, R. B., (1976), "Free Surface Effects for Yawed Surface-Piercing Plates", Journal of Ship Research, Vol. 20, pp. 125-136.

Faltinsen, O. M. and Zhao, R., (1991a), "Flow Prediction Around High Speed Ships in Waves", Mathematical approaches in hydrodynamics, SIAM

Faltinsen, O. M. and Zhao, R., (1991b), "Numerical Predictions of Ship Motions at High Forward Speed", Phil. Trans. R. Soc. London A, Vol. 334, pp. 241-252.

Faltinsen, O., Hoff, J.R., Kvalsvold, J. and Zhao, R., (1992), "Global Wave Loads on High-Speed Catamarans", Proceedings of *PRADS'92*, ed. J.B. Caldwell and G. Ward, Elsevier Applied Science, London and New York, Vol 1, pp.1360-1375.

Faltinsen, O. M., (1990), "Sea Loads on Ships and Offshore Structures", Cambridge University Press.

Fang, C. C., Chan, H. S. and Incecik, A., (1996), "Investigation of Motions of Catamarans in Regular Waves-I", Ocean Engineering, Vol. 23, No. 1, pp. 89-105.

Fang, C.C., (1996), "An Investigation of Motions of Catamarans in Regular Waves", PhD Thesis, Department of Naval Architecture and Ocean Engineering, University of Glasgow.

Frank, W., (1967), "Oscillation of Cylinders in or Below the Free-Surface of Deep Fluids", Report 2375, Naval Ship Research and Development Center, Washington D.C.

Fonseca, N., (1994), "Non-Linear Motion Response Simulation of Floating Vessels in Waves", MSc Thesis, Department of Naval Architecture and Ocean Engineering, University of Glasgow.

Fonseca, N. and Guedes Soares, C., (1994), "Time Domain Analysis of Vertical Ship Motions", Marine Offshore and Ice Technology, T. K. S. Murthy, P. A. Wilson and P. Wadhams (Eds), Computational Mechanics Publications, Southampton, pp. 224-243.

Gerritsma, J. and Beukelman, W., (1967), "Analysis of the Modified Strip Theory for the Calculation of Ship Motions and Wave Bending Moments", International Shipbuilding Progress, Vol. 14, No. 156, 1967.

Guedes Soares, C. et al, (1997) "Loads", Proceedings 13th International Ship and Offshore Structures Congress *(ISSC'97),* T. Moan and S. Berge (Eds), Elsevier Applied Science, London, Vol. 1, pp. 59-122.

Hamoudi, B, (1995), "Dynamic Response of Hull due to Bottom Slamming and Deck Wetness", PhD. Thesis, Department of Naval Architecture and Ocean Engineering, University of Glasgow.

Hudson, D. A., Price, W. G. and Temarel, P., (1995), "Seakeeping Performance of High Speed Displacement Craft", FAST95, Vol. 2, pp. 877-892.

Incecik, A., Morrison, B.F. and Rodgers, A.J. (1991), "Experimental Investigation and Seakeeping Characteristics of a Catamaran Design", Proc. of the 1st International Conference on Fast Sea Transportation, Norway, pp.239-258.

Inglis, R.B.I. and Price, W.G., (1982a), " A Three-Dimensional Ship Motion Theory: Calculation of Wave Loading and Responses with Forward Speed", Trans RINA, suppl paper, 124, pp. 183-192.

Inglis, R.B.I. and Price, W.G., (1982b), " A Three-Dimensional Ship Motion Theory: Comparison Between Theoretical Predictions and Experimental Data of the Hydrodynamics Coefficients with Forward Speed", Trans RINA, 124, pp. 141-157.

Korvin-Kroukovsky, B. V. and Jacobs, W. R., (1957), "Pitching and Heaving Motions of a Ship in Regular Waves", Transactions SNAME, Vol. 65, pp. 590-632.

Korvin-Kroukovsky, B. V., (1955), "Investigation of Ship Motions in Regular Waves", Soc. Naval Archit. Mar. Eng., Trans. 63, pp. 385-435.

Lee, C.M., Jones, H. D. and Bedel, J. W.,(1971),"Added Mass and Damping Coefficients of Heaving Twin Cylinders in a Free Surface", Report 3695, Naval Ship Research and Development Center, Washington D.C.

Lee, C. M., Jones, H. D. and Curphey, R. M., (1973), "Prediction of Motions and Hydrodynamic Loads of Catamarans", Marine Technology, Vol. pp.392-405, October 1973.

Lee, C. M.,(1976), "Theoretical Prediction of Motion of Small Water-Plane-Area Twin-Hull Ships in Waves" Report 76-0046, Naval Ship Research and Development Center, Washington D.C.

Lewis, E.V., (1989), "Principles of Naval Architecture", Vol. III, The Society of Naval Architects and Marine Engineers.

Newman, J.N., (1977), "Marine Hydrodynamics", MIT Press.

Newman, J.N., (1978), "The Theory of Ship Motions", Advances in Applied Mechanics, Vol. 18, pp. 221-283.

Ogilvie, T. F., and Tuck, E. O., (1969), "A Rational Strip Theory for Ship Motions", Part 1, Report No. 013, Department of Naval Architects and Marine. Engineers, University of Michigan, Ann Arbor.

Ohkusu, M. and Faltinsen, O., (1990), "Prediction of Radiation Forces on a Catamaran at High Froude Number", Proc. of 18th Symp. on Naval Hydrodynamics, Ann Arbour, Michigan.

Ohkusu, M. and Takaki, M., (1971),"On the Motion of Multihull Ships in Waves (II)", Reports of Research Institute for Applied Mechanics, Vol. XIX, No. 62.

Ohkusu, M., (1970),"On the Motion of Multihull Ships in Waves (I)", Rep. Research Institute for Applied Mechanics, Vol. XVIII, No. 60.

Rathje, H. and Schellin, T.E. (1997),"Viscous Effects in Seakeeping Prediction of Twin-Hull Ships", Schiffstechnick, Vol. 44, pp. 44-52.

Salvesen, N., Tuck, E. O., and Faltinsen, O., (1970), "Ship Motions and Sea Loads", Soc. Naval Archit. Mar. Eng., Trans. 78, pp 250-287.

Schellin, T.E., Rathje, H., (1995), "A Panel Method Applied to Hydrodynamic Analysis of Twin-Hull Ships", FAST95, Vol. 2, pp. 905-916.

St. Denis and Pierson, W.J., (1953), "On the Motion of Ships in Confused Seas", Transactions SNAME, Vol. 61.

The Selspot System", (1977), Technical Manual, Selective Electronic Company, Sweden.

Thwaites, B. (1960), "Incompressible Aerodynamics", Oxford University Press.

van't Veer, A. P. and Siregar, F. R. T., (1995), "The Interaction Effects on a Catamaran Travelling with Forward Speed in Waves", FAST95, Vol. 1, pp. 87-98, Lübeck, Germany.

Varyani, K.S., (1988), "The Effect of Forward Speed on Hydrodynamic Forces Acting on Cylindrical Bodies in Waves", PhD. Thesis, Kyushu University.

Wang, S. and Wahab, R. (1971), "Heaving Oscillations of Twin Cylinders in a Free Surface", Journal of Ship Research, Vol. 15, No. 1, pp. 33-48.

Appendix I

In the expressions of the viscous coefficients and viscous forces it is considered:

$$\dot{z}(x) = |\dot{z}_P(x)| + |\dot{z}_S(x)|$$

$$\dot{z}_P(x) = \dot{\xi}_3 - x\dot{\xi}_5 - \dot{\zeta}_v(x, b(x), -d_3(x))$$

$$\dot{z}_S(x) = \dot{\xi}_3 - x\dot{\xi}_5 - \dot{\zeta}_v(x, -b(x), -d_3(x))$$

$$\dot{y}(x) = |\dot{y}_P(x)| + |\dot{y}_S(x)|$$

$$\dot{y}_P(x) = \dot{\xi}_2 + x\dot{\xi}_6 + d_2(x)\dot{\xi}_4 - \dot{\zeta}_h(x, b(x), -d_2(x))$$

$$\dot{y}_S(x) = \dot{\xi}_2 + x\dot{\xi}_6 + d_2(x)\dot{\xi}_4 - \dot{\zeta}_h(x, -b(x), -d_2(x))$$

$$\dot{z}_r(x) = |\dot{z}_{rP}(x)| - |\dot{z}_{rS}(x)|$$

$$\dot{z}_{rP}(x) = b(x)\dot{\xi}_4 - \dot{\zeta}_v(x, b(x), -d_3(x))$$

$$\dot{z}_{rS}(x) = -b(x)\dot{\xi}_4 - \dot{\zeta}_v(x, -b(x), -d_3(x))$$

Viscous coefficients and viscous forces

$$\hat{B}_{33} = \rho a_l U \int_L B_m(x)dx + \rho \frac{4}{3\pi} C_D \int_L \dot{z}(x)\, B_m(x)dx$$

$$\hat{B}_{35} = -\rho a_l U \int_L x B_m(x)dx - \rho \frac{4}{3\pi} C_D \int_L x\, \dot{z}(x) B_m(x)dx$$

$$\hat{B}_{53} = -\rho a_l U \int_L x B_m(x)dx - \rho \frac{4}{3\pi} C_D \int_L x\, \dot{z}(x) B_m(x)dx$$

$$\hat{B}_{55} = \rho a_l U \int_L x^2 B_m(x)dx - \rho \frac{4}{3\pi} C_D \int_L x^2 \dot{z}(x) B_m(x)dx$$

$$\hat{B}_{22} = \rho a_l U \int_L d(x)dx + \rho \frac{4}{3\pi} C_D \int_L \dot{y}(x)\, d(x)dx$$

$$\hat{B}_{24} = \rho a_l U \int_L d_2(x)d(x)dx + \rho \frac{4}{3\pi} C_D \int_L \dot{y}(x)\, d_2(x)d(x)dx$$

$$\hat{B}_{26} = \rho a_l U \int_L x\, d(x)dx + \rho \frac{4}{3\pi} C_D \int_L \dot{y}(x)\, d(x)dx$$

$$\hat{B}_{42} = \rho a_l U \int_L d_2(x)d(x)dx + \rho \frac{4}{3\pi} C_D \int_L \dot{y}(x)\, d_2(x)d(x)dx$$

$$\hat{B}_{44} = \rho a_l U \int_L b^2(x)B_m(x)dx + \rho \frac{4}{3\pi} C_D \int_L \dot{z}_r(x)\, b^2(x)B_m(x)dx +$$

$$\rho a_l U \int_L d_2{}^2(x)d(x)dx + \rho \frac{4}{3\pi} C_D \int_L \dot{y}(x)\, d_2{}^2(x)d(x)dx$$

$$\hat{B}_{46} = \rho a_l U \int_L x d_2(x)d(x)dx + \rho \frac{4}{3\pi} C_D \int_L x\, \dot{y}(x)\, d_2(x)d(x)dx$$

$$\hat{B}_{62} = \rho a_l U \int_L x\, d(x)dx + \rho \frac{4}{3\pi} C_D \int_L \dot{y}(x)\, d(x)dx$$

$$\hat{B}_{64} = \rho a_l U \int_L x d_2(x)d(x)dx + \rho \frac{4}{3\pi} C_D \int_L x\, \dot{y}(x)\, d_2(x)d(x)dx$$

$$\hat{B}_{66} = \rho a_l U \int_L x^2\, d(x)dx + \rho \frac{4}{3\pi} C_D \int_L \dot{y}(x)\, x^2 d(x)dx$$

$$\hat{C}_{35} = \rho a_l U^2 \int_L B_m(x)dx$$

$$\hat{C}_{46} = -\rho a_l U^2 \int_L d(x)d_2(x)dx$$

$$\hat{C}_{55} = -\rho a_l U^2 \int_L x\, B_m(x)dx$$

$$\hat{C}_{66} = -\rho a_l U^2 \int_L x d(x)dx$$

$$F_2^V = -\rho\omega_0 a_l U \int_L d(x) e^{K_0(-d_2(x)+ix\cos\beta)} \cos(K_0 b(x)\sin\beta)dx$$
$$-\rho\frac{4}{3\pi}\omega_0 C_D \int_L d(x) e^{K_0(-d_2(x)+ix\cos\beta)} \left(e^{iK_0 b(x)\sin\beta}\left|\dot{y}_S(x)\right| + e^{-iK_0 b(x)\sin\beta}\left|\dot{y}_P(x)\right|\right)dx$$

$$F_3^V = -\rho\omega_0 a_l U \int_L B_m(x) e^{K_0(-d_1(x)+ix\cos\beta)} \cos(K_0 b(x)\sin\beta)dx$$
$$-\rho\frac{4}{3\pi}\omega_0 C_D \int_L B_m(x) e^{K_0(-d_1(x)+ix\cos\beta)} \left(e^{iK_0 b(x)\sin\beta}\left|\dot{z}_S(x)\right| + e^{-iK_0 b(x)\sin\beta}\left|\dot{z}_P(x)\right|\right)dx$$

$$F_4^V = -\rho\omega_0 a_l U \int_L b(x) B_m(x) e^{K_0(-d_1(x)+ix\cos\beta)} \sin(K_0 b(x)\sin\beta)dx$$
$$+i\rho\frac{4}{3\pi}\omega_0 C_D \int_L b(x) B_m(x)\, e^{K_0(-d_1(x)+ix\cos\beta)} \left(e^{iK_0 b(x)\sin\beta}\left|\dot{z}_S(x)\right| - e^{-iK_0 b(x)\sin\beta}\left|\dot{z}_P(x)\right|\right)dx$$
$$-\rho\omega_0 a_l U \int_L d(x) d_2(x) e^{K_0(-d_2(x)+ix\cos\beta)} \cos(K_0 b(x)\sin\beta)dx$$
$$-\rho\frac{4}{3\pi}\omega_0 C_D \int_L d(x) d_2(x)\, e^{K_0(-d_2(x)+ix\cos\beta)} \left(e^{iK_0 b(x)\sin\beta}\left|\dot{y}_S(x)\right| + e^{-iK_0 b(x)\sin\beta}\left|\dot{y}_P(x)\right|\right)dx$$

$$F_5^V = i\rho\omega_0 a_l U \int_L x B_m(x) e^{K_0(-d_1(x)+ix\cos\beta)} \cos(K_0 b(x)\sin\beta)dx$$
$$+i\rho\frac{4}{3\pi}\omega_0 C_D \int_L B_m(x) e^{K_0(-d_1(x)+ix\cos\beta)} \left(e^{iK_0 b(x)\sin\beta}\left|\dot{z}_S(x)\right| + e^{-iK_0 b(x)\sin\beta}\left|\dot{z}_P(x)\right|\right)dx$$

$$F_6^V = -\rho\omega_0 a_l U \int_L x d(x) e^{K_0(-d_2(x)+ix\cos\beta)} \cos(K_0 b(x)\sin\beta)dx$$
$$-\rho\frac{4}{3\pi}\omega_0 C_D \int_L x d(x) e^{K_0(-d_2(x)+ix\cos\beta)} \left(e^{iK_0 b(x)\sin\beta}\left|\dot{z}_S(x)\right| + e^{-iK_0 b(x)\sin\beta}\left|\dot{z}_P(x)\right|\right)dx$$

Appendix II

Added mass and damping coefficients

$$A_{33} = \int_L a_{33}dx - \frac{U}{\omega^2} b_{33}^A$$

$$A_{35} = -\int_L x a_{33}dx - \frac{U}{\omega^2} B_{33}^0 + \frac{U}{\omega^2} x_A b_{33}^A - \frac{U^2}{\omega^2} a_{33}^A$$

$$A_{53} = -\int_L x a_{33}dx + \frac{U}{\omega^2} B_{33}^0 + \frac{U}{\omega^2} x_A b_{33}^A$$

$$A_{55} = \int_L x^2 a_{33}dx + \frac{U^2}{\omega^2} A_{33}^0 - \frac{U}{\omega^2} x_A^2 b_{33}^A + \frac{U^2}{\omega^2} x_A a_{33}^A$$

$$B_{33} = \int_L b_{33}dx + U a_{33}^A$$

$$B_{35} = -\int_L x b_{33}dx + U A_{33}^0 - U x_A a_{33}^A - \frac{U^2}{\omega^2} b_{33}^A$$

$$B_{53} = -\int_L x b_{33}dx - U A_{33}^0 - U x_A a_{33}^A$$

$$B_{55} = \int_L x^2 b_{33}dx + \frac{U^2}{\omega^2} B_{33}^0 + U x_A^2 a_{33}^A + \frac{U^2}{\omega^2} x_A b_{33}^A$$

$$A_{22} = \int_L a_{22}dx - \frac{U}{\omega^2} b_{22}^A$$

$$A_{24} = A_{42} = \int_L a_{24}dx - \frac{U}{\omega^2} b_{24}^A$$

$$A_{26} = \int_L x a_{22}dx + \frac{U}{\omega^2} B_{22}^0 - \frac{U}{\omega^2} x_A b_{22}^A + \frac{U^2}{\omega^2} a_{22}^A$$

$$A_{44} = \int_L a_{44} dx - \frac{U}{\omega^2} b_{44}^A$$

$$A_{46} = \int_L x a_{24} dx + \frac{U}{\omega^2} B_{24}^0 - \frac{U}{\omega^2} x_A b_{24}^A + \frac{U^2}{\omega^2} a_{24}^A$$

$$A_{62} = \int_L x a_{22} dx - \frac{U}{\omega^2} B_{22}^0 + U x_A a_{22}^A$$

$$A_{64} = \int_L x a_{24} dx - \frac{U}{\omega^2} B_{24}^0 - \frac{U}{\omega^2} x_A b_{24}^A$$

$$A_{66} = \int_L x^2 a_{22} dx + \frac{U^2}{\omega^2} A_{22}^0 - \frac{U^2}{\omega^2} x_A^2 b_{22}^A + \frac{U^2}{\omega^2} x_A a_{22}^A$$

$$B_{22} = \int_L b_{22} dx + U a_{22}^A$$

$$B_{24} = B_{42} = \int_L b_{24} dx - \frac{U}{\omega^2} b_{24}^A$$

$$B_{26} = \int_L x b_{22} dx - U A_{22}$$

$$B_{44} = \int_L b_{44} dx + U a_{44}^A$$

$$B_{46} = \int_L x b_{24} dx - U A_{24}^0 + U x_A a_{24}^A + \frac{U^2}{\omega^2} b_{24}^A$$

$$B_{62} = \int_L x b_{22} dx + U A_{22}^0 + U x_A a_{22}^A$$

$$B_{64} = \int_L x b_{24} dx + U A_{24}^0 + U x_A a_{24}^A$$

$$B_{66} = \int_L x^2 b_{22} dx + \frac{U^2}{\omega^2} B_{22}^0 + U x_A^2 a_{22}^A + \frac{U^2}{\omega^2} x_A b_{22}^A$$

where the terms A_{jk}^0 and B_{jk}^0 refer to the speed independent part of A_{jk} and B_{jk}; x_A is the x-coordinate of the aftermost section of the ship; and a_{jk}^A and b_{jk}^A are the sectional added mass and damping coefficients of the aftermost section of the ship.

The sectional two dimensional added mass and damping coefficients are given by

$$a_{jj} = \mathrm{Re}\left[\frac{\rho}{\omega} i \int_{Cx} N_j \phi'_j dl\right] \quad ; \; b_{jj} = \mathrm{Im}\left[\rho \int_{Cx} N_j \phi'_j dl\right] \quad ,j=2,3,4$$

$$a_{24} = \mathrm{Re}\left[\frac{\rho}{\omega} i \int_{Cx} N_2 \phi'_4 dl\right] \quad ; \; b_{24} = \mathrm{Im}\left[\rho \int_{Cx} N_2 \phi'_4 dl\right]$$

where ϕ'_j is the sectional radiation potential of the two dimensional problem calculated by the Frank close fit method (Frank 1967). The integration is performed along the cross section contour *Cx*. In the sectional potential expressions N_j *(j=2,3)* are the two-dimensional unit normals to the hull surface in the *y-z* plane and $N_4 = yN_3 - zN_2$. To apply Frank close-fit method and calculate the sectional potentials the cross sections have to be defined by a finite number of straight-line segments as represented in the Figure below (in this work 14 segments are used).

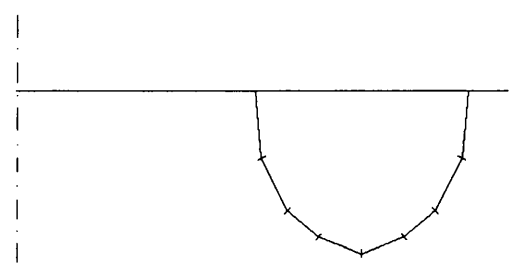

Figure AppendixII.1 - Definition of a hull section

The exciting forces, which include incident and diffracted forces, are given by:

$$F_j = \rho A \int_L \left(f_j^I + f_j^D\right) dx + \rho A \frac{U}{i\omega} f_j^D \Big|_{x_A} \quad ,j=2,3,4$$

$$F_5 = -\rho A \int_L \left[\left(f_3^I + f_3^D\right) x - \frac{U}{i\omega} f_3^D\right] dx - \rho A \frac{U}{i\omega} x_A f_3^D \Big|_{x_A}$$

$$F_6 = \rho A \int_L \left[\left(f_2^I + f_2^D\right) x - \frac{U}{i\omega} f_2^D\right] dx + \rho A \frac{U}{i\omega} x_A f_2^D \Big|_{x_A}$$

$$f_j^I(x) = -\frac{ig}{\omega_0} e^{ik_0 x \cos\beta} \int_{Cx} \left[i\omega_0 N_j e^{k_0(z - iy\sin\beta)} \right] dl$$

$$f_j^D(x) = -\frac{ig}{\omega_0} e^{ik_0 x \cos\beta} \int_{Cx} \left[k_0(-iN_2 \sin\beta + N_3)\phi_j' e^{k_0(z - iy\sin\beta)} \right] dl$$

where $f_j^D\Big|_{x_A}$ refers to $f_j^D(x)$ calculated at the aftermost section of the ship x_A.

GLASGOW UNIVERSITY LIBRARY